

Multi-Objective Structural Optimization of Repairs of Blisk Blades

Von der Fakultät für Bauingenieurwesen und Geodäsie
der Gottfried Wilhelm Leibniz Universität Hannover
zur Erlangung des Grades

DOKTOR-INGENIEUR

- Dr.-Ing. -

genehmigte Dissertation
von

Ricarda Berger M.Sc.

2022

Hauptreferent: Prof. Dr.-Ing. habil. Raimund Rolfes,
Leibniz Universität Hannover
Korreferent: Prof. Dr.-Ing. habil. Jörg Wallaschek
Leibniz Universität Hannover
Tag der mündlichen Prüfung: 9. Februar 2022

Abstract

Modern manufacturing technologies offer multiple options to extend the service life of expensive jet engine components through repairs. In this context, the repair processes of blade-integrated disks (blisks) are of particular interest, as the complex design makes replacement of this part very costly.

However, currently, repairs of blisks are mainly done manually and repair design decisions still rely on the expertise of maintenance technicians. From a scientific perspective, these subjective, experience-based decisions are a major drawback, as today's computational methods allow for systematic analysis and evaluation of design alternatives.

The present doctoral thesis contributes to the decision-making process related to the repair of blisk blades by blending and patching by providing an engineering optimization framework and simulation routines for structural assessment of different repair designs.

First, an object-oriented optimization framework is developed that is ideally suited to address engineering optimization problems such as blisk repair optimization. The design of the software architecture is chosen to achieve a high degree of flexibility and modularity. In particular, the framework provides a unified interface for global and local derivative-free optimization algorithms and custom engineering optimization problems. Thereby, optimization of single- as well as multi-objective problems is supported. The broad applicability of the framework in engineering optimization is demonstrated using examples from wind energy research. Furthermore, the optimization framework forms a suitable environment for structural multi-objective optimization of blend and patch repairs.

The second part of this thesis is devoted to the application of the optimization framework to blend repairs of a compressor blisk. The geometry of the removed blade part and the resulting blend is parameterized by three geometric design variables. The two objectives of the optimization correspond to two modal criteria, because especially the vibration behavior of blades is affected by this kind of geometric modification. To check if frequency requirements are harmed by the repair the first objective reflects the deviation of the natural frequencies of the repaired blade to the natural frequencies of the nominal blade. The second objective considers resonance conditions by evaluating the proximity of natural frequencies to excitation frequencies. Pareto optimal repair designs are found by solving the derived optimization problem using appropriate structural mechanics models of a blade sector and employing the developed optimization framework. By analyzing the optimal blend shapes for two different damage patterns, it is shown that the characteristics of Pareto frontiers, like the occurrence of discontinuities, are damage-specific. Therefore, it is concluded that design decisions on blend repairs have to be made on a case-by-case basis.

The third part of this thesis is concerned with the multi-objective optimization of patch repairs. While blend repairs change the blade geometry, patch repairs restore the original blade contour. In terms of structural integrity, the most significant modification due to patching is hence associated with the welding process to join patch and blade. The remaining residual stresses, affect the strength of the repaired blade, are therefore the most critical aspect of patch repairs. Utilizing the engineering optimization framework and the parametric

simulation model, a multi-objective optimization problem is solved considering the length of the weld and the fatigue strength of the repaired blade. In addition to fatigue strength properties, the weld length is selected as an optimization goal, since the manufacturing effort of the high-tech repair is of practical importance. Pareto optimal repair designs are presented for a damage pattern at the leading edge. The optimization results are further complemented by subsequent thermal and mechanical simulations of the welding and heat treatment process. Different patch geometries are classified from the Pareto optimal solutions. Depending on the preferences in terms of weld length and the High-Cycle Fatigue strength of different load cases, short or long patches are to be used. In addition, the results show that some potential patch designs are not optimal in any case, and therefore can be completely excluded.

Finally, the benefits of the unified interface of the engineering optimization framework are emphasized. Different optimization settings of a patch repair optimization are presented and compared utilizing the hypervolume metric. Concluding remarks on the potential of computational methods for improved repair design and an outlook on future maintenance of blisks complete this work.

Keywords: Blisk; Repair; Multi-Objective Optimization; Engineering Optimization; Compressor Blade; Blending; Patching

Kurzfassung

Moderne Fertigungstechnologien bieten vielfältige Möglichkeiten, die Lebensdauer von teuren Triebwerkskomponenten durch Reparaturen zu verlängern. In diesem Zusammenhang sind die Reparaturprozesse von blade-integrated disks (Blisks) von besonderem Interesse, da das komplexe Design einen Austausch dieses Bauteils sehr kostenintensiv macht.

Derzeit werden Reparaturen von Blisks jedoch hauptsächlich manuell durchgeführt, und Entscheidungen über das Reparaturdesign hängen weiterhin von der Expertise des Instandhaltungstechnikers ab. Aus wissenschaftlicher Sicht sind diese subjektiven, erfahrungsbasierten Entscheidungen ein großer Nachteil, da die heutigen rechnergestützten Methoden eine systematische Analyse und Bewertung von Designalternativen ermöglichen.

Die vorliegende Dissertation leistet einen Beitrag zur Entscheidungsfindung im Zusammenhang mit der Reparatur von Bliskschaufeln durch Blending und Patching, indem sie ein ingenieurwissenschaftliches Optimierungsframework und Simulationsroutinen zur strukturellen Bewertung verschiedener Reparaturdesigns bereitstellt.

Zunächst wird ein objektorientiertes Optimierungsframework entwickelt, das ideal geeignet ist, um ingenieurtechnische Optimierungsprobleme wie die Optimierung von Bliskreparaturen anzugehen. Das Design der Softwarearchitektur ist so gewählt, dass ein hohes Maß an Flexibilität und Modularität erreicht wird. Insbesondere bietet das Framework eine einheitliche Schnittstelle für globale und lokale gradientenfreie Optimierungsalgorithmen und individuelle ingenieurtechnische Optimierungsprobleme. Dabei wird sowohl die Optimierung von Einzel- als auch von Mehrzielproblemen unterstützt. Die breite Anwendbarkeit des Frameworks in der Ingenieursoptimierung wird anhand von Beispielen aus der Windenergieforschung demonstriert. Darüber hinaus bildet das Optimierungsframework eine geeignete Umgebung für die strukturmechanische Mehrzieloptimierung von Blend- und Patchreparaturen.

Der zweite Teil dieser Arbeit widmet sich der Anwendung des Optimierungsframeworks auf Blendreparaturen einer Verdichterblisk. Die Geometrie des entfernten Schaufelteils und der resultierenden Blendform wird durch drei geometrische Designvariablen parametrisiert. Die beiden Optimierungsziele entsprechen zwei Frequenzkriterien, da insbesondere das Schwingungsverhalten von Schaufeln durch diese Art von geometrischen Veränderungen beeinflusst wird. Um zu überprüfen, ob die Frequenzanforderungen durch die Reparatur beeinträchtigt werden, berücksichtigt das erste Ziel die Abweichung der Eigenfrequenzen der reparierten Schaufel von den Eigenfrequenzen der nominalen Schaufel. Das zweite Ziel berücksichtigt Resonanzbedingungen, indem die Nähe der Eigenfrequenzen zu den Anregungsfrequenzen bewertet wird. Pareto-optimale Reparaturdesigns werden gefunden, indem das abgeleitete Optimierungsproblem mit Hilfe von entsprechenden strukturmechanischen Modellen eines Schaufelsektors und unter Einsatz des entwickelten Optimierungsframeworks gelöst wird. Durch die Analyse der optimalen Blendformen für zwei verschiedene Schadensbilder wird gezeigt, dass die Eigenschaften der Paretofront, wie das Auftreten von Diskontinuitäten, schadensspezifisch sind. Daraus wird gefolgert, dass Designentscheidungen über Blendreparaturen abhängig vom Einzelfall getroffen werden müssen.

Der dritte Teil dieser Arbeit befasst sich mit der Mehrzieloptimierung von Patchreparaturen. Während sich bei der Blendreparatur die Schaufelgeometrie ändert, wird bei der Patchreparatur die ursprüngliche Schaufelkontur wiederhergestellt. In Bezug auf die strukturelle Integrität ist die bedeutendste Veränderung durch das Patching daher mit dem Schweißprozess zum Fügen von Patch und Schaufel verbunden. Verbleibende Eigenspannungen, die sich auf die Festigkeit der reparierten Schaufel auswirken, sind daher der kritischste Aspekt bei der Patchreparatur. Unter Verwendung des Optimierungsframeworks und des parametrisierten Simulationsmodells wird ein Mehrzieloptimierungsproblem unter Berücksichtigung der Schweißnahtlänge und der Ermüdungsfestigkeit der reparierten Schaufel gelöst. Neben den Festigkeitseigenschaften ist auch die Schweißnahtlänge ein Optimierungsziel, da der Fertigungsaufwand der Hightech-Reparatur von praktischer Bedeutung ist. Pareto-optimale Reparaturdesigns werden für ein Schadensbild an der Vorderkante vorgestellt. Die Optimierungsergebnisse werden außerdem durch anschließend durchgeführte thermische und mechanische Simulationen des Schweiß- und Wärmebehandlungsprozesses ergänzt. Aus den Pareto-optimalen Lösungen werden verschiedene Patchgeometrien klassifiziert. Abhängig von den Präferenzen in Bezug auf die Schweißnahtlänge und die hochzyklische Ermüdungsfestigkeit verschiedener Lastfälle sind kurze oder lange Patches zu bevorzugen. Darüber hinaus zeigen die Ergebnisse, dass einige potenzielle Patchdesigns in keinem Fall optimal sind und daher vollständig ausgeschlossen werden können.

Schließlich werden die Vorteile der einheitlichen Schnittstelle des ingenieurwissenschaftlichen Optimierungsframeworks hervorgehoben. Es werden verschiedene Optimierungseinstellungen für die Optimierung einer Patchreparatur vorgestellt und unter Verwendung der Hypervolumen-Metrik verglichen. Eine abschließende Darstellung über das Potenzial von Berechnungsmethoden für ein verbessertes Reparaturdesign und ein Ausblick auf die zukünftige Instandhaltung von Blisks vervollständigen diese Arbeit.

Schlagnworte: Blisk; Reparatur; Mehrzieloptimierung; Ingenieursoptimierung, Verdichterschaufel; Blending; Patching

Contents

List of Figures	III
Notation	V
1 Introduction	1
1.1 Motivation	1
1.2 State of the Art	3
1.2.1 Software for Engineering Optimization	3
1.2.2 Repair Technologies of Blisk Blades	6
1.2.3 Structural Optimization of Rotating Turbomachinery Components	10
1.3 Challenges and Research Gaps	16
1.4 Objectives	18
1.5 Outline	19
2 Theoretical Background	21
2.1 Introduction to Engineering Optimization	21
2.1.1 Optimization Problem Formulation	21
2.1.2 Structural Optimization	22
2.1.3 Classification of Optimization Algorithms	23
2.1.4 Concept of Pareto Dominance	24
2.2 Fundamentals of Blade Mechanics	26
2.2.1 Operating Conditions of Jet Engines	26
2.2.2 Loading of Rotating Blades	27
2.2.3 Blade and Blisk Modes	28
2.2.4 Vibrations and Resonance Conditions	29
2.2.5 Blade Fatigue	32
3 Engineering Optimization Framework	35
3.1 Research Context	35
3.2 Methods	36
3.3 Results and Outlook	36
3.4 Paper A: EngiO – Object-Oriented Framework for Engineering Optimization	37

4	Optimization of Blend Repairs	53
4.1	Research Context	53
4.2	Methods	53
4.3	Results and Outlook	54
4.4	Paper B: A Two-Objective Design Optimisation Approach for Blending Repairs of Damaged Compressor Blisks	54
5	Optimization of Patch Repairs	65
5.1	Research Context	65
5.2	Methods	65
5.3	Results and Outlook	66
5.4	Paper C: A Multi-Objective Approach towards Optimized Patch Repairs of Blisk Blades	66
6	Application of EngiO to Multi-Objective Optimization of Blade Repairs	99
6.1	Quality Indicators in Multi-Objective Optimization	99
6.2	Optimization Algorithms and Parameters	100
7	Summary and Outlook	103
7.1	Summary	103
7.2	Outlook	105
	Bibliography	107

List of Figures

- 1-1 Airplane (a) with jet engine CF34 and compressor blisk (b). 1
- 1-2 Compressor blisks with different scales of blade damages. 6
- 1-3 Different repair concepts of blades (a) and their relative number of use (b). 6
- 1-4 Blending tool used to manually grind down irregularities of a single compressor blade. [162] 8
- 1-5 Damaged blade portion (a) before and (b) after blending. [3] 8
- 1-6 Joining patch and blade in a welding process. [124] 9
- 1-7 Fan blade with a) defect, b) applied patch, and c) final shape. [12] 10
- 1-8 Concept developed for multi-objective optimization of blisk blades repaired by blending and patching. 18

- 2-1 Levels of structural optimization. [19] 22
- 2-2 Attributes for classification of state-of-the-art optimization methods [119]. . 23
- 2-3 Two-dimensional visualization of Pareto dominance. 25
- 2-4 Relative shaft speed and high-pressure turbine inlet temperature during a short-haul flight mission according to Hanumanthan et al. [76]. 26
- 2-5 Bending (mode 1), torsional (mode 3) and higher mode shape of a clamped blisk blade. 28
- 2-6 Cyclic symmetry modes of a blisk for different nodal diameters (ND). . . . 29
- 2-7 Schematic Campbell diagram showing the frequencies of the first two blade modes and the first three engine order (EO) lines). 30
- 2-8 Schematic SAFE diagram showing the frequencies of the first two blade modes and the excitation line. 31
- 2-9 Simplified load spectrum according to one flight mission. 32
- 2-10 Schematic constant life diagram. 33

- 6-1 Visualization of the hypervolume metric for a two-dimensional example. . . 100
- 6-2 Visualization of the hypervolume metric for the second two-dimensional example in paper C for different algorithms. 101
- 6-3 Visualization of the hypervolume metric for the second two-dimensional example in paper C for different population sizes. 102

Notation

Symbols

Symbol	Name
λ	Lebesgue measure
ω	Natural frequency
Ω	Exciting frequency
σ	Stress
\mathbf{a}	Point of approximation set
af	Amplitude frequency strength
A	Approximation set
CSM	Number of cyclic symmetry modes
\mathbf{f}, f	Objective functions
\mathbf{g}	Inequality constraints
\mathbf{h}	Equality constraints
HV	Hypervolume metric
k	Counter
m	Number of objectives
n	Number of design variables
	Number of nodal diameters
N	Number of blades
p	Number of inequality constraints
q	Number of equality constraints
r	Reference point
\mathbf{x}, x	Design variables
X	Set of solutions

Indices

Symbol	Name
a	Amplitude
e	Endurance
i	General index
lb	Lower boundary
m	Mean
max	Maximum
ub	Upper boundary
y	Yield

Abbreviations

Abbreviation	Name
Blisk	B lade- i ntegrated d isk
CFD	C omputational F luid D ynamics
CSM	C yclic S ymmetry M ode
DLR	D eutsche Z entrum für L uft- und R aumfahrt
EASA	E uropean U nion A viation S afety A gency
EngiO	E ngineering O ptimization
EO	E ngine O rders
ESA	E uropean S pace A gency
FE	F inite E lement
FOD	F oreign O bject D amage
HCF	H igh C ycle F atigue
LCF	L ow C ycle F atigue
LE	L eading E dge
LPT	L ow- P ressure T urbine
MDO	M ultidisciplinary D esign O ptimization
MRO	M aintenance R epair O verhaul
MAC	M odal A ssurance C riterion
MOGPS	M ulti- O bjective G lobal P attern S earch
NACA	N ational A dvisory C ommittee for A eronautics
ND	N odal D iameter
NSGA-II	N on-dominated S orting G enetic A lgorithm-II
NURBS	N on- U niform R ational B asis- S pline
SAFE	S ingh's A dvanced F requency E valuation
SFB	S onder F orschungs B ereich
TE	T railing E dge

1 Introduction

1.1 Motivation

The maintenance, repair, and overhaul (MRO) of jet engines account for a significant amount of the operating costs of civil airplanes. In terms of direct operating costs, up to ten percent is related to engine maintenance [147]. With new engine designs, underlying maintenance processes even get more important. Modern jet engines are designed to increase efficiency and decrease fuel consumption. One main driver in the design process is the thrust-to-weight ratio. Better performance is therefore gained by reducing the total weight of the engine. This weight reduction is especially achieved by more complex part designs within the engine. One example can be found in the jet engine of the Bombardier CRJ200. This short-track airplane, which is depicted in Fig. 1-1 (a), is operated by two GE engines of type CF34.



(a) Bombardier CRJ200 [58]



(b) Blisk

Figure 1-1: Airplane (a) with jet engine CF34 and compressor blisk (b).

The design of rotors in the first and second stages of the high-pressure compressor of the CF34 engine differs from conventional approaches. In conventional design, the rotor consists of a series of individual blades mounted on the central disk. In contrast, in the CF34 engine, the blade and disk assemblage is replaced by one single part. The **blade-integrated disk (blisk)** of the first compressor stage is shown in Fig. 1-1 (b). This kind of compressor blisk enables a weight reduction up to 20 % relative to the conventional design concept [33], but also leads to new challenges in maintenance processes.

While a single defective compressor blade in the conventional setup used to be simply replaced by a new one, the blade-integrated design forces the maintenance technicians to either repair the blisk blade or replace the entire blisk. To avoid scrapping and high spare part costs of blisks, special high-tech repair procedures are developed to preserve compressor blisks rather than replacing them.

In the aviation industry, every component of a jet engine must meet strict criteria to ensure safe flight operation. Just like the nominal components, repairs and repaired parts are hence subjected to high safety requirements. Repairs of blisks must be designed and carried out in such a way that structural integrity is maintained and the safe operation of repaired parts in the engine is ensured.

To check these safety requirements, experiments and simulations are carried out. Especially in the last decades, numerical simulations are increasingly used to verify crucial requirements for the components and thus partially replace expensive and time-consuming experiments. In the context of compressor blisks, the simulation models are mainly concerned with predicting and evaluating the functionality of the repaired blades in terms of aerodynamics and mechanics. Corresponding numerical simulations are already used in the initial design phase of jet engines and design decisions are made based on the computational results. However, unlike the initial simulation model, the models for repair assessment must also reflect repair-specific changes. Recent research, therefore, aims to accompany the real repair process with a virtual workflow and to improve repair decisions made in the real process [8]. When repairing compressor blisks, different repair procedures are used in accordance with the individual damage characteristics of blades. Depending on the technique used to refurbish the blade, this results in changes to the mechanical properties and strength of the jet engine blade. One repair technique, so-called blending, involves the removal of blade material such that the refurbished blade geometry always differs from the initial geometry. In the case of blending, the remaining geometric variation of the blade then affects the vibration behavior of the rotating blisk. Other repair procedures use welding processes, which locally impact the initial stress state and material strength. The fatigue strength of the remanufactured blade is hence affected. Consequently, all these repair-specific influences have to be represented by the computational models, like Finite Element (FE) models. Results of FE simulations provide insights into the blade's mechanics and established evaluation metrics allow the prediction of influences of repair parameters on design goals associated with vibration behavior and service life.

Since the engineer's motivation is to improve repair designs and find the best possible design alternative the application of numerical optimization methods is straightforward. To enable engineering optimization, the simulation models have to be embedded in an optimization scheme. This way, iterative and often manual design processes are accelerated by linking automated simulation with numerical optimization procedures. The design goals of the optimization tasks then are formulated as the objectives of the mathematical optimization and design alternatives are described by design variables of the repair.

In many cases, however, the optimal repair design is influenced by more than one single design goal and has to meet multiple objectives. For example, the service life of the repaired blisk blade is to be maximized while minimizing the machining effort of the repair. Reducing multiple objectives to a single one by the prior weighting of objectives is commonly beyond the intuition of engineers, especially when different disciplines are involved. Therefore, the optimization of blisk repairs benefits from multi-objective optimization approaches. Design goals are evaluated separately constituting one objective value each. The trade-off of design alternatives is presented in form of a Pareto frontier instead of an a priori articulation of preferences. The results of the multi-objective optimization supply an initial set of optimal repair designs to the engineer and therewith support the repair design decisions. The final decision on the repair design is taken by the engineer or maintenance technician according to the optimization results and individual preferences as well as experience-based knowledge.

Optimization results therewith complement the existing guidelines specified in the maintenance manuals of jet engines.

In this sense, this doctoral thesis develops a computational scheme that allows evaluating the influence of repair-specific changes on the blade structure and reveals optimal repair designs utilizing multi-objective optimization.

1.2 State of the Art

The following sections refer to the state of the art in engineering optimization and its application in turbomachinery design. In Sec. 1.2.1, state-of-the-art software for optimization in engineering and science is discussed. Subsequently, repair technologies of compressor blisks in jet engine applications are reviewed in Sec. 1.2.2. Special emphasis is placed on the repair by blending and patching. The last section (Sec. 1.2.3) is related to the application of optimization methods in the context of rotating turbomachinery components¹.

1.2.1 Software for Engineering Optimization

The use of optimization methods² in computational science, engineering, and research is widespread. As a result, various software implementations of optimization algorithms have been published in recent decades [101, 118, 4, 131]. These software implementations enable the application of optimization algorithms to engineering real-world optimization problems. In this context, the development of optimization software is often closely related to the development of new algorithms [123] or specific applications [180]. The term optimization algorithm refers to the scheme used to iterate to optimal solutions [102]. In contrast, software implementation denotes the realization of algorithms as a program. This section focuses on different levels of implementation of state-of-the-art optimization algorithms and considers the associated intentions. Current optimization software is presented in the context of algorithm-specific functions, collections of algorithm-specific functions, and optimization frameworks. Mathematical concepts and classification approaches of algorithms are covered in Sec. 2.1.

Implementation of Algorithm-Specific Functions

According to the target of the respective optimization software, optimization algorithms are implemented at different levels of complexity. At the lowest level, the optimization algorithm is implemented as a function or a set of functions respectively. For example, the C code of one of the most famous multi-objective algorithms, known as Non-dominated Sorting Genetic Algorithm-II (NSGA-II) [45, 46], is accessible via the developers' website [94]. The programming syntax of such functions is derived from the algorithm-specific parameters and is unique for the particular algorithm. Therefore, the programming syntax of the function (e.g. number and meaning of input arguments) can not be reused for the implementation of other state-of-the-art algorithms.

¹In this thesis, the term blade is used for compressor or turbine blades of conventional design as well as to describe blisk geometries. When the term blade is used in the context of blisks, it refers to the portion of the blisk that corresponds to a single blade in the conventional design.

²The terms optimization methods and algorithms are used synonymously in this thesis.

However, the functions containing the initial software implementation of NSGA-II or executable versions of this functions are still used by other optimization software, e.g., PyOpt [134]. In addition, several potentially slightly different implementations such as [154] may exist. For reasons of comparability, the original function is therefore often used in benchmark studies. Similarly, e.g., the initial implementation of whale search [123] is published as a function [122].

Collection of Algorithm-Specific Functions

On the next level, the code of multiple algorithms is implemented and collected in universal packages. These software packages bundle different algorithm-specific implementations and make them available to the user at once. Since the optimization algorithms are iterative schemes, which are in the first place independent from their specific application, optimization packages are equally applicable in various disciplines. One prominent open-source package for mathematics, science, and engineering is the SciPy package [167]. It has been developed over around 20 years and includes well-tested methods for general scientific computing. The optimization capabilities are bundled in the `scipy.optimize` subpackage. The algorithm implementations of this subpackage further provide the basis for packages with more specialized applications. For example, the packages named PyGMO and PyKEP [91] are based on SciPy routines. They were developed at the European Space Agency (ESA) to allow for parallel multi-objective optimization in the field of astrodynamical computation. SciPy also supports the Python-based optimization software Pyomo [79, 78], which aims to facilitate optimization through using a syntax similar to the mathematical notation of optimization problems (Sec. 2.1.1).

Software implementations of optimization algorithms are also part of the frequently used Matlab programming environment developed by MathWorks. The standard Matlab programming environment can be extended by two optimization-related packages. The Matlab Optimization Toolbox [121] provides some basic optimization functionality and the Matlab Global Optimization Toolbox [120] is targeted to solve global and multi-objective optimization problems. Further, the toolbox Tomlab [88] is an optimization package developed for the Matlab environment. It aims to facilitate optimization for practitioners and is also compatible with the MathWorks Optimization Toolbox. Moreover, a Matlab toolbox, named YALMIP, targeted to application in the field of systems and control theory is published by Löfberg et al. [109].

Optimization Frameworks

From the software engineering point of view, the most elaborate designs of optimization software are frameworks. Optimization frameworks, unlike packages, provide an entire scaffold for implementing algorithms and optimization problems. This additional structure enables to organize processes and facilitates the application of numerical optimization.

The design of frameworks, in general, is closely linked to the object-oriented design paradigm. According to Gamma et al. [61], an object-oriented framework consists of cooperating classes and "provides architectural guidance by partitioning the design into abstract classes and defining their responsibilities and collaborations". Therefore, an optimization framework offers a standard way to build e.g. optimization algorithm classes. Recurring routines are centralized and customized routines are implemented in associated subclasses. One of the

early software contributions to engineering optimization is DAKOTA [56], the Design Analysis Kit for OpTimizAtion. The C++ framework includes object-oriented design patterns and provides e.g. an optimizer class for the algorithm. Recent journal publications in totally different scientific fields such as composites [6], turbomachinery [2] or chemical kinetics [60] indicate that DAKOTA is still in use and is thus a notable optimization software. More elaborated object-oriented approaches towards state-of-the-art framework design could be found in more recent publications e.g. [134, 52].

In addition, the choice of programming language significantly influences the readability and usability of source code of optimization frameworks. High-level programming languages facilitate coding and make debugging of source code easier. Extensive optimization frameworks, therefore, benefit from the appropriate choice of programming language. The C++ programming language, which is the basis of DAKOTA, used to be considered as a high-level language. With the appearance of programming languages like Python, Java, and Matlab, however, this classification is debatable. Optimization frameworks implemented in high-level languages are Python-based implementations like PyOpt [134], ParadisEO-MO [90], and OpenMDAO [70, 69] or Matlab-based frameworks like UQLab [113], COSSAN [133] or PolyTop [163].

A further aspect, which is tackled by state-of-the-art optimization software is parallelization capabilities. Parallel computing of objective function values is of great importance since for many real-world problems extensive numerical simulations have to be performed. Especially in the case of structural or aerostructural optimization, the running times of simulations are too long that objective functions values can be computed sequentially within manageable time [97]. The Python-based framework FOM [130] for example misses this feature, while the architecture of PyOpt [134] supports parallel computation.

Finally, the design of most optimization frameworks is driven by a particular application. Depending on the field of engineering optimization different categories of optimization methods (Sec. 2.1.3) are used. Usually, the architecture of the optimization framework is specifically targeted to a certain group of optimization algorithms. For example, Opt4J [110], is designed for evolutionary optimization algorithms only, and therefore the architecture implements classes related to genetic representations. The interface definitions are hence not compatible to implement optimization algorithms like pattern search approaches. Equally, for multi-objective optimization problems, the architecture of the framework has to enable processing multiple objectives. This feature is found in frameworks like jMetal [52] but not in Easylocal [50], which focus on local single-objective optimizers. Optimization frameworks designed for uncertainty quantification and related methods like sampling approaches are UQLab [113] and COSSAN [133].

Overall, the current developments of optimization software take place in all three software categories presented in this section. The programming concept depends on the respective purpose and intention of the software. For the development of new logic of optimization algorithms, simple functions are often sufficient. However, for application-oriented optimization, as is common in engineering optimization, frameworks prove to be advantageous. Major design criteria of engineering optimization frameworks refer to object-oriented programming, high-level programming languages, parallelization techniques, and implementations of optimization algorithms.

1.2.2 Repair Technologies of Blisk Blades

During flight operation, the components of jet engines are subjected to wear and may be damaged. In particular, the stationary and rotating blades in the compressor and turbine are susceptible to so-called foreign object damage (FOD) [64]. FOD is caused by small to large particles entering the engine with the airflow. These objects hit the blade and leave damage to the blade material. The objects or particles can be e.g. small sand particles, garbage at the runway, or even bird strikes. Depending on the size of the object that passes through the jet engine, slight or severe damage is caused to the blades [75]. In Fig. 1-2 some typical damage patterns of compressor blisks are shown.

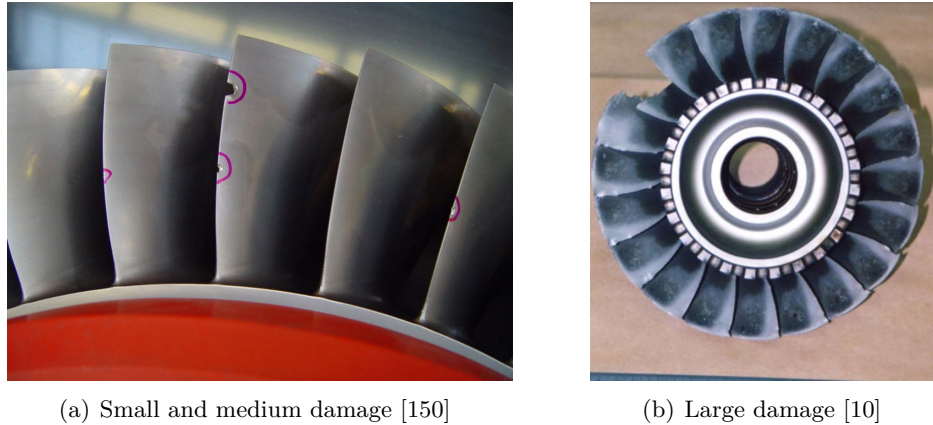


Figure 1-2: Compressor blisks with different scales of blade damages.

The foreign object usually hits the blades from the upstream direction and therefore FOD mainly occurs at the leading edges as illustrated in Fig. 1-2 (a). As depicted in Fig. 1-2 (b), blade defects can become large, such that they even lead to the complete destruction of blades. To be able to reuse damaged blades in jet engines different repair concepts are developed for compressor blisks [35, 33]. Fig. 1-3 gives an overview of state-of-the-art concepts and their usage in the maintenance of compressor blisks.

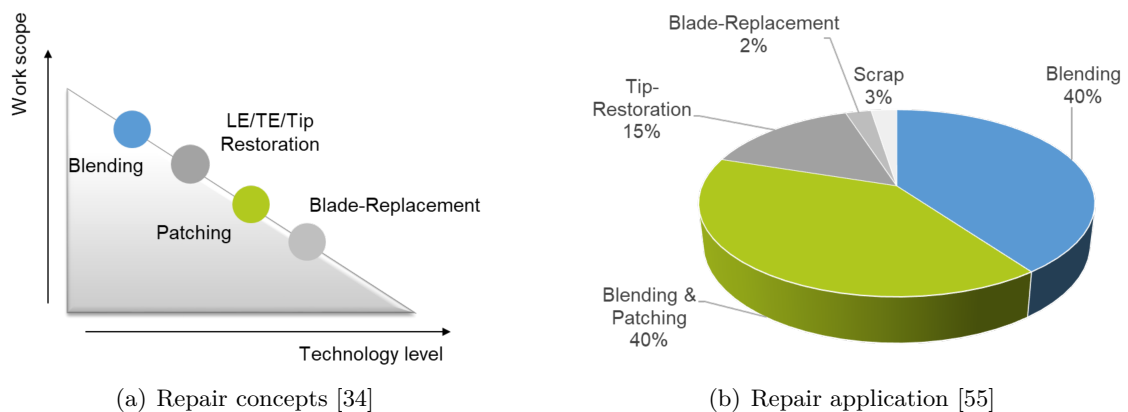


Figure 1-3: Different repair concepts of blades (a) and their relative number of use (b).

In Fig. 1-3 (a), according to Bussmann et al. [34] four repair technologies are ranked by the level of technology and their work scope. The most frequently used, but also simplest repair is the repair by blending. A blend repair is the removal of damaged areas of the blade via a grinding process. Since blending can be carried out with little effort, it is applied to compressor and turbine blades of the conventional blade-disk assemblage as well.

The second repair concept refers to the restoration of the leading edge (LE), the trailing edge (TE), or the tip region of the blade. Initially, the damaged portion is removed and the missing part is rebuilt using a cladding process. The surface of the additive manufactured part is restored via a milling process. Due to this multi-step procedure, the repair is significantly more elaborated than blending. For economic reasons, restoration of blades is only of interest for components with high spare part costs such as blisk or single crystalline turbine blades. The third concept is patching. This repair also involves the removal of the defect. However, after the removal of the damaged blade portion a new material, the so-called patch, is attached using a welding process. A final milling process recovers the aerodynamic shape of the blade. In contrast to the two repair concepts introduced previously patching is only applied to blisk blades, because it is inappropriate for single crystalline turbine blades and is not commercially viable for conventional compressor blades.

Finally, the most extensive repair designed exclusively for blisks is a blade replacement. Instead of removing damaged regions only, the whole blade is removed. The new blade and the blisk are joined by a welding process such that the new blade replaces the missing damaged one. According to the impact of the repair, the technology level of the repair process increases for the mentioned concepts. Especially, the welding processes involved in the last three repairs described here lead to further challenges from a manufacturing point of view.

The aforementioned work scope of the four repair concepts is also reflected in the statistics, which is shown in Fig. 1-3(b). According to Eberlein et al. [55], about 80 % of overhauled blisks are repaired by blending and patching. At two percent, blade replacements are very rare. Since this doctoral thesis focuses on repairs of blisks by blending and patching, in the following the two repair processes are elaborated in more detail. For further information on other repair concepts it is referred to [178, 177, 164, 145, 47].

Blending

Blending is a repair procedure, which is applied to turbomachinery blades with small defects. During a blend repair, the defect area is *blended out* by grinding as it is shown in Fig. 1-4.



Figure 1-4: Blending tool used to manually grind down irregularities of a single compressor blade. [162]

The high-speed grinding tool is used to get the final contour. The tool can also be applied in a boroscope blending procedure [65]. In this case, there is no need to disassemble the engine, and the blending tool and optical instruments are inserted into the engine using inspections ports. Regardless of the specific process, the general idea of blending is to remove stress concentrations caused by dents, nicks, or cracks and therewith prevent further crack propagation. In Fig. 1-5, a defect at a blade edge is documented before and after the repair process by blending.



Figure 1-5: Damaged blade portion (a) before and (b) after blending. [3]

Comparing the blade before and after repair, it can be seen that the repaired blade significantly differs from its original contour. At the same time, the shape of the removed portion is smooth and has a reduced risk of crack formation. In this context, it should be noted that the modification of the blade profile also impacts the flow around the blade. As shown by Keller et al. [96], the aerodynamic performance of blended blades thus decreases with blends. The influence of blend repairs on blade frequencies is studied by Beck et al. [14].

They analyze the scatter of frequencies of blisk blades due to a blend in two different sizes. The main focus of their work is further on the amplification of vibration amplitudes resulting from blade-to-blade variations known as mistuning. The paper published by Schwerdt et al. [152] is about the influence of repairs and further scattering material parameters on natural blade frequencies. In addition, the flutter tendency of different blend repairs is considered. Further investigations on mistuning caused by blend repairs and the accuracy of associated reduced-order models are presented in [151].

Although there are scientific contributions about geometric modifications due to blends [96, 152, 14] as well as unintended geometric variances [62, 30, 28, 29, 84, 57] current maintenance guidelines are very limited. Guidelines ensure the aerodynamic and structural functionality of repaired blades by restricting repairs to certain blade areas and blend sizes. These engine- and blade-specific repair limits are documented in the confidential engine manufacturer's service and overhaul instruction manuals.

Patching

Patching is a more complex repair concept than blending. A patch repair is carried out for greater damages, where the blend size would exceed allowable limits and is hence not applicable anymore. In the case of a patch repair, the defect is initially removed via a milling process and prepared for the welding procedure. Subsequently, a plate is joint to the blade via a welding process as it is shown in Fig. 1-6.

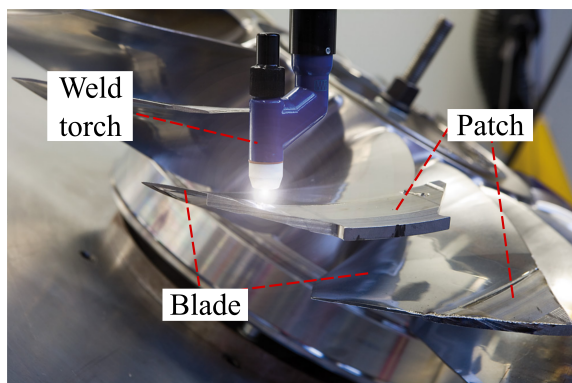


Figure 1-6: Joining patch and blade in a welding process. [124]

The new part (patch) is typically made out of the same material as the blade, which is a titanium alloy for most compressor applications. The patch, as it is illustrated in Fig. 1-7, is initially larger and thicker than the replaced blade portion. The excessive material allows for later machining to nominal geometry. In the final step, the aerodynamic contour of the blade is recovered in a milling process, named recontouring [49] or reprofiling [25]. The final repaired blade is also shown in Fig. 1-7.

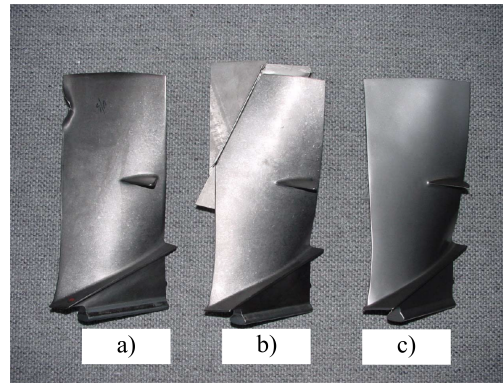


Figure 1-7: Fan blade with a) defect, b) applied patch, and c) final shape. [12]

Furthermore, the joint between blade and patch has to meet high quality standards. Conventional welding methods like tungsten-inert gas are not capable of manufacturing a precise weld and lead to unfavorable microstructural changes [23]. Only high-tech welding processes like electron beam welding [11] or plasma arc welding [48] ensure high-quality welds and are suitable to manufacture these joints. Nevertheless, all kinds of welding processes induce residual stresses into the material and hence may lower the fatigue strength of the repaired blade. To minimize remaining stresses in the blade, heat treatment is carried out in a final step [17].

Since the patch repair process involves significantly more processing and manufacturing effort than blending, the repair concept is applied to blisk blades only. If the rotor is designed the conventional way as a blade and disk assemblage, the exchange of single blades is more cost-efficient than the time-consuming patch repair. At the moment, the repair by patching is so demanding that only some MRO companies like MTU have certified the repair technology and offer patch repairs to their costumers [41].

1.2.3 Structural Optimization of Rotating Turbomachinery Components

In the last decades, researchers are increasingly using optimization approaches to improve the design of rotating turbomachinery components such as blades [99], disks [170], or blisks [59]. However, according to the definition of structural optimization stated in Sec. 2.1.2, these optimization approaches can rarely be assigned to the field of pure structural optimization [51]. Most approaches primarily target aerodynamic performance rather than structural integrity [108]. Nevertheless, many aspects, e.g. the parameterization of blade geometries, are relevant for structural as well as for aerodynamical optimization. The literature presented in the following paragraphs, therefore, also includes optimization tasks from other disciplines. The focus remains on aspects of structural modeling and optimization.

The following section is divided into three parts. The first part summarizes existing optimization approaches for blades, disks, or blisks from a design (variable) perspective. It deals with the choice of design variables and automated numerical modeling of design alternatives in recent scientific contributions. The second part, on the contrary, focuses on the optimization goals and the formulation of optimization problems associated with the design of blades, disks, or blisks. Objective functions and constraints corresponding to structural criteria are highlighted.

While these first two paragraphs refer to optimization during the initial design phase only, the third paragraph is concerned with design variables, models, objectives, and constraints related to the structural optimization of repair procedures. Differences and similarities between optimization of repair designs and optimization of initial designs are emphasized.

Design Variables and Models for Design Optimization

Size optimization, as the simplest form of structural optimization, is rarely found in recent optimization approaches of rotating turbomachinery components. The geometries of disks, blades, and blisks are usually too complex to be described by a set of simple quantities such as lengths and diameters. An early work that can be considered as an example of size optimization was published by Brown et al. [27]. The authors optimized a cross-section of a turbine disk. Five geometric design variables, e.g., the thickness of the rim of the disk, were used to model the turbine disk. A coarse FE mesh was adjusted in a mesh morphing procedure to allow for an automated evaluation process.

Both size and **shape optimization** was performed by Wagner et al. [169] aiming for the optimal geometry of a fir-tree root³. The main focus of their work was on the parameterization of the fir-tree geometry rather than the optimization process. In particular, they compared three models with a different number of design variables and found that the optimization is strongly influenced by the selected approach. In the study, only the most extensive shape optimization approach captured the required features and therefore led to the best results. A similar approach was presented by Song et al. [160, 161]. The authors modeled the geometry of the fir-tree using a rule-based computer-aided design system and applied a Non-Uniform Rational Basis-Spline (NURBS) definition for local notch profiles. The optimization problem was formulated based on six geometric design variables. Wagner et al. [169], as well as Song et al. [160, 161], further used automated meshing for their structural simulation models.

The majority of shape optimization approaches in the field of rotating turbomachinery components, though, do relate to the design of an aerodynamically effective blade contour. Modern jet engine blades (i.e. turbine blades, compressor blades, and blisk blades) have complex three-dimensional geometries to reach optimal fluid mechanical properties. As a result, it is difficult to describe their geometries with a few design variables. In the past, mainly two parameterization concepts have been used in industrial applications and academic research.

The first one refers to the specification of aerodynamic contours introduced by the National Advisory Committee for Aeronautics (NACA). Developed in the mid of the 20th century the NACA profiles provide a standardized description for cross-sections of aerodynamic structures like airfoils or turbomachinery blades [1]. The particular shape is defined according to a single-digit number of variables like the maximum thickness of the profile. For today's curved blade design, however, the two-dimensional profile description enabled by NACA is no longer adequate. Nevertheless, for example, the method developed by Lange et al. [105] is still based on the fundamental ideas of the NACA system. The specification of the meanline and the thickness of the NACA profile was modified by Lange et al. and the three-dimensional blade was reconstructed combining multiple cross-sections. According to the proposed method, one two-dimensional profile was defined by 14 design variables

³The fir-tree root attachment is named after its contour, which is reminiscent of a fir-tree. It is a design concept used for highly loaded rotating turbine blades.

such as chord length or thickness of LE or TE. The discretization of the blade for CFD simulations was maintained and updated according to the particular design via a mesh morphing procedure. An optimization approach for turbine blades, which is also based on multiple NACA profiles, was published by Gezork et al. [63]. The authors used 19 profiles to describe the blade geometry, which results in more than a hundred design variables. In contrast to Lange et al. [105], in this study, a new mesh was generated for each blade design. Further, equivalent approaches were applied by Heinze [83] or Backhaus et al. [13]. Both authors did not use the blade model for optimization purposes but performed sensitivity studies concerning scattering blade parameters. In the latter publication, the whole blade model comprised a large number of 686 parameters.

The second concept widely used in recent blade design is based on parametric curves [148]. In this case, the contour of the blade profile is described by polynomials like Bézier curves or Basis-splines (B-splines). The actual shape of these curves depends on the positions of so-called control points. Keskin [100], as well as Öksüz and Akmandor [127], implemented Bézier curves for their geometric modeling approaches. While Keskin directly used the coordinates of control points as design variables, Öksüz and Akmandor reshaped the Bézier curve of the two-dimensional profile according to aerodynamic parameters like the wedge angle of the LE. Considering six layers per turbine blade the latter optimization problem consisted of 36 geometric design variables. Automatic meshing was employed for the evaluation of design alternatives. To account for three-dimensional blade design, Dutta [53] utilized a Bézier surface to describe the camber-line angle distribution as a function of blade chord and blade height.

Accordingly, there are several approaches that model blade profiles using B-splines. The works of Gräsel et al. [71], Keskin [99], and Otto [127] were all based on the software Parablading, which is a tool for blade design developed by Rolls-Royce. The blade geometry was modeled using B-splines and exported as a CAD model, which has to be meshed for further numerical simulation. In the study carried out by Gräsel et al. [71] 14 design variables were needed to describe one two-dimensional profile.

A similar parametric modeling tool, named Bladegenerator, was also employed by [168]. The software Bladegenerator, which was developed at Deutsches Zentrum für Luft- und Raumfahrt (DLR), manipulates the control points of four B-splines to generate the shape of the LE, TE, suction as well as pressure side. In Buske et al. [32] this approach was combined with an automated meshing procedure to optimize a three-dimensional turbine blade geometry. According to a large number of design variables of 154 involved in the optimization, a surrogate-based optimization procedure was proposed. More recently, Adjei et al. [2] applied B-splines for fan blade optimization. They combined this geometric parameterization with a free-form-deformation, which is a method originating from computer graphics, to morph the simulation mesh.

The last type of structural optimization, which is not yet widely used in the context of turbomachines, refers to the concept of **topology optimization**. In topology optimization with continuous variables, the structure is specified using a material distribution function instead of geometry parameters (see Sec. 2.1.2). Such a topology optimization approach was presented by Boccini et al. [21, 22] finding optimal structural designs of disks and blisks. The density method, typical for structural topology optimizations, was used to achieve a weight reduction and avoid resonances. A more recent contribution of Wang et al. [170] addressed the compressor disk geometry as well. A special interest FE code, T-Axi Disk [72], was utilized to evaluate structural stresses. Turbine blades were considered by Amedei et

al. [5] and Pinelli et al. [135], investigating aerostructural aspects. In general, all of these approaches differ from size and shape optimization, because they leave substantial more freedom to the topology. With regard to additive manufacturing technologies, which allow for more complex geometries, this category of structural optimization may become more important in the future.

State-of-the-art approaches towards a parameter-based description of blades were mainly targeted to aerodynamical optimization and derive the three-dimensional blade geometry from two-dimensional blade profiles. Since multiple cross-sections were needed to construct the whole blade, the number of design variables increased rapidly. This significantly harmed the numerical efficiency of associated optimization processes. To avoid unmanageable computation times the optimization was either carried out with a reduced set of design variables or on a surrogate derived from the full model. To simulate different design alternatives and implement an automated simulation chain remeshing or mesh morphing was applied.

Objectives and Constraints for Design Optimization

As stated at the beginning of this section, the geometry of blades is rarely considered in terms of pure structural optimization. In most cases, aerodynamic functionality is part of the optimization formulation. When structural and aerodynamic aspects are addressed in the same optimization, it is referred to as aerostructural or more general multidisciplinary design optimization (MDO)[118]. In the following, contributions to the state of the art are analyzed with special attention to structural design goals and types of optimization problems.

A pure structural optimization approach was applied by Frischbier [59], who utilized optimization techniques for a redesign process. The redesign was necessary because a conventional blade-disk assemblage of a compressor was planned to be replaced by a blisk. Since the change in mechanical conditions at the blade root led to increased natural frequencies and resonance occurred, the blade design of the blisk had to be adjusted. The objective of the single-objective formulation was thus to minimize the first blade bending frequency. Inequality constraints limited the frequencies corresponding to the second bending and first torsional blade mode to an allowable range. Further, constraints ensured that the blade thickness decreased from root to tip and that the blade mass did not exceed the allowable limit. The maximum mass was previously calculated in a rotor dynamics analysis for the case of blade loss. Frequency constraints were also part of the structural optimization problems discussed by Grandhi [68]. In his work, he reported on the minimization of the mass of blades or disks with frequency constraints. However, he pointed out that in more practical optimization additional constraints are necessary to account for stress distributions and potential mode-switching phenomena.

In 2009, Hecker and Mücke [81] utilized a two-objective structural optimization to improve the geometry of a compressor blade root. The first objective was to minimize the first blade bending frequency, and the second objective was the reduction of von Mises stress in the most loaded part of the root. Later, Hecker et al. [80] extended their idea of an automated design process by optimizing a whole compressor blade of a stationary gas turbine. In the latter case, they evaluated the distances between natural frequencies and harmonic excitation frequencies for the first twelve vibration modes at different operating

speeds. A single-objective function was formulated summing up the frequency values and weighting them with penalty values. The penalty values were determined according to the mode-specific risk of increased vibration amplitudes of blades. Additionally, due to the practical experience of the authors, the minimum allowable first eigenfrequency was constrained. Hecker et al. achieved improved blade designs but pointed out that a good understanding of the physical meaning of penalty values is necessary to obtain appropriate results.

In addition to the vibration frequencies, static and alternating stresses are central counterparts of the structural objective functions. A structural and an aerodynamic objective were pursued by Luo et al. [111], who implemented a two-objective MDO approach for a NASA transonic compressor blade. While the first objective optimized aerodynamic properties in terms of isentropic efficiency, the second objective function resulted from the maximum static von Mises stress under centrifugal loading. Natural blade frequencies of four vibration modes were additionally restricted using inequality constraints. In a later publication [112], the authors compared the optimization results of the MDO with a single-objective aerodynamical approach. They found that purely single-objective aerodynamic optimization led to infeasible blade designs and therefore concluded that a multi-objective formulation was required to make progress in the design procedure.

The consideration of maximum static stresses by means of constraint values was further presented in the works of Brown and Grandhi [27] and Roos et al. [143]. Both contributions combined optimization with uncertainty quantification methods. Instead of static stresses, the probability of failure calculated based on scattering stresses was evaluated. Furthermore, an approach towards the structural optimization of a blisk geometry under uncertainty was published by Song et al. [159]. In their multi-objective formulation, the mean values of maximum stress and maximum blade deformation served as the two optimization objectives. Blade design optimization, which includes criteria from blade dynamics and service life evaluation, was proposed by Martin et al. [116, 115, 117]. The first publication [116] was concerned with the automated evaluation of blade dynamics. In this case, a mode-recognition technique based on the Modal Assurance Criterion (MAC) was tested in order to check, if the first ten vibration modes could be differentiated automatically. In their work, the authors found that the MAC, in general, was suitable to identify modes and only failed, if completely new mode forms compared to the reference blade were triggered. Later [115, 117] the authors used a three-objective formulation tackling aerodynamic and manufacturing design goals. Structural requirements were guaranteed by imposing constraints. Low-Cycle Fatigue (LCF) behavior was ensured by limiting maximum von Mises stresses below the Yield strength, crack initiation was prevented restricting local static von Mises stresses at the TE and LE, and High-Cycle Fatigue (HCF) strength was maintained by limiting alternating von Mises stresses to the endurance limit of the material. Resonance conditions were checked according to constraint equations proposed earlier by Hecker et al. [80] and geometric constraints on the shape of the LE and TE accounted for manufacturing processes. In addition, the aeroelastic behavior was considered using a flutter criterion [7], which is the ratio between blade vibration frequency and flow excitation frequency.

A similar selection of design goals can be found in the doctoral thesis of Otto [128]. The author optimized the aerodynamic loss and flutter of compressor blades in a two-objective optimization task. Frequency criteria related to the relative distances of natural frequencies to excitation frequencies and HCF requirements were imposed as inequality constraints. The amplitude frequency value [83] was chosen as an indicator of HCF strength. Moreover,

structural optimization of a blisk aiming for improved HCF strength was carried out by Simpson et al. [155]. They optimized the fatigue properties according to the Goodman relation. To assess the alternating and mean stress level during operation FE simulations were performed and the most critical resonance point was identified via the Campbell diagram. The pressure loading of the blades was taken from CFD simulations.

In recent optimization tasks dealing with the design of disks, blades, and blisks, aspects from structural mechanics were present either as constraints or as objective functions. In addition to the basic structural properties, such as volume, mass, and size, frequency conditions were formulated very frequently. Objectives aimed at the service life of blades mainly referred to static stresses in the sense of LCF strength. In some works, however, the HCF behavior was also considered by taking alternating vibratory stresses or the amplitude frequency strength into account. When the design tasks involved conflicting goals, which were initially of similar importance, the calculation of Pareto optimal solutions provided additional insights.

Design Variables, Models, Objectives, and Constraints for Repair Optimization

Up to now, the majority of scientific publications focus on the initial design of turbomachinery components during the preliminary design phase and only a few approaches exist, that emphasize repair procedures. When applying optimization methods to repair processes, both similarities and differences to design optimization arise.

With regard to blend repairs, one of the most important contributions to repair optimization can be found in the work of Karger and Bestle [95]. The authors performed shape optimization of a blend repair using a D-shaped cut-out. The dimensions of the blend were specified with five geometric parameters which served as design variables in the optimization. Blisk blades with different blends were meshed in an automated procedure and static stresses caused by centrifugal loading are determined in a FE analysis. Alternating stresses and frequencies were further calculated in modal analysis. The optimization task involved two structural objectives and ten inequality constraints. The first objective was the mass ratio between the nominal and the repaired blade because the cut-out size had to be minimized. The second objective resulted from multiple amplitude frequency strengths. Relative af-values associated with six relevant vibration modes were calculated by dividing the repair-specific values by corresponding nominal values. The final objective value was formed averaging the six relative af-strength. Moreover, the constraint equations were imposed to control the flutter stability (for the first flap and torsion mode), maximum von Mises stress (for nominal and surge conditions), and relative af-values (for six modes shapes). Selected designs corresponding to Pareto optimal solutions showed a variety of potential blend shapes. The subsequent analysis of individual fatigue strength values of modes showed that some values could even be improved relative to the reference design. Finally, the authors, however, pointed out that aerodynamics have to be considered before selecting a final solution out of the presented Pareto optimal set.

Fundamental considerations modeling blend repairs were further described by Day et al. [44]. In their work, they proposed a parametric model of blends using a cylindrical volume such that the resulting cut-out is C-shaped. The blend geometry was defined via three geometric design variables. Vibratory and centrifugal stresses were evaluated for individual designs using different FE meshes for each blend design. HCF was evaluated exemplary for the first bending mode visualizing the stresses using a constant life diagram (Sec. 2.2.5). Although

numerical optimization was not part of the paper, the automated workflow developed can be considered as the first step towards an optimization scheme for blend repairs.

Both works on blend repairs demonstrated that blend repair design benefits from structural optimization schemes. Even though, blend designs are geometric in nature, the parameters greatly differ from geometric parameters associated with the initial blade design. In the past, several researchers [62, 104, 106] analyzed the geometry of worn blades, also including blades with blend repairs in their geometric data set. They used blade profile parameters common for initial blade design processes. It should be noted that the classical parameterization of blade profiles reaches its limits when it comes to blend repairs. For smaller blend shapes, sticking to the two-dimensional profile representation may be reasonable, but becomes inaccurate for larger geometric modifications [96].

Concerning other repair processes such as patching or blade replacement, there have been no notable approaches towards repair design optimization. Conceptual considerations on blisk repairs were presented by Eberlein et al. [55]. They showed blisk blades repaired by patching and discussed the significance of patch designs on vibratory (HCF) strength. In particular, residual stresses in the proximity of the joint between blisk blade and patch were measured. However, the publication contained only normalized values to protect the industrial knowledge.

Work with a focus on numerical analysis of patch repairs was conducted by Schönenborn and Reile [150]. They computed the remaining residual stresses in the repaired blade using uncoupled thermomechanical FEM. The numerical model was prepared manually and no attempt was made to parameterize or automate the simulation, e.g. for optimization or probabilistic analysis. Simulation results were validated with corresponding measurements. The analytic approach and measurements were in good agreement and residual stresses deviated less than 2%. A very similar approach was followed by Azar et al. [11, 12], who analyzed fan blade repairs. In their work, the authors concentrated on patching using an electron beam welding procedure and investigated HCF and LCF strength of repaired blades and proved that the patch repair meets the strict aerospace requirements.

Overall, it can be concluded that optimization applications are state of the art in the design process of new blade designs [129, 59], but rarely used to improve associated repair processes. Concurrently, an increased interest in automated repair processes [25] and repair-specific numerical simulation [8] is evident. The objectives and evaluation metrics for repair optimization partly equal the design goals of initial design optimization. Nevertheless, objectives and constraints regarding deviations to nominal designs (e.g. mass deviations) were also added to formulations of optimization problems.

1.3 Challenges and Research Gaps

The previous sections reveal that automated design and numerical optimization offer several advantages for many technical applications in the field of turbomachinery. However, the initial prerequisite for the use of optimization methods is to establish a suitable link between the engineering optimization task and mathematical optimization algorithms.

The first challenge in the structural optimization of repairs of blisk blades is therefore to create an environment in which all the required routines can be organized with little effort. This scaffold for structured implementation of optimization algorithms and support for

solving optimization problems can only be provided within the scope of an optimization framework. The particular challenge in designing such a framework is to include all required functionalities for engineering optimization while maintaining the necessary flexibility. For this purpose, aspects related to an object-oriented programming scheme, a high-level programming language, parallelization capabilities, implementation of derivative-free optimization algorithms, code complexity, and visualization options for results have to be addressed with no compromise. To the author's knowledge, existing **engineering optimization software** [120, 141] only partly satisfies these requirements.

Moreover, repairs conducted at blades of compressor blisks rarely received attention in scientific publications, because researchers mainly focus on the improved nominal three-dimensional design of blades and their aerodynamic performance [108]. Nevertheless, maintenance processes are of particular interest for compressor blisks, which are already installed and currently operating in jet engines. Since **blisk repairs** are not part of the preliminary design phase, there is a lack of unified or parameterized modeling thereof.

In the case of a **blend repair**, this means that the local change of the blade geometry has to be described in relation to the nominal geometry of the blade. The design variables hence have to capture the geometric features of the blend. When aerodynamic blade shapes are described for the purpose of design optimization, there is some consensus on parameterization. Three-dimensional blades are engineered using cross-sections and parametric curves [92, 1]. Applying this approach to repair designs and using a fully parameterized blade geometry would however result in a high number (>100) of design variables. For the optimization of blending shape, where most of the nominal blade geometry is maintained, many of these variables would not even be required to describe the local modification. Furthermore, when the cross-section of repaired blades significantly deviates from standard two-dimensional profiles, these conventional approaches are no longer applicable. The models developed specifically for cut-out shapes [95, 44] showed promising initial results, but still need to be tested with other blisks and extended to other blend geometries.

Further, in the context of blisks more elaborated repair concepts such as patching have to be analyzed. Considering **patch repairs**, the geometric description of the patched blade is trivial at first, since the patch has a triangular shape and the original blade geometry is reconstructed entirely. Geometrically more challenging at this point is the description of the actual weld path, which is required for welding simulation. The path along with the interface between blade and patch material has to follow the curved surface of the three-dimensional blade.

In terms of engineering optimization of blisk repairs, the **formulations of objectives and constraints** are at first equivalent to the formulations from the process of blade design, since the same structural requirements also apply to repaired blades. Design criteria related to the structural integrity of blades commonly relate to natural frequencies and stresses [59, 115]. In repair design optimization, the challenge is to recheck these criteria and simultaneously keep differences small with respect to the nominal design. The objective functions for repair optimization must consequently be selected in such a way, that individual structural design criteria, that could be particularly endangered by the repair, are rechecked and optimized. For blend repairs, especially the tuning of frequencies has to be considered [152, 14], whereas residual stresses in the joint decrease the HCF strength of patched blades [150]. Furthermore, objectives referring to relative deviations to the nominal reference design and manufacturing effort are of practical interest. Combining these structural requirements on repair designs in one optimization task is difficult and has not been addressed yet. However, multi-objective

approaches applied, e.g. to aerostructural design optimization [2], already showed great potential to find Pareto optimal design alternatives.

Additionally, the **parametric evaluation** and **numerical optimization** of blade repair designs necessitate fully automated simulation and analysis of design alternatives. Recent automated processes [81, 83] were mainly based on remeshing procedures, which had the major drawback that simulation results of different designs had different discretizations and hence could not be compared directly. Moreover, with more extensive structural analysis, like thermomechanical analysis of welding processes, automated simulation without manual adjustment is hard. Since the FE analyses and computations are part of the optimization, special attention has to be paid first to the accuracy of required structural responses and secondly to the run time of involved simulations. To complete the optimization in a reasonable time, the numerical effort has to be reduced to an acceptable extent using feasible model simplifications [169] or surrogate-based optimization [137].

1.4 Objectives

To fill the research gap illustrated in the previous section, this doctoral thesis identifies two key aspects of optimized blisk blade repairs. The first one is related to engineering optimization and the development of an object-oriented optimization framework for multi-objective structural optimization. The second aspect is targeted to two distinct repair processes of blades of blisks. The derived objective of this thesis and the central aspects contributing to this work are shown in Fig. 1-8.

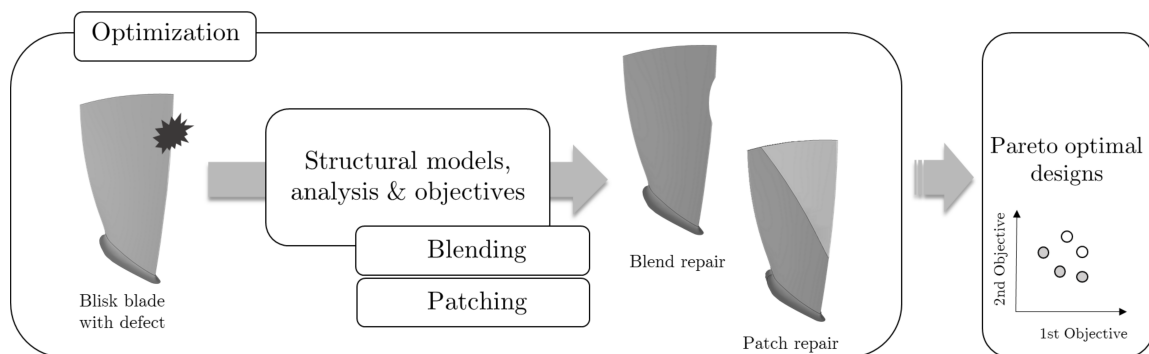


Figure 1-8: Concept developed for multi-objective optimization of blisk blades repaired by blending and patching.

According to the size of their defects, blisk blades can be repaired in different repair procedures, namely blending or patching. However, the best out of multiple design alternatives is initially unknown. The goal of this thesis is to develop a scheme that allows optimization of repairs either by blending or patching by embedding relevant structural models and analysis in a customized optimization framework.

To this end, structural modeling of repair alternatives first requires the specification of design variables that uniquely describe the repair design. Secondly, the structural models corresponding to design alternatives are created automatically on the basis of this repair-specific representation and are prepared for FE analysis. The analyses, like static, modal, or thermomechanical simulations, are used to calculate relevant structural responses. In

the case of blending, the analysis focuses on changes in vibration of blades, because blade frequencies are relevant to the design and are strongly influenced by geometric changes. On the other hand, the structural property that is most affected by patching is local residual stress formation and decreased material properties in the weld. Therefore, FE analysis is used to predict the HCF strength of the welded regions. The pure natural blade frequencies, fatigue strength values (af-values), or normalized values thereof form the basis for objective functions. Imposed constraints ensure, that the repair determined removes the damaged portion completely. Since more than one objective drives the structural design of blade repairs multiple objectives are formulated and multi-objective optimization methods are utilized to reach the outlined goal. The outcome, as illustrated in the right part of Fig. 1-8, are Pareto optimal repair designs, which represent the trade-off between design alternatives according to objectives. The final design decision is supported by the optimization results and can be taken based on the Pareto frontier according to further preferences.

In this sense, the main objectives of this doctoral thesis are

- the design of an engineering optimization framework,
- the parametric modeling of blend repairs,
- the parametric modeling of patch repairs,
- the automated evaluation of vibration and fatigue properties,
- and finding Pareto optimal designs for blisk repairs.

Addressing these objectives, this work is a step towards a more profound understanding of repair design alternatives in the context of blade repairs of compressor blisks.

1.5 Outline

The objectives of this doctoral thesis are reflected by three scientific publications. The first one in Sec. 3 is dedicated to engineering optimization. An engineering optimization framework named EngiO is developed, which subsequently enables the numerical optimization of optimization tasks derived. This first part, therefore, is seen as the basis for all further contributions.

The second and third publications of this thesis are built upon the introduced optimization framework. The papers, which are presented in Sec. 4 and 5, focus on two different repair technologies, respectively. Since the repairs lead to process-specific changes, the parametric description of the repair design, FE modeling, and the evaluation of results in terms of vibration behavior and fatigue strength are of major concern.

Moreover, the theoretical basis of the scientific contributions is described in Sec. 2. Firstly, a brief summary of engineering optimization is provided in Sec. 2.1. Secondly, important aspects in the context of jet engine blades are reviewed in Sec. 2.2. Special emphasis is on the vibration of blisk blades and the failure of blades associated with fatigue.

The scientific publications in Sec. 3, 4 and 5 are further followed by Sec. 6, which considers the application of the developed optimization framework and settings selected for the optimization of blade repairs in more detail. Finally, the thesis is enclosed with a summary of findings and a discussion of further aspects the developed concept can be extended to in the future (Sec. 7).

2 Theoretical Background

2.1 Introduction to Engineering Optimization

In this section, basic definitions related to numerical optimization are provided. In the first part (Sec. 2.1.1), the generalized formulation of optimization problems is introduced. The mathematical problem formulation is followed by the definition of structural optimization in Sec. 2.1.2. An overview of optimization algorithms and their classification is presented in Sec. 2.1.3. Finally, the concept of Pareto dominance, which is a central definition in multi-objective optimization, is presented in Sec. 2.1.4.

2.1.1 Optimization Problem Formulation

The general aim of optimization is to find the best or the best set of solutions to a given problem. The individual optimization task may vary, but all optimization problems can be reduced to a common form. In a mathematical sense, all optimization problems are expressed by

$$\begin{aligned} & \underset{\mathbf{x}}{\text{minimize}} && \mathbf{f}(\mathbf{x}) \\ & \text{subject to} && \mathbf{g}(\mathbf{x}) \leq \mathbf{0} \\ & && \mathbf{h}(\mathbf{x}) = \mathbf{0} \end{aligned} \tag{2.1}$$

for $\mathbf{f} \in \mathbb{R}^m, \mathbf{g} \in \mathbb{R}^p, \mathbf{h} \in \mathbb{R}^q, \mathbf{x} \in \mathbb{R}^n,$

where $\mathbf{f}(\mathbf{x})$ is the objective function, $\mathbf{g}(\mathbf{x})$ the inequality constraint equation, $\mathbf{h}(\mathbf{x})$ the equality constraint equation, \mathbf{x} the design variables. The integers $m, p, q,$ and n denote the dimension of the respective expressions. In the single-objective case ($n = 1$), the vector-valued objective function $\mathbf{f}(\mathbf{x})$ simplifies to a scalar function. The objectives are formulated such that minimal values are favorable and the optimal design corresponds to minimal values of $\mathbf{f}(\mathbf{x})$. In the optimization process, the design variables are varied by the optimization algorithm to determine the best design. The range of possible design variables is given by

$$\mathbf{x}_{\text{lb}} \leq \mathbf{x} \leq \mathbf{x}_{\text{ub}} \tag{2.2}$$

where \mathbf{x}_{lb} and \mathbf{x}_{ub} are the lower and upper bounding vectors, respectively.

Further, equality as well as inequality constraints limit the feasible search space of the optimization. In Eq. (2.1), the notation implies that all solutions leading to negative values of the constraint equation $\mathbf{g}(\mathbf{x})$ are feasible solutions. However, since there is no consensus on the notation of inequality constraints ($\mathbf{g}(\mathbf{x}) \leq \mathbf{0}$ or $\mathbf{g}(\mathbf{x}) \geq \mathbf{0}$) the sign convention of the particular software has to be followed.

The notation in Eq. (2.1) suggests that the objective function $f(\mathbf{x})$ and the constraints $g(\mathbf{x})$ and $h(\mathbf{x})$ are analytical functions. In the field of engineering optimization, these relations are typically not known in an analytic form and thus are determined by numerical simulation. Further, for engineering problems, some design variables might be restricted to take on integer values only. This type of optimization is referred to as mixed integer optimization.

Finally, it should be noted that the formulation of the optimization problem as presented here is initially independent of the optimization approach or optimization algorithm used. In some cases, the formulation of the optimization problem is modified prior to numerical optimization. An example is the transformation of the constrained problem into an unconstrained one by extending the objective function with a penalty value instead [39].

2.1.2 Structural Optimization

A subset of engineering optimization is structural optimization. In structural optimization, the design of a load-carrying mechanical structure or component is optimized concerning its mechanical properties [38]. In the pure sense of this definition, in structural optimization, the objective functions, constraint equations, and design variables (Eq. (2.1)) correspond to structural aspects only.

Objective functions and constraints of structural optimization problems, therefore, refer to the structural performance of the optimized component. Typical measures for structural performance are weight, stiffness, maximal forces, stresses, or displacements of the structure. Design variables of structural optimization tasks define the properties of the component in terms of its geometry or material parameters like Young's Modulus or density. In this context, three levels of structural optimization, namely size, shape, and topology optimization, are differentiated. This classification, which is illustrated in Fig. 2-1, is derived from the physical meaning and choice of design variables.

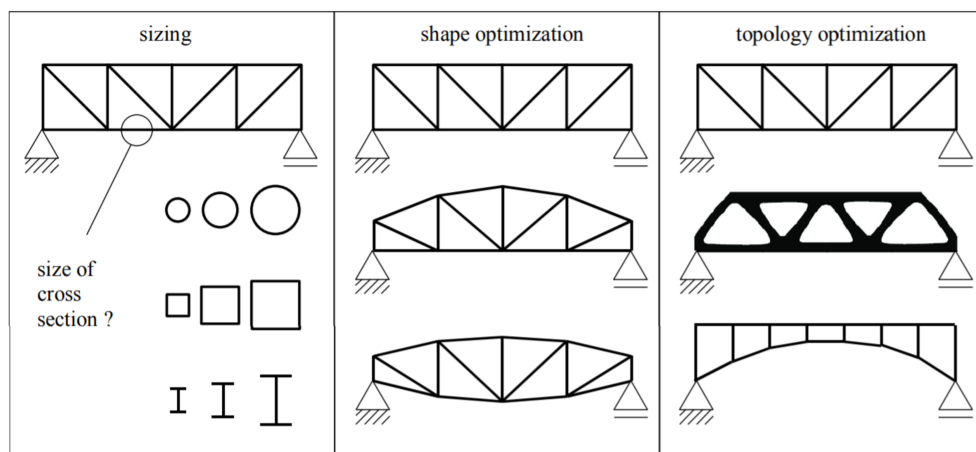


Figure 2-1: Levels of structural optimization. [19]

In size optimization, design variables refer to predefined geometric or material measures e.g. the diameter or density of a bar in a truss. The connectivity between bars remains untouched. In shape optimization, the design variables are chosen such that the shape of the structure can be manipulated. One approach common for shape optimization is to use the

position of control points of parametric curves. Finally, topology optimization is the most general form of structural optimization, where only the initial domain of the structure is predefined. Concerning the truss shown in Fig. 2-1, in a discrete approach (bottom picture), this allows changing the connectivity by completely removing some bars. In a continuous topology method (top picture) the geometric design is described with density-like variables, which can take values between zero and one. This approach allows very different topologies, which also could contain holes or cavities.

2.1.3 Classification of Optimization Algorithms

Due to the diversity of optimization methods, a uniform and unambiguous grouping of all optimization algorithms is not possible [119]. Attributes suitable to classify established optimization algorithms are shown in Fig. 2-2. All attributes listed are initially independent of each other but may interfere at some point.

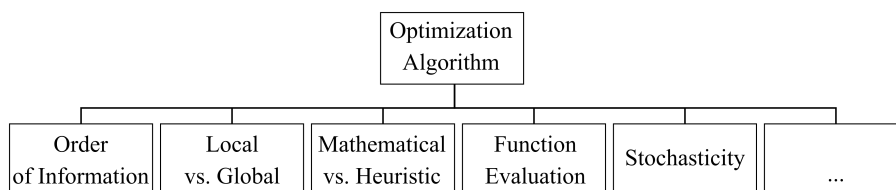


Figure 2-2: Attributes for classification of state-of-the-art optimization methods [119].

The first attribute is related to the order of information processed by the algorithm. The minimal information, which has to be provided to the algorithm are objective and constraint values, so-called zeroth-order information. Algorithms that use purely zeroth-order information are classified as derivative-free algorithms [40]. Algorithms of this class frequently used in simulation-based engineering are e.g. variants of the Genetic Algorithm [66] or Particle Swarm Optimization [98]. Although many of the zeroth-order approaches are related to evolutionary methods also deterministic methods like Pattern Search [89] are part of this class. The performance of state-of-the-art derivative-free algorithms is reviewed by Rios and Sahinidis [141] and Schälte et al. [149]. Gradient-based optimization algorithms use the gradients of objective functions to iterate to the optimum. Since first- or higher-order derivatives provide richer information about the objective function, gradient-based optimization needs less iterations to converge to the optimum than derivative-free optimization [9]. Secondly, algorithms are classified as local or global search approaches. Global optimization algorithms seek to find the best solution in the entire search space, even if there are multiple local optima. Global methods are therefore required when objective functions are multimodal⁴. If multiple local minima exist, local search approaches are often combined with a multi-start approach to explore the whole design space [149].

The third attribute distinguishes between mathematical and heuristic algorithms. This attribute refers to the principles the algorithm logic is based on. Heuristic algorithms are based on stochastic processes and do not rely on pure mathematical principles. Hence, their convergence is not proven for some heuristic approaches [175], but nevertheless have a huge practical relevance. Gradient-based approaches as denoted by the name rely on local

⁴A function with multiple peaks or valleys is a multimodal function, and its landscape is multimodal [176]

gradients of objectives and are classified as mathematical methods. Moreover, optimization algorithms are classified by the way of objective function evaluation. In engineering optimization, the objective function values are mostly computed using a numerical simulation model. If the simulations are too time-consuming to be carried out in each iteration of the optimization, the initial simulation model is approximated by a surrogate model. Surrogates, as discussed by Wang et al. [171], are used instead of direct model evaluation.

The fourth attribute shown in Fig. 2-2 refers to the stochasticity of optimization algorithms. As mentioned previously, heuristic or metaheuristic approaches use random numbers during the iteration and decisions rely on certain probabilities. The stochasticity leads to different spreading of samples for each optimization run and thus to potentially different results. In contrast, pattern search approaches [107] have a deterministic nature.

One additional attribute, which is of particular importance for this thesis, refers to the distinction between single- and multi-objective approaches. If more than one objective has to be optimized at the same time, further approaches to handle contradicting objectives are necessary. A survey about current multi-objective methods is provided by Marler and Arora [114]. They define basic terms and present different methods for the articulation of preferences. Unlike single-objective optimization, in the multi-objective case, there is not a single solution, which solves the problem. Instead, the result is a set of optimal solutions. Algorithms, which are able to find the whole set of solutions, the so-called Pareto optimal set. For example, the Non-dominated Sorting Genetic Algorithm (NSGA-II) [45] is based on its single-objective counterpart, but includes a further sorting and ranking schemes to extract the whole solution set. More detailed information on multi-objective approaches is presented in the following section.

As implied by the illustration in Fig. 2-2 there are several other categories or attributes for the classification of optimization algorithms. Therefore, the presented selection does not claim to be exhaustive. For further attempts to classify optimization algorithms, the reader is referred, for example, to Roy et al. [146].

2.1.4 Concept of Pareto Dominance

Multi-objective optimization refers to the optimization of problems where the optimization goal is not limited to one single objective. As indicated by the vector-valued notation $\mathbf{f} \in \mathbb{R}^m$ in Eq. (2.1), the objective function includes m different objectives. These kinds of objective functions are frequently used in engineering design, if there is a conflict between two or more optimization objectives and not all objectives can be achieved equally. In contrast to the single-objective case, the result of a multi-objective optimization hence presents a trade-off between different solutions.

The selection of optimal candidates with respect to contradicting objectives is based on the definition of Pareto dominance [132] and plays a central role in multi-objective approaches. Pareto dominance is a concept to compare solutions according to their relative position to other solutions in objective value space. According to Marler et al. [114] Pareto optimality, which is also referred to as Pareto dominance, it is defined as follows:

Definition. *Pareto Optimality:* A point, $\hat{\mathbf{x}} \in X$, is non-dominated if there does not exist another point, $\mathbf{x} \in X$, such that $\mathbf{f}(\mathbf{x}) \leq \mathbf{f}(\hat{\mathbf{x}})$, and $f_i(\mathbf{x}) < f_i(\hat{\mathbf{x}})$ for at least one function.

This dependency between design points $\mathbf{x} \in X$ is graphically shown in Fig. 2-3. For visualization purposes, six samples corresponding to a two-objective optimization are shown in the two-dimensional objective value space.

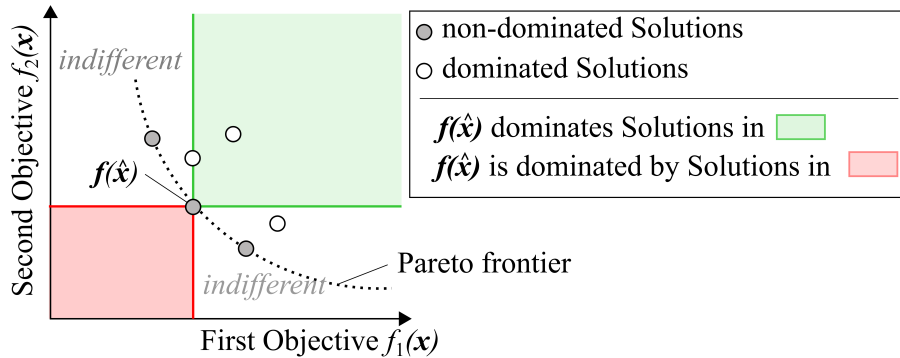


Figure 2-3: Two-dimensional visualization of Pareto dominance.

The three points in Fig 2-3, which are highlighted in gray, correspond to non-dominated solutions, while the other three points (white) are dominated solutions. The definition of dominance is further visualized for the non-dominated candidate \hat{x} . This solution \hat{x} dominates all solutions located in the area highlighted in green. The two samples (gray and white) in the lower right area are in contrast indifferent to \hat{x} . A further candidate (white), which is dominated by \hat{x} , has the same first objective value as \hat{x} and is therefore located at the boundary to the indifferent area. Since \hat{x} improves the second objective value compared to this solution, the candidate on the boundary is still dominated by \hat{x} .

As also shown in Fig. 2-3, all non-dominated solutions together form some kind of front or frontier. The set of non-dominated solutions is therefore referred to as the Pareto frontier. The solutions being non-dominated are also called Pareto optimal set.

The shape of the Pareto frontier can have a lot of different appearances and is specific for each optimization task. In some case, like it is shown in Fig. 2-3, the Pareto frontier has a continuous course. However, in the optimization of real engineering problems, it is also common that there are several disconnected parts. These result from concavities of solution sets or separated feasible regions in the objective value space. An example of a Pareto frontier with four parts is the solution related to the Kursawe test problem [103].

Since the Pareto frontier represents a set of solutions, the weighting of design alternatives and the final design decision could be taken subsequent to the optimization procedure without restarting the optimization. The slope of the frontier in the objective value space additionally visualizes the dependencies and correlations of objectives involved. This is a significant advantage compared to single-objective optimization formulation, where the weighting of objectives is specified prior to optimization.

2.2 Fundamentals of Blade Mechanics

In the following, the design of rotating turbomachinery blades is reviewed with emphasis on the blade mechanics. The first sections (Sec. 2.2.1 and 2.2.2) are concerned with the flight operation of jet engines and the resulting load spectrum. Blade and blisk vibrations are considered in Sec. 2.2.3. The design criteria and graphical concepts related to resonance detection are presented in Sec. 2.2.4. A summary of established fatigue assessment is part of Sec. 2.2.5.

2.2.1 Operating Conditions of Jet Engines

The operating conditions of turbomachinery blades strongly depend on the type of engine considered. In the following, the focus is on the operating conditions of jet engines, because compressor blisks are only installed in jet engines and not in stationary gas turbines. Nevertheless, the fundamental aspects can be found similar in other turbomachines like stationary gas turbines or steam turbines as well.

First, the operation of jet engines is clearly linked to the flight mission of airplanes. The particular flight missions may differ in type of airplanes (e.g. military, civil airplane), application (e.g. long-haul, short-haul), and other environmental conditions. However, all flight missions comprise the same flight phases. In Fig. 2-4, relevant key data of one flight mission are visualized for this purpose. The diagram (Fig. 2-4) shows the rotational speed of the turboshaft (blue) and the turbine inlet temperature (orange) during a short-haul route of a civil airplane. The qualitative altitude profile of the flight mission is emphasized in the diagram with a black dotted line.

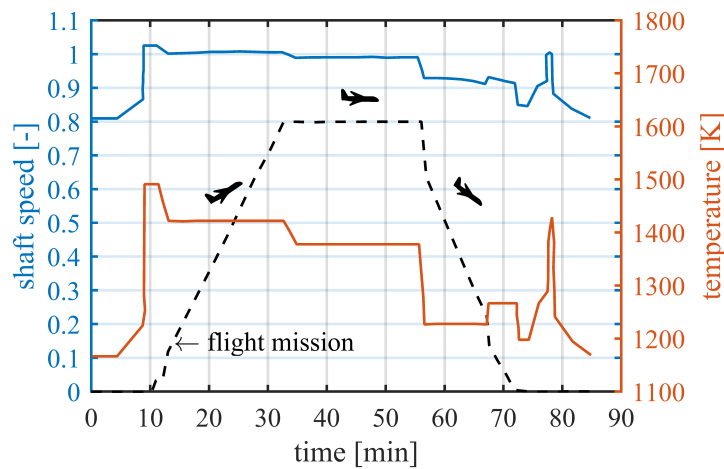


Figure 2-4: Relative shaft speed and high-pressure turbine inlet temperature during a short-haul flight mission according to Hanumanthan et al. [76].

One regular flight mission begins with the start-up of the jet engines about 10 min before the flight. In this time period, the shaft rotates at about 80 % of the nominal speed and the turbine inlet temperature⁵ is increased. The engine and its components are warmed up until a stabilized temperature distribution is reached in order that the spacing between the assembled components meets the required standards. The airplane is taxiing-out and awaits the final take-off.

During take-off, the highest shaft speeds and temperatures are temporarily reached. The take-off operation is followed by a climb phase in which the airplane further increases altitude up to its cruising altitude. During the climb phase, which makes about one-third of the actual short-haul flight, the engine operates at a constant speed at nominal operating point. Due to the stationary operation of the engine, the temperature is approximately constant. The second actual flight phase, which is typically the longest time interval, is the cruise phase. The shaft speed is still about 100 %, but the temperature level is slightly lower compared to climb, because the maximum travel altitude of the airplane is reached.

After cruise, the flight is terminated by descent, approach and landing phases in which the altitude gradually decreases up to ground level. At ground level, the use of reverse thrust enables the deceleration of the airplane. The effect of the transient operations are also visible in the graphs of shaft speed and temperature. At the end of the flight mission, the airplane taxis to a parking position and finally the jet engines are cooled and shut down.

2.2.2 Loading of Rotating Blades

The loads acting on the jet engine components, such as blisk blades, directly result from the flight mission presented in the previous section. Blades and blade repairs have to be designed to withstand these operating loads. The corresponding loads thus have to be addressed in the lifetime assessment (see Sec 2.2.5). In terms of rotating blades, the significant loads mainly fall into the three categories of

- rotational forces,
- fluid forces of the working fluid,
- and thermal loading [165].

The rotation of the shaft and blisk lead to centrifugal forces in the blades, which increase quadratically with the rotational speed. As the rotational speed remains almost constant during the climb, cruise, and descent (Fig. 2-4), the blade loading has a steady nature in the related flight intervals.

The second category refers to fluid forces caused by the combustion airflow or combustion gas flow, respectively. The forces acting on the blades correspond to the flow field and have a static and fluctuating component. The pressure difference between the pressure and suction side implies a steady bending moment on the blade. Variations and disturbances of the flow passing the blades, on the other hand, lead to alternating loading on the blade.

⁵The turbine inlet temperature is the temperature of exhaust gases measured at the exit of combustion chamber before entering the high-pressure turbine of the engine. Although it is not significant for the temperature in the compressor, it is considered here, because it is known as a key performance indicator for jet engines.

Finally, the last category concerns thermal effects in the jet engine. This load case is primarily associated with blades operating at the hot end of the engine. Hot combustion gases in a transient operation (see turbine inlet temperature in Fig. 2-4) lead to thermal gradients e.g. in turbine blades. Especially in combination with centrifugal forces, temperature-dependent creep processes can be of importance for the life of turbine blades. For components upstream to the combustion chamber, such as blisk blades, the thermal effects are not as significant as in the high-pressure turbine.

In addition to the three categories mentioned, loads on the blades can be caused, for example, by deposits or by chemical interactions with the blade material. However, these load cases are not considered in this work, as they describe physical phenomena that are not directly associated with blade mechanics.

2.2.3 Blade and Blisk Modes

The vibration modes of one single compressor blade or of one blisk sector have a similar appearance as the eigenmodes known for beams or rectangular plates. For illustration, three typical vibration modes of blades are exemplarily shown in Fig. 2-5. The depicted mode shapes are computed for one sector of a blisk, where the two cyclic faces to neighboring sectors are clamped.

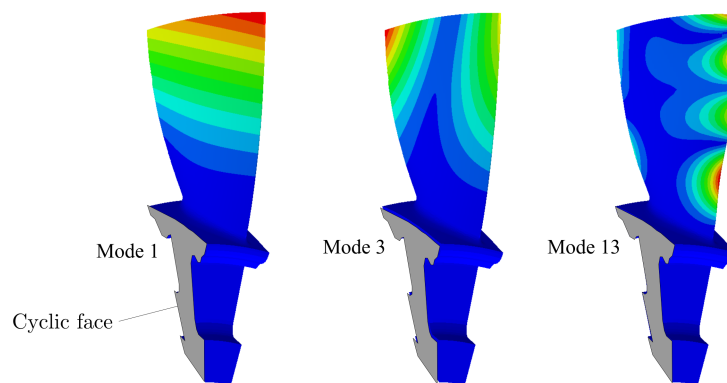


Figure 2-5: Bending (mode 1), torsional (mode 3) and higher mode shape of a clamped blisk blade.

As depicted in Fig. 2-5, the first mode shape is commonly a bending mode, while the third mode corresponds to a torsional movement. In general, blade modes can be classified as bending modes, torsional modes, or a combination thereof. Since the higher mode shapes are more complex, a distinct classification is not possible. Each of the mode shapes corresponds to a certain natural frequency, which is referred to as a blade-alone frequency. The rest of the cyclic structure is not considered.

However, due to the cyclic symmetry of blade assemblies and blisks, they exhibit special modal dynamics [126]. When considering the whole cyclic structure, different vibration patterns so-called cyclic symmetry modes (*CSM*) occur. Three *CSMs* are shown in Fig. 2-6.

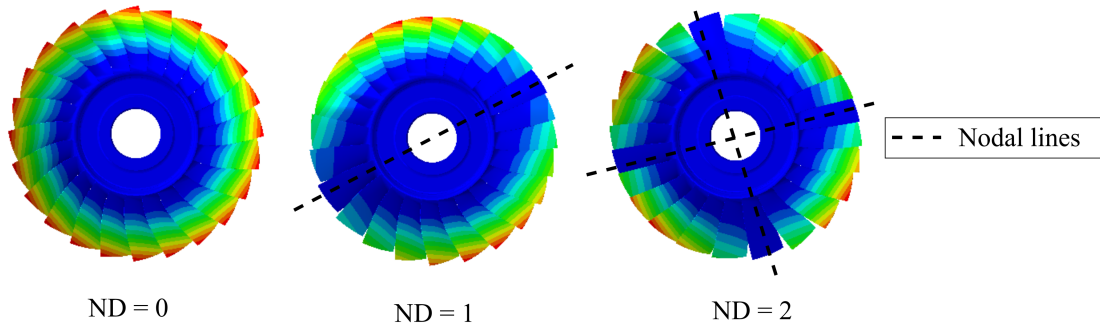


Figure 2-6: Cyclic symmetry modes of a blisk for different nodal diameters (ND).

All blades depicted vibrate in the first bending mode, but the phase angles between the blades are different for each pattern. This phase shift between the blades leads to geometric areas with low vibration amplitude, named nodal lines. The occurrence of these nodal lines is characteristic of the *CSM* and the number of nodal lines is referred to with the term nodal diameter (ND). In the first picture of Fig. 2-5 the blades all move synchronously. No nodal line exists and the ND is zero. Due to the association of the blade movement with a closing and opening umbrella, this mode is also named umbrella mode. The maximum number cyclic symmetry modes CSM_{max} is calculated as follows

$$\begin{aligned}
 CSM_{max} &= \frac{N}{2} + 1 && \text{for even } N \\
 \text{and } CSM_{max} &= \frac{N+1}{2} && \text{for odd } N,
 \end{aligned} \tag{2.3}$$

where N refers to the number of blades. If, for example, a blisk comprises four blades ($N = 4$) the maximum number of *CSM* calculates to three ($CSM_{max} = 3$). This is reasonable, because the blades can either vibrate in umbrella mode (ND=0) or in *CSMs* with one or two nodal lines.

2.2.4 Vibrations and Resonance Conditions

During the operation of the jet engine, the blades tend to vibrate at high frequencies. In general, there can be multiple reasons for the blade vibrations. Major excitation sources, which may cause the vibration of the jet engine blades, are the gas flow around the blades, mechanical vibrations of other engine parts, imbalances of rotating structures, combustion vibrations, and tooth forces from gears [7, 42, 125, 144]. These excitations become critical to jet engine operation when they have the potential to cause resonant vibrations e.g. of blisk blades. Two conditions have to be met to cause resonance with a cyclic symmetric structure [156]:

1. The frequency of the exciting forces coincides with the natural frequency of the cyclic symmetric structure.

2. The profile⁶ of the exciting force equals the shape of the cyclic symmetry mode corresponding to the natural frequency.

Only, if both conditions are satisfied the structure enters resonance. According to these two criteria, there are two common evaluation concepts.

Campbell Diagram

The first concept for the evaluation of matching frequencies was developed by Wilfried Campbell [36]. The so-called Campbell diagram, which is schematically shown in Fig. 2-7, presents the natural frequencies of the blade and possible excitation frequencies over the rotational speed of the operating range of the engine.

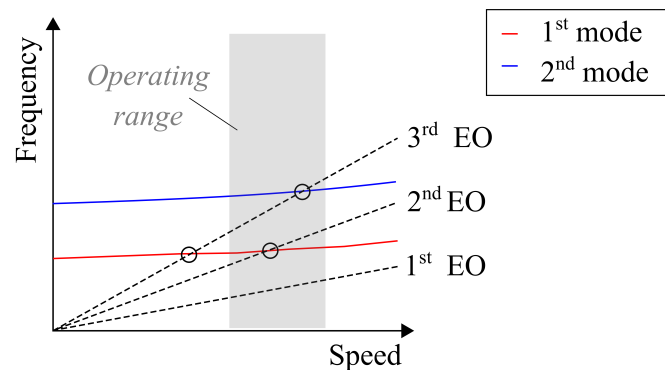


Figure 2-7: Schematic Campbell diagram showing the frequencies of the first two blade modes and the first three engine order (EO) lines).

The red and blue curves in the diagram correspond to the natural frequencies of the first and second modes. As indicated by the nonlinear slope, the natural frequencies depend on the rotational speed of the shaft. In most cases, stiffening effects act on the blades, so that the natural frequency during operation is higher than at standstill. In rare cases, e.g., with torsional modes, a frequency reduction can also be observed. The dashed lines are engine order (EO) lines representing harmonic excitations at operating speed. They show multiples of the rotating frequency of the engine.

The crossings between EO lines and natural frequency lines denote possible resonances. Since the engine should not operate at resonance conditions, this intersection of lines has to be avoided in the main operating range and especially for nominal shaft speed. In the case depicted, two crossings are located within the operating range of the engine. To judge, whether the excitation due to the particular harmonic leads to critical states, the excitation force related to the EO has to be considered. Not all EO are equally important and so they lead to far different blade vibration amplitudes. In this context, special attention has to be paid to a certain EO, which is referred to as nozzle passing frequency. The nozzle passing excitation results from disturbances in the fluid flow. Upstream obstacles, i.e. stator

⁶The term refers to the harmonic pressure distribution resulting from the fluid flow. It can be thought of as a circumferential wave.

blades, lead to fluctuation in the fluid flow. Each time the rotating blade passes the spacing between upstream stator blades (vanes) the pressure changes and causes blade vibration. The frequency of this excitation results from the rotational frequency multiplied by the number of spacing between the upstream vanes. The disturbed fluid flow commonly results in relatively high excitation forces and thus high magnification of blade vibrations.

Interference Diagram

The second condition for resonances refers to the shape of the vibration mode and profile of the excitation. To check, if these two shapes match, a diagram as shown in Fig. 2-8 is used.

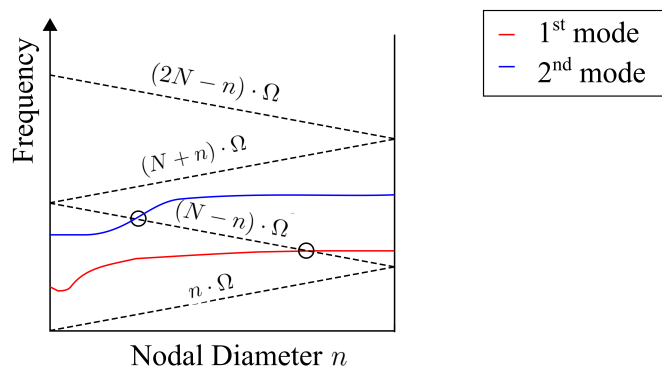


Figure 2-8: Schematic SAFE diagram showing the frequencies of the first two blade modes and the excitation line.

Similar to the Campbell diagram, the y-axis refers to the natural frequency. However, the frequencies are shown for a constant operating speed but different NDs. The courses of the blue and red lines indicate the influence of the cyclic symmetry mode on the natural frequencies. Further, the black dashed line is the (zig-zag) excitation line associated with the second criterion for resonance (see page 29).

The condition can also be expressed as

$$\omega_n = (kN \mp n) \cdot \Omega \text{ with } k = 0, 1, 2, \dots, \quad (2.4)$$

where ω_n is the natural frequency, k the counter, n the number of NDs and Ω the exciting frequency [126]. As previously in the Campbell diagram, in Fig. 2-8 the intersections of both lines denote possible resonances. In the presented example, two resonance points are identified.

This visualization of natural frequencies and excitation lines in Fig. 2-8 is referred to as Interference diagram, SAFE (Singh's Advanced Frequency Evaluation) [157], or ZZENF (Zig Zag Excitation line in Nodal diameter vs. Frequency) [173] diagram. Together with the Campbell diagram, the SAFE diagram is widely used during the design process of blades to prevent the occurrence of resonances in the final design.

2.2.5 Blade Fatigue

As with any component, jet engine blades and blisks have a finite life expectancy. The failure of turbomachinery blades is strongly influenced by the aforementioned operating conditions (Sec. 2.2.1) and loads (Sec. 2.2.2) and can be caused by various failure mechanisms. In particular, failure due to fatigue, creep, corrosion, foreign object damage, and oxidation are the most important mechanisms in a jet engine [179].

Since fatigue is one of the major damage mechanisms [42], the fundamentals of blade failure due to fatigue are considered in the following. First of all, the damage mechanism known as fatigue denotes the progressive deterioration of material that occurs under cyclic loading [125]. In this context, commonly two ranges of the fatigue regime are distinguished. The first, known as Low-Cycle Fatigue (LCF), corresponds to fatigue due to repetitive loads with relatively high amplitude. The cyclic loads result in stresses that exceed the yield point of the material, so that plastic deformation occurs. In contrast, fatigue due to a lower load level is classified as High-Cycle Fatigue (HCF). No appreciable plastic deformation occurs in the structures and the load cycles (the structure can withstand) increase compared to the LCF case. The distinction between LCF and HCF is primarily based on the number of load cycles to failure. The transition between the two regimes is usually considered to be around 10^4 to 10^5 cycles [139].

In the context of blades, operating in a jet engine, the two fatigue classes are directly associated with the load conditions during a flight mission (Sec. 2.2.1). A generalized load spectrum [179], which simplifies one ground-air-ground cycle, is shown in Fig. 2-9.

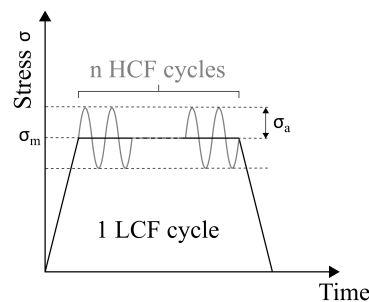


Figure 2-9: Simplified load spectrum according to one flight mission.

During each flight mission, those blade stresses, which are mainly caused by the shaft rotation, increase rapidly, stay at a certain stress level σ_m and decrease subsequently. Since the induced stresses have a high amplitude but low frequency, this load cycle is also referred to as the LCF cycle.

In addition to this start-stop operation, the blade is subjected to in-flight vibrations. In Fig. 2-9, these vibratory stresses are indicated by the gray curve.⁷ The large amplitude of the LCF cycle is superimposed with small stress amplitude σ_a but high-frequency vibrations. These n load cycles associated with blade vibrations, therefore, contribute to the HCF failure of blades.

⁷As Fig. 2-9 shows a schematic diagram, the proportion between different stress levels and cycles does not correspond to real conditions.

In the design process, the failure of blades due to fatigue is estimated by well-established evaluation concepts. These concepts are based on fatigue testing data, which is determined in fatigue experiments under cyclic loading. The relation between the number of cycles to failure and the applied stress amplitude is reported in S-N curves [139]. Together with the measured or predicted stresses in the structure the service life is assessed. When the load spectrum is available, often a damage accumulation theory is used to calculate the lifetime to failure [140, 37].

The relation reported in S-N curves is further influenced by the mean stress level of the load cycles. The effect of mean stresses, is especially important for the evaluation of HCF considering the in-flight vibrations. The degradation of fatigue strength due to increased mean stresses is shown in so-called constant life curves. The decrease in allowable stress amplitudes at higher mean stresses using a constant life curve is schematically illustrated in Fig. 2-10.

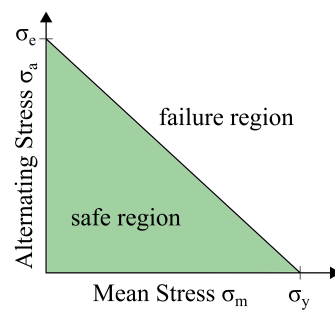


Figure 2-10: Schematic constant life diagram.

In Fig. 2-10, according to the mean stress σ_m and alternating stress σ_a two regions are distinguished. If the alternating and mean stresses in the structure lead to a point within the safe region (highlighted in green), the structure withstands the required cycles. Otherwise, if the combination of stresses refers to a state in the failure region, the structure is likely to break before hitting the required cycles. There are various ways to draw the boundary between the safe and failure region [139]. In particular, in Fig. 2-10, a linear relation using the yield strength σ_y and endurance limit σ_e is illustrated.

In turbomachinery design, based on the representation in the diagram of Fig. 2-10, the strength of the blade is often measured using the definition of amplitude frequency strength [83]. The amplitude frequency strength is defined as

$$\text{af} = \frac{\sigma_e}{\sigma_a} \left(1 - \frac{\sigma_m}{\sigma_y} \right), \quad (2.5)$$

where σ_e is the endurance limit of the material, σ_a the stress amplitude, σ_m the mean stress and σ_y the yield strength. The af-strength is a standardized measure to qualitatively compare the strength of blades. It basically states the ratio between allowable loading and actual loading. Large values of the amplitude frequency strength therefore indicate long lifetimes.

3 Engineering Optimization Framework

3.1 Research Context

As described in Sec. 2.1, there is a variety of optimization software used in the scientific and technical community. Each of the codes developed is more or less targeted to a specific application. Thus, the design of the optimization framework EngiO, which is presented in paper A, is precisely oriented to the application of optimization in the field of blade repairs and to the requirements resulting from engineering research. In this sense, five aspects have driven the development of EngiO and make the framework unique compared to other established optimization software.

The first aspect refers to the basic architecture of the framework, which is the key to the modularity and functionality of all further implementations. The core of EngiO is built according to an object-oriented programming scheme, which has also provided the basis for other recent developments [52, 134]. Furthermore, the structure of EngiO leads to a separation of algorithm and optimization problem. The strict separation of the optimization algorithm and the optimization problems is the central idea of the PISA interface [20], where the link between both is established by exchanging text files. The architecture of EngiO is also built on this separation premise, but in contrast, realizes the separation via its class definitions.

The second aspect relates to the programming language. EngiO is programmed in Matlab/Octave syntax, which has great benefits in terms of code readability. Thus, EngiO achieves simple handling of optimization problems due to the high-level language. This distinguishes EngiO from historically grown projects like DAKOTA [56], where the main part is programmed in C. At the same time, the choice of programming language makes EngiO competitive with respect to the ease of use offered by commercial Matlab optimization toolboxes [121, 120].

The third aspect refers to the optimization algorithms included in EngiO and the implementation of further algorithms. Due to its application in engineering, the interface is designed for gradient-free global optimization. The majority of algorithms included in EngiO are hence metaheuristics and have a similar application range as the frameworks reviewed by Parejo et al. [131]. Moreover, implementations of algorithms can be modified and tested using EngiO. This transparency contrasts EngiO from commercial software [54], where the implementation is often not accessible for the user.

The fourth aspect, which is considered in the design of EngiO, is code complexity. Since the code is also intended to be used by students, a clear structure of the code is essential. The centralization of routines in the base class increases the clarity and significantly reduces the number of lines of code implemented. This idea of a comprehensible structure and a reduced code can also be found in other approaches [78, 24].

The last aspect deals with the visualization of optimization results. By the choice of the programming language, many visualization possibilities are available in EngiO. Several functions, which are included in EngiO, enable to display the results in objective and design variable space. From the literature known behaviors of algorithms and characteristics of optimization problems [67, 93] become visible to the user.

Finally, it should be noted that EngiO is not only the basis for the results published in papers B and C of this thesis. It is also used in other recent publications written by the author of this thesis [15, 16] and other researchers [74, 31, 87, 166, 73].

3.2 Methods

The focus of paper A is on the development of an architecture for engineering optimization. The object-oriented approach presented here is in the first place a design concept to organize optimization problems and optimization algorithms in a concise fashion. The basic functionality is provided by an optimization class, which contains the main optimization loop and abstract class definitions for algorithm implementations. The interface definition is further designed such that it is suitable to implement zeroth-order optimization algorithms. To enable constrained optimization a penalty handling concept is implemented in an object-oriented manner as well.

The optimization problems addressed in paper A are used exclusively for demonstration purposes of the framework. The methods behind the problem formulations are therefore not the main innovation of this paper. All simulations and methods are the result of extensive research activities at the Institute of Structural Analysis and are accordingly the core of other scientific publications.

3.3 Results and Outlook

Since the key aspect of paper A lies in the particular design of the framework and the parent class definition, the functionality and flexibility provided by the code is the most important outcome. Thus, with the resulting framework, all the requirements imposed on the optimization environment for optimization in papers B and C are met. A special feature of this work is the open-source code made publicly accessible in the sense of the open science idea. All versions of the code are hence available in the ISD github repository (<https://github.com/isd-luh/EngiO>).

Since the benefits and advantages of the developed code only become apparent when the framework is applied to optimization problems several exemplary computations are presented. Utilizing three engineering optimization tasks the applicability of the framework is demonstrated. All three examples are taken from wind energy research but greatly differ in optimization goals and type of optimization problem.

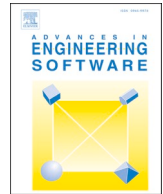
As the initial version of EngiO only includes a limited number of state-of-the-art optimization algorithms, more algorithms should be implemented in the future to extend the range of optimization possibilities. In doing so, the interface provided by the framework can be exploited.

3.4 Paper A: EngiO – Object-Oriented Framework for Engineering Optimization

The following paper is published in *Advances in Engineering Software* Volume 153, March 2021, pages 102959 (<https://doi.org/10.1016/j.advengsoft.2020.102959>).

Author Contribution

The main work was done by the author of this thesis. Marlene Bruns provided the software for the engineering problem on damage localization presented in Sec. 5.1 of paper A. Andreas Ehrmann gave technical and editorial suggestions for the improvement of the entire publication. Ayan Haldar provided the simulation model of bistable laminates, which is optimized in Sec. 5.3 of paper A. Jan Häfele supported the development of the framework in the initial phase and provided the example on jacket substructure optimization in Sec. 5.2 of paper A. Benedikt Hofmeister contributed to the implementation of the framework and provided the Global Pattern Search algorithm. Clemens Hübler contributed with advisory work and technical suggestions during the writing and review process of paper A. Raimund Rolfes gave technical and editorial suggestions for the improvement of the entire publication and performed the final proofreading.



Research paper

EngiO – Object-oriented framework for engineering optimization

Ricarda Berger^{*,a}, Marlene Bruns^a, Andreas Ehrmann^a, Ayan Haldar^a, Jan Häfele^a,
Benedikt Hofmeister^a, Clemens Hübler^a, Raimund Rolfes^a

Leibniz Universität Hannover, ForWind, Institute of Structural Analysis, Appelstraße 9A, Hannover 30167, Germany

ARTICLE INFO

Keywords:

Optimization framework
Engineering optimization
Global derivative-free optimization

ABSTRACT

This paper presents an object-oriented optimization framework for engineering optimization using the Matlab programming syntax. The novelty of the developed framework lies in its approach to remove redundancies by providing an interface for central routines of the optimization processes. Object-oriented programming is used to implement an abstract optimizer class, which controls the optimization process and provides unified interfaces for optimization. The software architecture reduces code complexity and allows concise implementation of derivative-free algorithms and optimization tasks. Therefore, it is ideal for students and researchers to improve and develop algorithms or to solve optimization problems. The proposed framework features parallel evaluation of objective functions and handles global optimization including single-objective, multi-objective and constrained problems. In this paper, the versatility of the framework is demonstrated by using analytic test problems as well as practical engineering problems.

1. Introduction

Through mathematical models and numerical simulation, researchers and engineers are able to predict the behavior of physical systems. Although numerical simulations provide a good prediction of properties of the physical systems, the best design of many alternatives is initially unknown. Aiming to find designs with improved properties, they ultimately enter the field of engineering optimization. It is intuitive to formulate an optimization goal – the objective – since it results from technical requirements or costs. When searching for the optimal solution, one is then confronted with a countless number of optimization methods. However, it is proven by the no free lunch theorem [1] that there is no universal optimization algorithm performing best for all optimization problems. Hence, as newcomers in the field of optimization, scientists and engineers make use of optimization frameworks to find the optimal solution of their specific problem.

To date, a multitude of optimization libraries and frameworks has been published to facilitate the optimization of practical engineering problems. Each of the frameworks targets different communities and a wide variety of programming languages are used [2,3]. One of the first notable contributions in engineering design optimization was DAKOTA [4], the Design Analysis Kit for OpTimizAtion. The framework is programmed in C++ and follows an object-oriented design approach providing an iterator and an optimizer class. Optimization capabilities

are included by linking third-party libraries of global derivative-free optimizers like NCSUOpt, SCOLIB and JEGA. Another C++ framework for academic and industrial application is ParadisEO-MO [5], which presents a unified interface exclusively targeted at single-objective metaheuristic approaches. The platform PISA [6] particularly addresses the strict separation of the optimization problem and the algorithm. This concept enables maximum flexibility and independence of both parts. The text-based interface links the C-based optimizer, denoted as selector, with the problem-specific part, called variator. Tazowski et al. [7] developed a programming concept for finite element topology optimization which makes use of functors. Implementing this programming concept creates advantages in code simplicity and maintenance. Frameworks programmed in low-level languages like C/C++ may provide a broad spectrum of optimization capabilities, but are hard to cope with for computer science beginners.

More prevalent are tools that are available in higher scripting languages like Python. A very prominent engineering optimization framework programmed in Python is OpenMDAO [8,9], which was developed by NASA. OpenMDAO implements several local gradient-based optimizers as well as a Genetic Algorithm. The framework concept mainly addresses multidisciplinary optimization tasks, splitting the analysis into so-called components for each discipline. Several high-dimensional aerodynamics and spacecraft problems, like satellite or wing design optimization, were solved using this framework. One optimization tool

* Corresponding author

E-mail address: r.berger@isd.uni-hannover.de (R. Berger).

originating from the same research field is PyGMO [10], which was part of an ESA project. It features the strong parallelization of algorithms to speed up global single- and multi-objective optimization of computationally costly models. It implements several metaheuristic approaches like Differential Evolution or Particle Swarm Optimization. The package pyOpt [11], which follows an object-oriented programming scheme, further demonstrates that optimization frameworks benefit significantly from advanced software design. It comes with a strict separation of problem and optimizer and therewith simplifies the handling for the developer as well as for the practical user. Just like the Python library SciPy [12], the optimizers of pyOpt are also used by OpenMDAO. Another approach is Pyomo [13], a freely available optimization package, that allows the formulation of the optimization problem based on a syntax common for Algebraic Modeling Languages. DEAP [14], an optimization tool for evolutionary optimization, further improves the handling of the optimization process by a lean implementation of its core with less than 2000 lines of Python code.

In addition to the Python frameworks, similar approaches can also be found in Java. The Java-based framework jMetal [15] is designed to solve multi-objective optimization problems using metaheuristics. In jMetal, no parallelization effort is made, which is a major drawback in terms of computing time. Another Java tool is Opt4J [16], which aims at the decomposition of the optimization problem into subtasks.

Due to its ease of use, a large community prefers the programming language Matlab. Matlab itself already contains two optimization toolboxes [17,18], which provide multiple functionalities for optimization purposes. The optimization under uncertainties was addressed by the Matlab tool UQLab [19], which is available under academic as well as commercial license. UQLab is used to study uncertainties in various engineering disciplines.

Frameworks are also developed in the area of topology optimization, which is of particular interest to aerospace and automotive applications. The structural design of a body-in-white model is considered by Zuo [20] and Qin et al. [21], where the latter has implemented his ideas in a Matlab toolbox.

Moreover, software environments like COSSAN [22] or YALMIP [23] facilitate virtual prototyping in engineering design. The Matlab framework TOMLAB [24] was initially developed for research and teaching purposes and is currently available under commercial license. It addresses usability aspects by incorporating a graphical user interface. A further Matlab code is GODLIKE [25], which includes four basic implementations of evolutionary algorithms. Multi- and single-objective problems are solved running a combination of metaheuristic optimizers. Therewith, the robustness of the optimization is improved.

As discussed, various optimization frameworks have been introduced for solving engineering optimization problems. However, for specific applications, it can be beneficial to implement a specialized framework. In teaching and as an introduction to the field of optimization, it is particularly important that the framework is easy to understand. By introducing EngiO – an Engineering Optimization framework – we aim to lower the barrier for practical engineering optimization by a high level of usability.

As Matlab is widely used in academia as well as in engineering, all functions of EngiO are implemented in Matlab. In the spirit of the open source idea and to reach a large community, EngiO is licensed under GNU General Public License version 3 (GPLv3) and also compatible with GNU Octave. The use of GNU Octave and Matlab increases usability and enables multiplatform compatibility. The object-oriented architecture of the framework allows the user to quickly customize EngiO to his or her own individual needs and focus on the optimization rather than on the framework. External research codes (e.g. FAST [26]) or commercial solvers (e.g. ABAQUS [27]) can be easily integrated in the optimization process. Single- and multi-objective optimization including constraints are supported. EngiO is thus suitable for research as well as for taking first steps into optimization.

Students, researchers and engineers predominantly interested in the

development of user-defined algorithms are further supported by a unified interface that follows the premise of strict separation between algorithm and problem. Like other frameworks, EngiO comes with multiple analytic test functions and includes implementations of local and global derivative-free state-of-the-art optimizers. The comparison of different implementations of algorithms is thus possible. In the context of numerically costly simulations, users of EngiO benefit from parallelization of objective function evaluations and restart capabilities. Finally, EngiO strikes a balance between ease of use and numerical efficient optimization of engineering problems.

In the first part of the paper, the unique architecture and related features of EngiO are presented. The basic features are demonstrated using well-established test functions and state-of-the-art algorithms. Subsequently, the framework is applied to three engineering optimization problems related to current research topics.

2. Engineering optimization framework

The framework is specifically intended for teaching purposes and tailored to engineering optimization. To this end, trade-off decisions in the design process are resolved favoring readability as well as usability. The software design of the framework and the associated advantages are presented in the following sections.

2.1. Architecture of the optimization interface

One of the main design requirements of the framework is the strict separation between algorithm and problem formulation. The optimization framework is therefore subdivided into problem-specific objective functions and optimizers. The link between both parts is established by the unified optimization interface, which is realized using class inheritance. Since all optimization processes follow a similar pattern, the main iteration loop can be implemented in a common way. The optimization process hence is controlled by an abstract class, which provides the interface definition and basic functionalities.

Parallel computing capabilities are centralized within the parent class. It therefore handles the parallelization of the objective function evaluation and the associated thread pools. Parallel evaluation of generated samples is possible without loss of generality, because all samples of an iteration can be computed separately. As the evaluation of the objective function by far makes up the largest part of the processing time in engineering problems, the parallel evaluation enables full utilization of the available processing power. While parallelization of the objective evaluation leads to a significant performance gain, the optimization algorithm's logic itself runs sequentially, since it makes up for an insignificant amount of run-time. Additionally, the framework can store the current state of the optimization process. Thus, the optimization can be restarted based on a previously computed optimization result.

According to abstract methods of the parent class the specific algorithm's logic is split into three steps. These steps are similar for all algorithms and include the initialization, sample generation and processing of results. By leaving basic functionalities to the parent class, the algorithm routines can be written in a clear and concise fashion. This speeds up the implementation process of new algorithms while also minimizing the potential for programming errors.

Both single- and multi-objective optimization problems can be solved with the framework. Therefore, the architecture is capable of handling multi-objective optimization by design.

To prevent errors associated with a mismatched number of objectives, the calling convention for unconstrained single- and multi-objective functions is the same. The number of objectives is signalled by the objective function when it is called with an empty set of design variables. The architecture of EngiO is visualised in Fig. 1 using the Unified Modelling Language (UML).

As shown in the UML class diagram, the core of the framework is

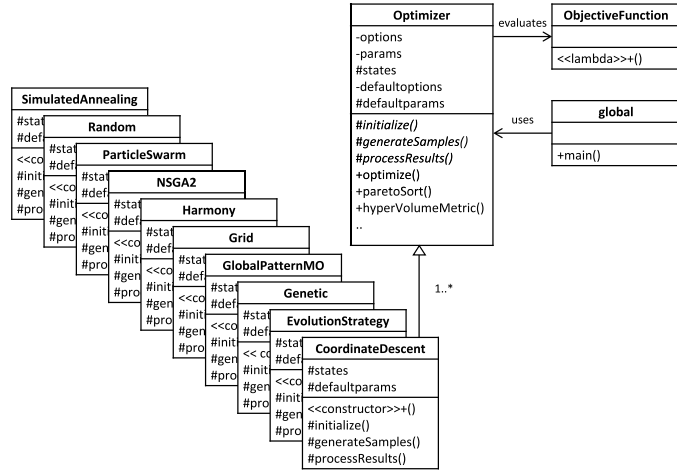


Fig. 1. UML class diagram of the basic framework.

formed by the **Optimizer** class, which controls the optimization process and connects the algorithm to the objective function. General optimization settings are specified via the options property of the **Optimizer**. Termination conditions or settings for parallel evaluation are part of the options property. The default options can be overwritten when calling the optimize method. Parameters can also be provided, which are defined individually for each optimization algorithm. They encompass population size, mutation rate and the like. Internal states of algorithms are passed using a shared state variable.

The **Optimizer** acts as a parent class for each algorithm and includes concrete as well as abstract methods. As outlined above, the parent class has three abstract methods which have to be overloaded by the derived algorithm class, e.g. the **CoordinateDescent** class. These methods constitute the optimization interface between algorithm and **Optimizer** class and necessitate splitting the optimization algorithm logic into several parts. As most engineering optimization problems are not convex and derivatives of the objective function are not available, the architecture focuses on derivative-free algorithms. Hence, the handling of derivatives is not supported by the framework.

Moreover, the **Optimizer** class contains public methods to start the optimization, to sort the evaluated multiple objectives according to the concept of Pareto dominance and to calculate the hypervolume metric. The **Optimizer** treats all problems as multi-objective formulations by default. To increase performance, efficient Pareto sorting is implemented in variants for single-, two- and many-objective cases. For the single-objective case, the sorting reduces to finding the minimum objective value. After the final iteration loop, the Pareto frontier is extracted from all prior objective function evaluations, providing the final result of the optimization. For comparisons between multi-objective algorithms, the optimization parent class includes the calculation of the hypervolume metric [28]. This metric measures the volume enclosed between a reference point and the Pareto frontier. It is influenced by both convergence and distribution of the Pareto-optimal set.

The user of the framework implements a main routine on a **global** level, which uses and creates an instance of the algorithm class. The objective function (**ObjectiveFunction**) is passed as a named or anonymous function handle. It can thus be either a global function or a method of an object. Information on boundaries of the design variables, options and parameter properties are passed using parameters when calling the optimize function. A collection of analytic test functions (**TestFunctions**) is also part of the framework. User-provided objective functions as well as the analytic test functions can be supplied when calling the optimize function. Optimization results are visualized using centralized plot functions, which are included in EngiO.

2.2. Architecture of the constraint interface

Following the modular and object-oriented approach taken for the optimization algorithm interface, the constraint interface is designed in a similar way. However, the constraint interface is implemented separately and is not part of the optimization class itself. This design decision achieves maximum modularity of the framework and allows for a fast implementation of handling approaches. The constraint handling considered in the constraint interface are so-called penalty methods only, because these techniques can be used independently of the optimization algorithm [29]. In particular, the framework does not consider constraint handling that involves a modification of the processes within optimization algorithms. Further, the interface is designed for static penalty methods. Static penalty methods are not influenced by internal states of the algorithm, such as the number of iterations. This property is necessary when optimization approaches are applied, which take the whole sampling history into account.

The additional classes forming the constraint handling interface are shown in Fig. 2. As previously, the optimization procedure is driven by the **Optimizer**. But instead of an objective function a penalized objective function is evaluated by the optimizer.

The penalization of objectives is implemented using the **PenalizedObjectiveFunction** class. The properties of this class therefore include handles of the objective function and equality as well as inequality constraint equations. To allow for multi-objective cases, the number of objectives is stored in the object properties of the **PenalizedObjectiveFunction**. In addition to the constructor, the class implements a concrete method to evaluate constraints. In this method, penalty values are added to objective values according to the constraint violation. The method individually handles the different penalization of each inequality and equality constraint. This design of the class scheme allows to select the penalty technique for each constraint separately. The framework provides several well-established penalty formulations like death penalty or quadratic penalty.

The techniques for the calculation of penalty values are implemented in related classes. Due to the architecture, specific implementations contain only a few lines of code, which greatly reduces redundancy. The specific penalty values are calculated upon calling the penalty function method. An example for a penalty function is given in Section 3.3. The weighting factors, which parameterize the penalty function, are defined in the global main routine and are passed to the penalty object via a vector during initialization.

To perform constrained optimization, the user of the framework implements a main routine, which creates instances of the

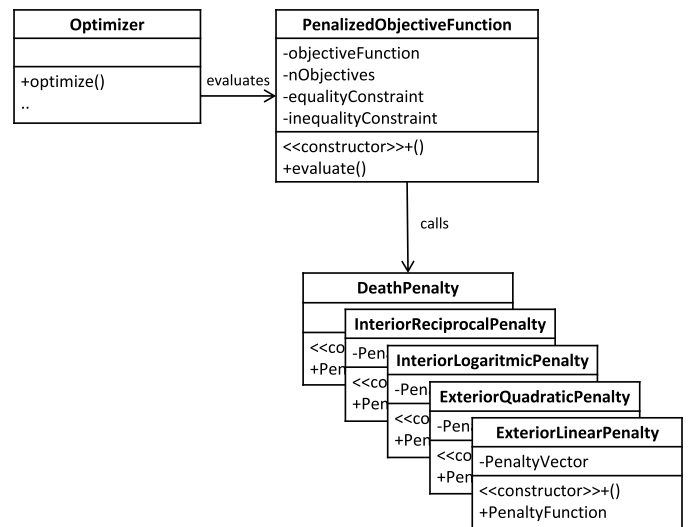


Fig. 2. UML class diagram of the static constraint handling framework.

PenalizedObjectiveFunction and penalty class in addition to the optimizer object. The evaluate method of the **PenalizedObjectiveFunction** class is then used as the objective function. In order to be compatible with the constraint interface, objective functions need to provide constraint equation values in addition to the objective value vector. Upon initialization, the number of objectives as well as the number of inequality and equality constraints are communicated to the **PenalizedObjectiveFunction**. The optimization scheme illustrated in Fig. 1 in Section 2.1 thus remains untouched.

2.3. Comparison with other optimization software

The properties of EngiO are illustrated by an exemplary comparison with three established optimization software codes. The software codes are compared objectively in terms of architecture, programming language, available optimization algorithms, complexity, result visualization and software license. The advantages of EngiO, which become clear through the differentiation from the other optimization software, are addressed in Section 2.4.

The Matlab Global Optimization Toolbox [18] is part of the Matlab product family and provides the functionality to solve global optimization problems. As it is a toolbox rather than a framework, the methods are implemented separately and have no common interface. Thus, the toolbox provides a collection of various algorithms, but the code has many redundancies. In contrast, EngiO is designed using unified interfaces for optimization and penalization.

Since the Global Optimization Toolbox belongs to the Matlab product family, it is completely programmed using the Matlab programming language. EngiO is written with the same language but is additionally compatible with GNU Octave.

The methods included in the Global Optimization Toolbox comprise global derivative-free algorithms as well as a gradient-based multi-start solver. EngiO considers global and local derivative-free methods, because gradients are not available in most complex engineering optimization problems. The collection of derivative-free methods in EngiO is similar to the algorithms provided by the toolbox. Multi-objective optimization is supported by both software codes.

The main script of the Global Optimization Toolbox, which starts the optimization process, has a comprehensible structure and usually contains about 20 lines of code. Main scripts of EngiO are of comparable length, as shown in Section 2.4. Unlike the toolbox, the unified interface of EngiO leads to very concise implementations of each algorithm. For instance, the Genetic algorithm implementation included in EngiO has about 200 lines of code. The corresponding implementation of the Global Optimization Toolbox comprises of 600 lines. Most of this extra complexity is caused by features like parallelization or argument checking, which are centralized in the optimization class of EngiO.

In both optimization software codes, optimization results are reported to the user via the command window. Visualisation of results via plot functions is supported by the Matlab Optimization Toolbox as well as by EngiO. The creation of publication-grade diagrams is facilitated by the broad range of graphical output options integrated in Matlab.

Finally, the Matlab Global Optimization Toolbox is an extension of a commercial software and requires the purchase of both the toolbox and the standard Matlab programming environment. EngiO is an open-source research code under GPLv3 license, freely downloadable, and can be run in GNU Octave.

An optimization software sharing the free and open source code approach is pyOpt [11]. PyOpt, like EngiO, is an optimization framework with an object-oriented architecture. In pyOpt, the optimization problem as well as the optimizer are implemented using classes. EngiO does not enforce a class-based definition of the objective function, allowing for more flexibility. Boundaries of the optimization problem are specified in the main script and objective functions and constraint equations are implemented using custom functions. In pyOpt, the optimization loop itself is implemented separately for each algorithm. In the

architecture of EngiO, such redundancies are avoided, since the optimization loop is implemented as a concrete method of the optimizer class.

PyOpt is a mainly Python-based framework, but also includes routines written in C, C++ as well as Fortran. The source code of pyOpt therefore is a mix of different languages, while EngiO is consistently programmed using one syntax.

The algorithms integrated in the pyOpt framework are gradient-based as well as derivative-free methods for single- and multi-objective optimization. In terms of derivative-free methods, pyOpt provides a similar range of algorithms as EngiO.

The python-based glue code of the pyOpt framework is structured in a clear way due to its object-oriented design. However, pyOpt uses the original implementations of many algorithms, which are mostly not object-oriented and written in low-level programming languages. Thus, the majority of the source code of PyOpt consists of functions that have a less understandable syntax. Due to the uniform programming language used in EngiO, the source code is much shorter. For example, the interface class implementation of NSGA-II in pyOpt contains about 400 lines of code written in Python, in addition several thousand lines of C code for the algorithm implementation itself. The whole algorithm is implemented in EngiO in about 350 lines of Matlab code. The main scripts used by pyOpt and EngiO are of comparable length and design.

The visualization of optimization results is not covered by the core of pyOpt. Contrary to pyOpt, EngiO supports the creation of graphics using a collection of plot functions.

The source code of pyOpt is freely available under GNU Lesser General Public License (LGPL). EngiO is also freely available under GPLv3.

Another well known optimization software is the DAKOTA toolkit [4]. DAKOTA is a vast collection of optimization-related tools and defines a unified interface between simulation codes and the DAKOTA components. In contrast to EngiO, DAKOTA follows the idea of exchanging data between the simulation model and the optimizer by writing and reading text files. Only for some applications, direct solvers are available.

DAKOTA is written in C and features interfaces to Python and Matlab code. However, the DAKOTA source code has to be adapted and recompiled for this purpose. In EngiO, it is assumed that the engineering optimization task can be triggered using the Matlab syntax, including calls to any external program.

In the choice of optimization software discussed here, DAKOTA has the broadest spectrum of functionalities. Beside pure optimization tasks, DAKOTA enables parameter studies, uncertainty quantification or sensitivity analysis. In contrast, EngiO is a special-purpose framework for complex engineering optimization tasks, so its functionality is limited to gradient-free optimization.

The quantity of code reflects this broad scope of DAKOTA. Even the executable version of DAKOTA (6.12.0) contains more than 6500 files. The complete source code of EngiO is contained in about 60 files.

For visualization of optimization results, DAKOTA features a GUI with various graphical options. The code base of the GUI contains over 2000 files. EngiO does not include a GUI in favor of a lean code and uses the Matlab plotting capabilities for graphical output.

The components of DAKOTA are mainly released under LGPL and are distributed via the DAKOTA homepage. EngiO is publicly accessible at Github.

2.4. Advantages of the framework in teaching and research

At university, students of computer-aided and engineering subjects learn the foundations for solving engineering tasks on their own. Especially during their bachelor or master thesis, they are encouraged to develop solutions for challenging simulation problems. These problems often include a numerical optimization component. With EngiO we aim to provide a framework, which can be used by students. Thus, we

address the aspects of code complexity, readability and visualization.

First, the code complexity, with regard to the quantity of source code lines, is an decisive aspect in teaching. The architecture of EngiO allows a clear and lean source code, which lowers the barriers for students and allows a quick familiarization even for inexperienced users, such as undergraduate students. User-defined optimization problems and algorithms can be implemented quickly and good programming practices are encouraged by the interface design.

Second, the utility of the framework is closely linked to the programming language used. For teaching purposes, the comprehensible Matlab syntax is advantageous, because of its good readability and debugging capabilities. The limitation of EngiO to this single language facilitates its usage for users with little programming experience. The usage is demonstrated by the main script in Listing 1, which starts the optimization of the analytic Himmelbau test function (see Appendix A Eq. (A.1)) using the Genetic algorithm.

The optimization problem is defined in lines 5-9 followed by the selection of algorithm and optimization settings. The optimization is started in line 19 calling the optimization method. The advantages of the underlying architecture become apparent, when the user wants to select an alternative optimization algorithm. Due to the architecture, only the instantiation of the optimization object in line 12 and the algorithm-specific parameters in line 15 have to be adjusted. However, the rest of the routine remains untouched. Changes in the function calls are not necessary, which demonstrates the flexible usage of EngiO. In our experience, this accessibility of the code encourages students and researchers to focus on creative approaches rather than being frustrated by programming bugs. Moreover, due to its ease of use, Matlab is part of many engineering courses and often introduced in undergraduate

programs of universities. Therefore, students are familiar with the syntax and environment used for EngiO.

Finally, the visualization of optimization processes is of great importance to impart knowledge to students. Differences between algorithms and influence of optimizations settings are more easily understood, if they are shown graphically. Hence, analyzing the design space is encouraged, instead of treating the optimal value as the result of a black-box process. Due to the plotting capabilities of Matlab and easy handling of figures, a GUI is not required. With the plot functions provided by EngiO, students can display their results with a single line of code like it is done in line 23 of Listing 1. The sampling pattern in Fig. 3 corresponds to this example. In the displayed run, an optimal value of $f_{opt} = 1.64625 \cdot 10^{-11}$ is found at $x_{opt} = [-2.805119 \quad 3.131312]^T$, which corresponds to results reported in literature (see Appendix A).

In addition to teaching, EngiO is used by doctoral and postdoctoral researchers to find optimal solutions for engineering problems or benchmarking their own algorithms. Hence, implementation effort, parallelization capabilities and open sourcing were the three main aspects considered in the design of EngiO with respect to the scientific community.

First, the object-oriented architecture of EngiO provides a clear structure for the implementation of newly developed algorithms. The user benefits from the central implementation of the main iteration loop in the parent class and can focus on the algorithm-specific routines for initialization, sample generation and processing of results. Splitting the algorithmic logic into this three steps and leaving basic functionalities to the parent class, greatly reduces the implementation effort and eliminates potential for programming bugs. Furthermore, running all algorithms within the same framework facilitates benchmarking and

```

% Add folders to path
addpath('OptAlgorithms', 'TestFunctionsUncon', 'Plots');

% Set optimization problem
prob = @Himmelblau;

% Set lower and upper bounds for problem
x_lb = [-6, -6];
x_ub = [ 6,  6];

% Create instance of optimization algorithm
algo = Genetic();

% Settings for optimization run
aParams = struct('popSize', 25);
aOptions = struct('maxEvals', 1000);

% Run optimizer
[x_opt, y_opt, nEvals, mSamples, vResults]...
    = algo.optimize(prob, [], x_lb, x_ub, aOptions, aParams);

% Create plots
fig = plot2DSamplingPattern(x_opt, mSamples, prob, x_lb, x_ub);

% Remove folders from path
rmpath('OptAlgorithms', 'TestFunctionsUncon', 'Plots');

```

Listing 1. Main script of EngiO running the optimization process.

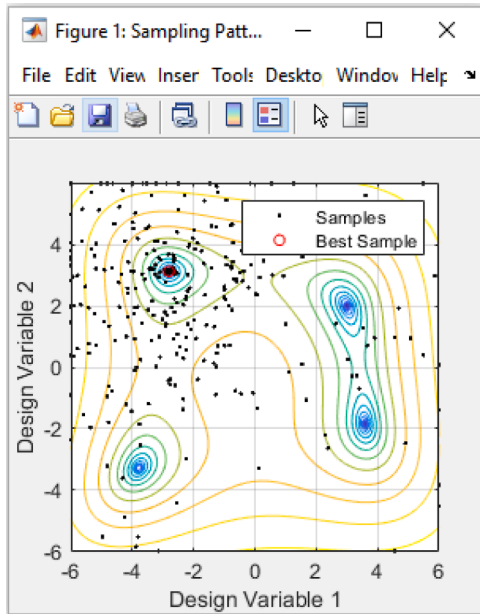


Fig. 3. Screenshot of two-dimensional sampling pattern plot in Matlab with the best sampled solution highlighted in red.

scientists benefit from the algorithms already implemented in EngiO.

Second, engineering simulations typically need a significant amount of computation time. To speed up the process, parallel evaluation of objectives is of great interest. The architecture of EngiO has the advantage that parallel treatment of objective functions is handled by the optimizer class. The parallel evaluation of simulation models is therefore possible without any additional code development in the algorithm implementation. Further, the restart capability enables the efficient use of computing time in case of stoppages in the optimization run.

The third advantage refers to the idea of open source code. EngiO as a research code is freely accessible via its Github repository. All changes and implementations are visible for the worldwide scientific community.

3. Optimization formulation and algorithms

Depending on the engineering application at hand, the optimization problem comprises one or more objectives and may involve constraint equations. In the following section, the single- and multi-objective formulations are introduced and constrained handling strategies are discussed.

3.1. Single-objective optimization

Numerous basic engineering optimization problems fall in the category of scalar, bounded, unconstrained, nonlinear and derivative-free optimization problems

$$\text{minimize } f(\mathbf{x}) \quad \text{for } f \in \mathbb{R}, \mathbf{x} \in \mathbb{R}^n, \quad (1)$$

where f is the scalar objective function and \mathbf{x} is the n -dimensional vector of design variables. The space of the design variables is bounded to the volume of a hypercube

$$\mathbf{x}_{lb} \leq \mathbf{x} \leq \mathbf{x}_{ub}, \quad (2)$$

where \mathbf{x}_{lb} and \mathbf{x}_{ub} are the lower and upper bounding vectors, respectively. The optimization framework includes several state-of-the-art algorithms suitable for derivative-free single-objective optimization. Table 1 lists the implemented algorithms in the order of the year of

Table 1

Algorithms implemented for single-objective optimization.

Optimization algorithm	
Coordinate Descent	[30]
Evolution Strategy	[31]
Genetic Algorithm	[32]
Simulated Annealing	[33]
Particle Swarm Optimization	[34]
Harmony Search	[35]
Global Pattern Search	[36]

publication.

Coordinate Descent is one of the oldest and simplest local, derivative-free, deterministic optimization algorithms. It employs a round-robin variation of each variable around a base point in the design variable space. An overview including extensions of Coordinate Descent is given by Wright [30]. In addition to this well-known local optimizer, the framework includes a second deterministic derivative-free algorithm called Global Pattern Search [36]. This is a global deterministic optimizer and represents a generalization of the local derivative-free Pattern Search [37].

Metaheuristics are the most commonly used global derivative-free algorithms. They rely on pseudo-random numbers to stochastically explore the design variable space of the underlying problem. Many metaheuristic optimization algorithms are inspired by natural processes like biological phenomena or swarm intelligence [38]. The earliest metaheuristic optimizers belong to the class of evolutionary algorithms, whereby our framework includes Evolution Strategy [31] and Genetic Algorithm [32]. The essence of both algorithms is the abstraction of the Darwinian evolution as well as natural selection of biological systems. The natural process “survival of the fittest” is represented in terms of mathematical operators like crossover, recombination, mutation or fitness evaluation. More recent examples of metaheuristic algorithms are Simulated Annealing [33], inspired by the annealing process of metals, Particle Swarm Optimization [34], inspired by swarm intelligence of fish and bird behavior, and Harmony Search [35], inspired by arrangement of musical harmonies.

3.2. Multi-objective optimization

In multi-objective optimization, the bounded, unconstrained, nonlinear and derivative-free optimization problem is solved

$$\text{minimize } f(\mathbf{x}) \quad \text{for } f \in \mathbb{R}^m, \mathbf{x} \in \mathbb{R}^n, \quad (3)$$

where f , in contrast to Eq. (2), is the m -dimensional objective function. In the case of multi-objective optimization, the concept of Pareto dominance is followed. This means that a point $\hat{\mathbf{x}}$ is on the Pareto frontier, if there exists no point \mathbf{x} such that $f(\mathbf{x}) \preceq f(\hat{\mathbf{x}})$ [39]. This means that the solutions on the frontier are better than others at least in one objective. As stated in Section 1, an efficient Pareto sorting code is part of the driver class and thus accessible from all algorithm implementations. Currently, the two multi-objective algorithms listed in Table 2 are implemented.

Non-dominated Sorting Genetic Algorithm-II (NSGA-II) [40,41] is an expansion of the evolution-inspired Genetic Algorithm and known to perform well on most problems [42]. Solutions are ranked by the computation of non-dominated sets and a crowding distance is assigned to find members of the new population. Additionally, the

Table 2

Algorithms implemented for multi-objective optimization.

Optimization algorithm	
Non-dominated Sorting Genetic Algorithm-II (NSGA-II)	[40]
Multi-Objective Global Pattern Search (MOGPs)	[36]

single-objective Global Pattern Search is extended to a multi-objective version. The so-called Multi-Objective Global Pattern Search (MOGPS) optimizes problems in a deterministic manner.

3.3. Constrained optimization

Some engineering problems require the use of constraints, which define a feasible region inside the bounded design space. The constrained optimization problem can be stated similar to Eqs. (2) and (3) as

$$\begin{aligned} & \text{minimize } f(\mathbf{x}) \quad \text{s. t. } \mathbf{g}(\mathbf{x}) \geq \mathbf{0} \\ & \mathbf{h}(\mathbf{x}) = \mathbf{0} \end{aligned} \quad (4)$$

for $f \in \mathbb{R}^m$, $\mathbf{g} \in \mathbb{R}^p$, $\mathbf{h} \in \mathbb{R}^q$, $\mathbf{x} \in \mathbb{R}^n$,

where $\mathbf{g}(\mathbf{x})$ is a one-sided inequality and $\mathbf{h}(\mathbf{x})$ an equality constraint equation comprising p and q constraint equations, respectively. In general, static penalty techniques expand the objective function such that the constrained optimization problem is defined as

$$\begin{aligned} & \text{minimize } f(\mathbf{x}) + \Phi(\mathbf{g}(\mathbf{x}), \mathbf{h}(\mathbf{x})) \\ & \text{for } f, \Phi \in \mathbb{R}^m, \mathbf{g} \in \mathbb{R}^p, \mathbf{h} \in \mathbb{R}^q, \mathbf{x} \in \mathbb{R}^n, \end{aligned} \quad (5)$$

where Φ is the vector-valued penalty function. The implemented static penalty constraint handling techniques are listed in Table 3.

According to Coello Coello [29], the techniques are divided into interior and exterior approaches. Interior methods restrict the design space to feasible solutions only. On the one hand, if there is only a very small feasible region, an application of these approaches can result in entirely missing the feasible region. On the other hand, in case of success they will definitively provide feasible solutions only. In contrast, exterior methods do not restrict the design space and thus are suited for problems with small or even non-existent feasible regions. However, the optimal solution obtained using an exterior approach will often not be inside the feasible region.

As an example, using the linear penalty technique, the violation of an inequality constraint $g(x)$ is penalized by

$$\Phi_i^g = \begin{cases} -r_i^g \cdot g(x) & g(x) < 0 \\ 0 & g(x) \geq 0, \end{cases} \quad (6)$$

where r_i^g are the corresponding penalty vector entries and i denotes the objective function index. In the case of one equality constraint $g(x)$, the linear penalty function

$$\Phi_i^h = r_i^h \cdot |h(x)| \quad (7)$$

evaluates the constraint violation weighted by penalties r_i^h specified for each objective i . This vector formulation of the penalty functions enables imposing constraints on multi-objective optimization problems as well. The final penalty added to the objective function is expressed by the sum over all equality as well as inequality penalty values

$$\Phi_i = \sum_g \Phi_i^g + \sum_h \Phi_i^h. \quad (8)$$

4. Optimization of analytic test functions

Several single- and multi-objective analytic test functions are implemented in the framework. This way, newly implemented or

Table 3
Static penalty constraint handling techniques provided by the framework.

Exterior	Interior
Linear penalty	Logarithmic penalty
Quadratic penalty	Reciprocal penalty
	Death penalty

modified optimization algorithms can be easily tested and compared to each other as well as to established methods. In the following subsections, optimization algorithms are exemplarily applied to different analytic test functions and optimization results are presented. A single-objective unconstrained, a single-objective constrained and a two-objective unconstrained problem are considered.

4.1. Single-objective optimization without constraints

Firstly, the unconstrained Himmelblau test function (see Appendix A Eq. (A.1)) is chosen to illustrate the optimization process using two different optimization methods. This multimodal test function possesses four local minima, which are also global minima. As the implemented optimization algorithms are based on several different, mostly nature-inspired approaches, the sampling patterns shown in Figs. 4 and 5 are stochastic.

All samples are displayed as black dots and the red circle represents the best value found after reaching the limit of 1000 evaluations. The sampling patterns of Evolution Strategy and Harmony Search are quite different. Evolution Strategy samples in a cloud-like structure around the initial set of samples, whereas Harmony Search explores the design variable space in a crosswise pattern.

As indicated by the contour plot, the Himmelblau function has four optimal, equally valued solutions $f_{opt} = 0$. For the displayed runs, significant differences emerge during convergence. While Evolution Strategy converges to the optimum in the lower right corner, Harmony Search finds the optimal solution in the upper left corner of the design value space. As the applied algorithms are metaheuristic, they will reach a different optimum with every run and the four solutions will only become apparent to the user when a sufficient number of runs is conducted. The minimum objective function values for the displayed run are $f_{opt} = 1.72 \cdot 10^{-7}$ for Evolution Strategy and $f_{opt} = 1.60 \cdot 10^{-6}$ for Harmony Search.

4.2. Single-objective optimization with constraints

As many engineering optimization problems have constraints attached to them, the framework provides several different static penalty constraint handling techniques. To give an example of a single-objective test problem with one inequality constraint, the two-dimensional Simionescu function (see Appendix A Eq. (A.2)) is used. This multimodal test function features a geometrically complex constraint definition. For this example, the constraint equation is solved using the exterior linear penalty method. Particle Swarm Optimization and Genetic Algorithm are applied to this analytic test function with the maximum number of evaluations limited to 2000.

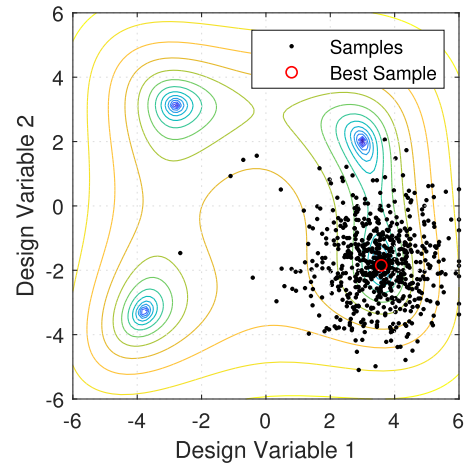


Fig. 4. Sampling pattern of Evolution Strategy on Himmelblau function.

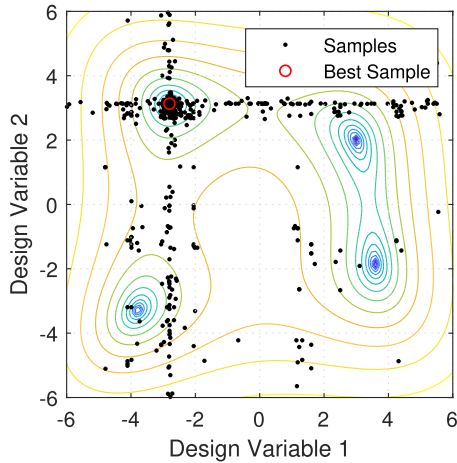


Fig. 5. Sampling pattern of Harmony Search on Himmelblau function.

Figs. 6 and 7 show the history of objective function evaluations for both optimization runs. The objective values determined for 2000 samples are represented by black dots. The best constraint-satisfying objective function values found in the optimization are highlighted in red. All samples located below the red line violate the constraint.

Regarding the convergence of the best objective function value, it is apparent that both algorithms reach the optimal solution $f_{opt} = -0.072$ after approximately 250 objective function evaluations. However, the spread of the samples in the objective value space differs. There are only few samples of Genetic Algorithm that scatter in the objective value space, whereas the samples of Particle Swarm Optimization are widespread.

Figs. 8 and 9 display the convergence of the related constraint equation value itself. According to the problem definition in Eq. (4), negative constraint values denote infeasible designs. In general, the evolution of constraint values shows the same tendency as discussed for the constrained objective value space. The constraint value calculated when applying Genetic Algorithm clearly converges to zero after approximately 300 objective function evaluations. On the contrary, a convergence of the constraint value calculated when applying Particle Swarm Optimization is only visible after approximately 1000 evaluations.

4.3. Multi-objective optimization without constraints

Engineering applications often have more than one goal and the objectives are contradictory. This is where multi-objective optimization can be of great importance, as it can calculate Pareto-optimal solutions.

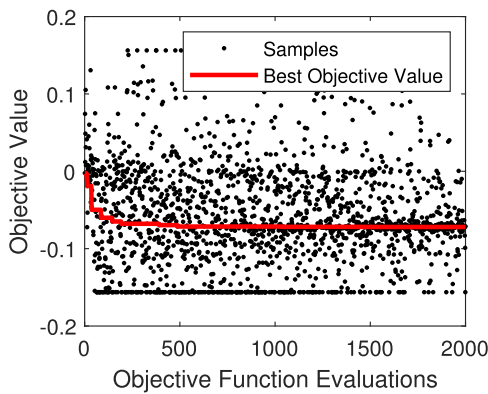


Fig. 6. Objective values of Particle Swarm Optimization on Simionescu function.

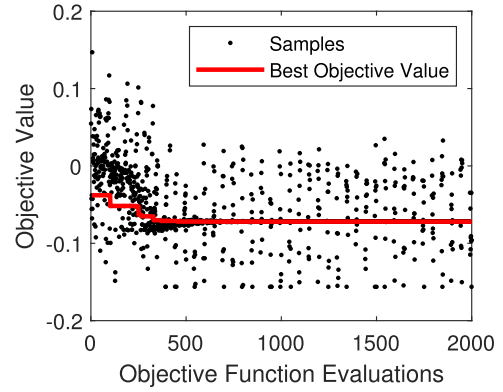


Fig. 7. Objective values of Genetic Algorithm on Simionescu function.

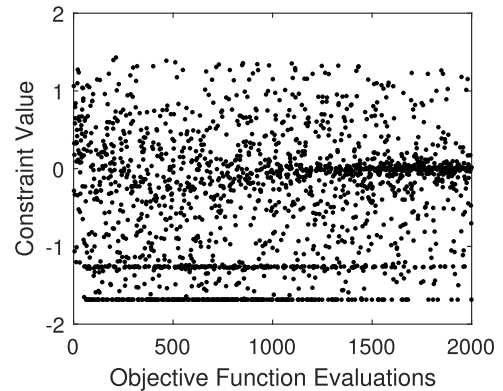


Fig. 8. Constraint values of Particle Swarm Optimization on Simionescu function.

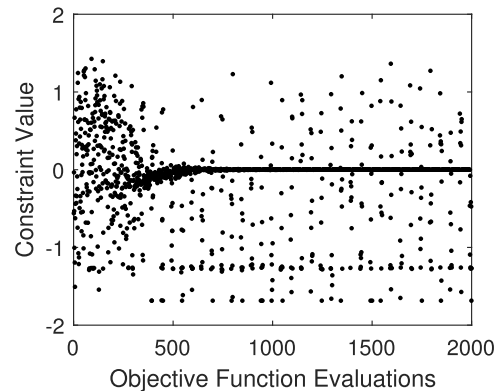


Fig. 9. Constraint values of Genetic Algorithm on Simionescu function.

Of course, it is the user's decision to pick a suitable solution out of the (possibly infinite) set of optimal solutions to the problem at hand.

Figs. 10 and 11 show the optimization results of the two implemented multi-objective optimization algorithms on the three-dimensional, two-objective, unconstrained test function Kursawe (see Appendix A Eq. (A.3)). The Kursawe test function has Pareto-optimal regions which are volumetric, flat, linear as well as point-like. In each case, the number of objective function evaluations is set to 1000.

Both algorithms find the four separated Pareto-optimal regions in the objective value space, which are three S-shaped sections and one isolated point close to a second objective value of zero. Still, the difference in the resolution and thus the clarity of the Pareto-optimal regions is apparent. In this case, the Pareto frontier calculated with deterministic

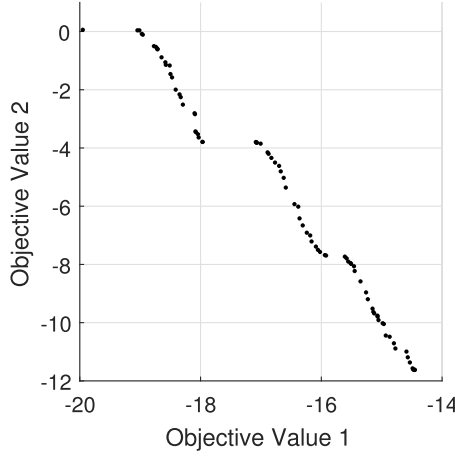


Fig. 10. Pareto frontier of NSGA-II on Kursawe function.

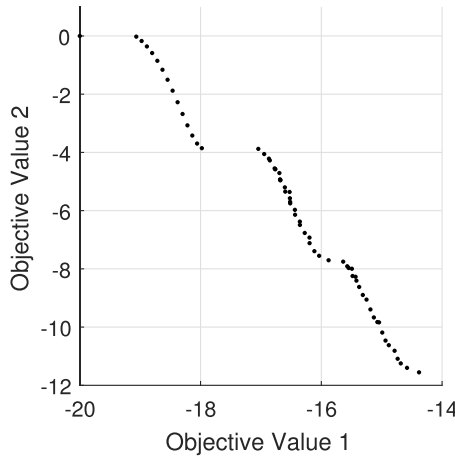


Fig. 11. Pareto frontier of MOGPS on Kursawe function.

MOGPS is more evenly sampled than the Pareto frontier calculated with NSGA-II.

5. Application to engineering problems

Subsequent to the optimization of test functions, this section shows three engineering problems in the field of wind energy. As before, a single-objective unconstrained, a single-objective constrained and a two-objective unconstrained problem are considered.

5.1. Damage localization using finite element model updating

Finite element (FE) model updating is based on the assumption that differing mechanical properties cause detectable changes in the structural behavior [43]. In terms of damage assessment, this means that damage-induced variations in the mechanical properties can be detected by updating specific parameters of the FE model to the structural behavior [44]. Thus, FE model updating can be employed as a vibration-based, non-destructive damage assessment method. In this contribution, changes in the structural behavior are to be found in terms of stiffness deviations.

As a practical engineering problem, the FE model updating of the offshore wind turbine rotor blade shown in Fig. 12 is conducted. Here, only a brief summary of the approach is given to understand the resulting optimization task. For more detailed information, it is referred to Bruns et al. [45]. Specifications of the NREL offshore 5-MW baseline wind turbine [46] are used to create the FE model of the 63 m long



Fig. 12. CAD model of a wind turbine rotor blade.

blade.

The FE model with nominal properties represents the healthy state of the rotor blade and is therefore referred to as reference model. Additionally, a model with a fictitious damage is created by reducing the edgewise bending stiffness of certain elements by two percent. This model of the damaged blade is named the target state. The position of the damage of the target state is illustrated in Fig. 13, where EI_i^0 corresponds to elements with nominal and EI_i^θ elements with reduced stiffness.

The goal of the model updating procedure is to iteratively change the properties of the reference model to meet the target state, where the stiffness deviation along the blade is described by a set of design variables. In favor of a minimal set of design variables and FE mesh independence, a stiffness distribution function is introduced for the considered beam model as it is shown in Fig. 14.

The respective design variable vector is

$$x = [\mu, D, \sigma]^T, \quad (9)$$

where μ represents the spanwise position, D represents the intensity of the damage, and σ represents the width of the normal distribution. As the FE model is meshed with a discrete amount of beam elements, elementwise stiffness scaling factors

$$\theta_i = 1 - \left(D \cdot F(s_i, \mu, \sigma) - \sum_{j=1}^{i-1} 1 - \theta_j \right) \quad (10)$$

are calculated, where $F(s_i, \mu, \sigma)$ is the cumulative distribution function, s_i the spanwise position and θ_j the stiffness scaling factors of previous elements.

To match the structural properties of the target state, the objective function compares the mode shapes of the current model to the mode shapes of the target state. The objective function

$$f(x) = \sum_{i=1}^N (1 - \text{MAC}_i(x))^2 \quad (11)$$

is formulated using the Modal Assurance Criterion (MAC) defined by Allemang and Brown [47] for a number of $N = 10$ mode shapes. This objective function contains multiple local minima, which result from the mode shape geometry [36]. The optimization problem is solved using Genetic Algorithm. The convergence behavior is shown in Fig. 15, where the history of the design variables is illustrated for 1000 objective function evaluations.

Although Genetic Algorithm generates samples broadly along the defined design bounds, featuring a scattering sampling pattern, it finally converges to an optimal design.

The design variables corresponding to the computed optimum localize the damage position with a good accuracy. The computed

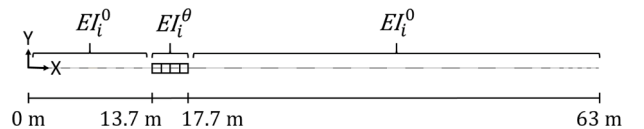


Fig. 13. Spanwise position of the fictitious damage on the 63 m long blade.

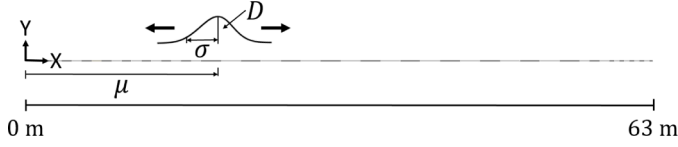


Fig. 14. Parameterization of the stiffness distribution function by design variables (μ, D, σ) along the blade span.

damage position $\mu = 15$ m is close to the true position of the defect, which is at 15.7 m (Fig. 13). The obtained damage intensity $D = 7.7\%$ quantifies the artificially induced damage of 8% correctly. The design variable σ is determined to be close to 1. According to the 2σ interval, this means that about a region of ± 2 m of the blade is damaged. Compared with Fig. 13, it turns out that the optimization results fit the target state.

5.2. Jacket substructure design optimization

Support structures of offshore wind turbines in water depths of more than 40 m are often constructed using jacket substructures (Fig. 16). The design of jacket substructures includes a series of decisions with regard to the topology and the dimensions. In many cases, these decisions are based on experience and expert knowledge. However, current research results [48,49] show that state-of-the-art jackets can still be improved by incorporating numerical optimization.

The optimization of jacket substructures is challenging in two respects. Firstly, jacket substructures are complex structures that differ in topology as well as in size of the assembled parts. For the accurate description of the structure, a relatively large set of parameters is necessary. In the context of optimization, this is disadvantageous, because the dimension subsequently determines the number of objective function evaluations and thus the numerical effort. Based on the work of Häfele et al. [49], the jacket model comprises ten design variables

$$\mathbf{x} = [R_{\text{foot}}, \xi, q, D_L, \beta_b, \beta_t, \gamma_b, \gamma_t, \tau_b, \tau_t]^T, \quad (12)$$

where R_{foot} is the foot radius of the jacket, ξ is the ratio between head and foot diameter, q is the ratio of two consecutive bays, D_L is the leg diameter, β_b and β_t are the brace-to-leg diameter ratios, γ_b and γ_t are the leg radius-to-thickness ratios and τ_b and τ_t are the brace-to-leg thickness ratios at bottom and top. For details and visualizations of the design variables, it is referred to Häfele et al. [50]. The number of legs is set to three and the number of braces layers (bays) is set to four.

Secondly, jacket designs have to be evaluated according to the engineering requirements. Time-domain simulations are needed for various load cases to assess the fatigue life and the ultimate limit state of the jacket. To improve the efficiency, the fatigue and ultimate limit state assessments are approximated a priori by surrogate models (Gaussian Process Regression) [51]. Further, an analytic cost model calculates the total expenses due to material, fabrication, coating, transport, connectors and installation. Based on the engineering problem statement, we formulate the optimization problem

$$\begin{aligned} & \text{minimize} && C_{\text{total}}(\mathbf{x}), \\ & \text{s.t.} && g_1(\mathbf{x}) \geq 0 \text{ and} \\ & && g_2(\mathbf{x}) \geq 0, \end{aligned} \quad (13)$$

where the objective function $C_{\text{total}}(\mathbf{x})$ represents the jacket costs, while the imposed constraints refer to fatigue $g_1(\mathbf{x})$ and ultimate limit state $g_2(\mathbf{x})$ assessments [52,53]. For detailed information on application of guidelines it is referred to Häfele et al. [49]. The constrained problem formulation is optimized using Particle Swarm Optimization and a linear exterior penalty expression. Figs. 17 and 18 show the constraint values for 40000 objective function evaluations.

In both cases, a clear convergence of constraint values towards zero is noticeable after approximately 35000 evaluations. The optimization

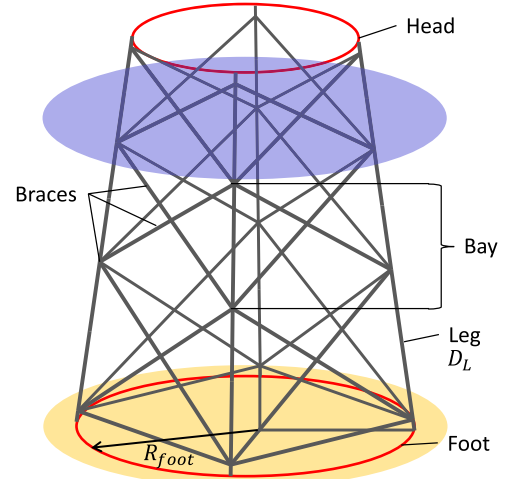


Fig. 16. Schematic design of jacket substructures.

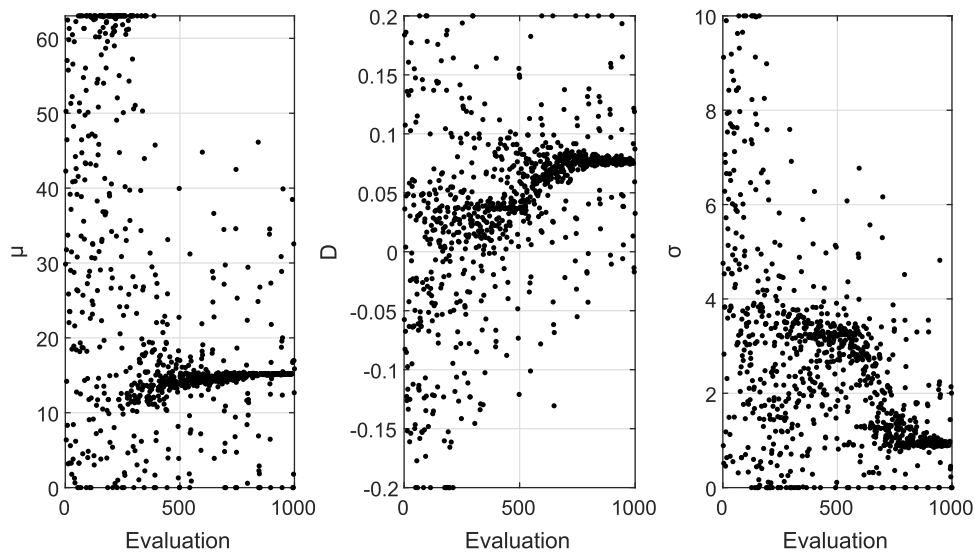


Fig. 15. Convergence of the design variables using Genetic Algorithm.

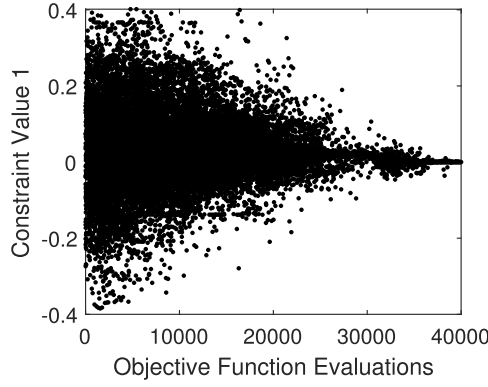


Fig. 17. First constraint values of Particle Swarm related to fatigue.

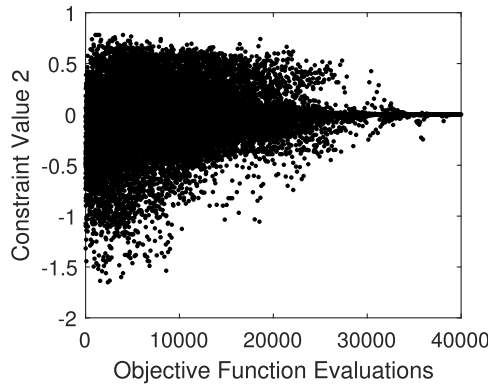


Fig. 18. Second constraint values of Particle Swarm related to ultimate limit state.

history with regard to the objective values reflects this tendency and is shown in Fig. 19. The optimal design

$$\mathbf{x}_{opt} = [R_{foot}, \xi, q, D_L, \beta_b, \beta_t, \gamma_b, \gamma_t, \tau_b, \tau_t]^T = [12.73, 0.53, 0.87, 1.04, 0.80, 0.80, 12.04, 18.00, 0.50, 0.46]^T \quad (14)$$

determined after 40000 objective function evaluations is depicted in Fig. 20. It has a foot radius of $R_{foot} = 12.7$ m, a head radius of $R_{head} = 6.8$ m and a leg diameter of $D_L = 1.0$ m. The costs for one jacket substructure are $C_{total} = 2922400$ \$ in the optimal case with the two constraints satisfied. In this example, the jacket substructure is optimized according to a lifetime of 30 years.

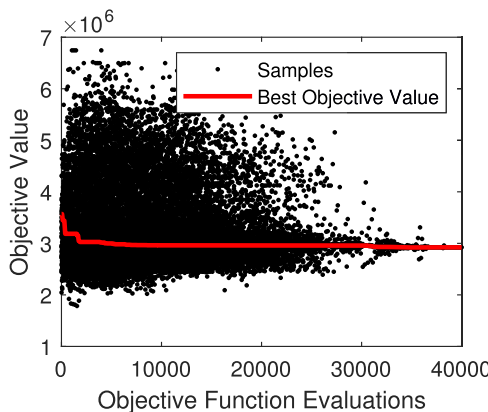


Fig. 19. Objective values of Particle Swarm on jacket cost function.

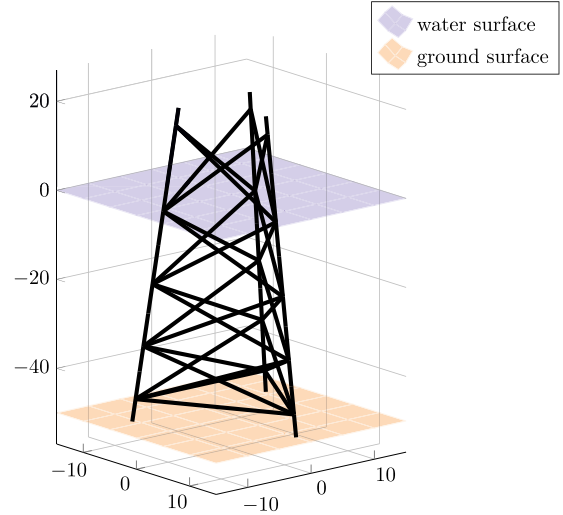


Fig. 20. Topology of optimal jacket design.

5.3. Analysis of morphing trailing edge flap with integrated multistable laminates

Morphing trailing edge flaps are promising candidates for alleviating loads in large wind turbine rotor blades. In this concept, the inflexible trailing edge of rotor blades is replaced by a flexible flap. This flap shown in Fig. 21 can be actuated dependent on variable wind conditions and improves the efficiency of the wind turbine. The morphing of the flexible flap can be achieved using multistable laminates and piezo actuators [54]. For background information regarding morphing trailing edge flaps with integrated multistable laminates, it is referred to Haldar et al. [55].

The multistable laminate considered has two stable states that are depicted in Figs. 22 and 23. The changes between the curved and straight shape are called snap-through and snap-back. They are triggered by a set of actuators placed on both sides of the bistable laminate. The bistability enables the flap to remain in one stable state, unless the actuators are triggered.

As the location of the actuators plays a crucial role in triggering the snap-through and snap-back process, the optimization is an apparent need to achieve an optimal design. Since the simultaneous optimization of all actuator locations would result in a high-dimensional design variable space, which is computationally prohibitive, only two actuators are considered. In this case, the snap-through actuators, which are placed on the bottom surface, are optimized. The actuator positions at the top surface are therefore fixed during the optimization.

As shown in Fig. 24, the snap-through actuators should be placed symmetrically on the plate, and their position can be specified by two coordinates a and b . Therefore, the two-dimensional design variable vector

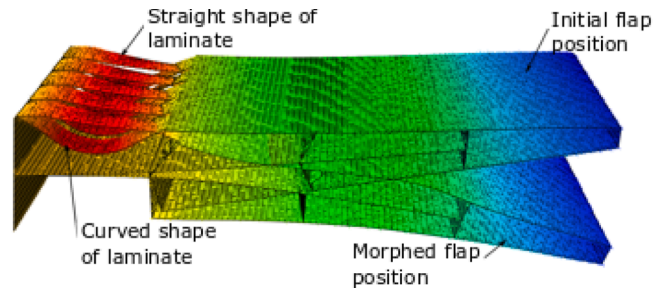


Fig. 21. FE model of a flap with bistable laminates.

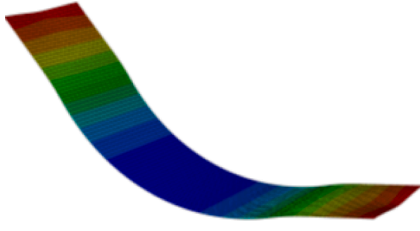


Fig. 22. Curved shape of rectangular bistable laminate.

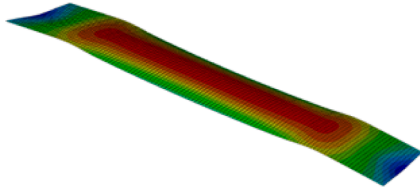


Fig. 23. Straight shape of rectangular bistable laminate.

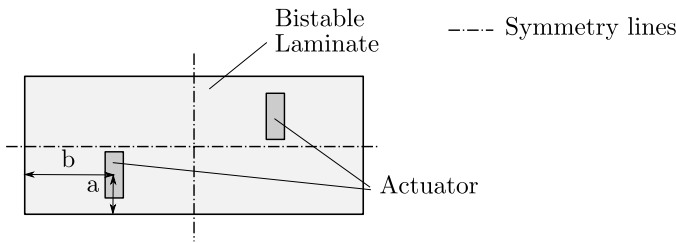


Fig. 24. Bottom view of the bistable laminate with two snap-through actuators.

$$\mathbf{x} = [a, b]^T \quad (15)$$

includes the horizontal and vertical coordinate of the geometrical center of one actuator. The second snap-through actuator is placed symmetrically to the first one.

To find the best location of the actuators, two conflicting objectives have to be considered. Firstly, it is favorable to increase the maximum out-of-plane displacement of the curved shape $|u_o|$ to maximize morphing movements of the flap. Secondly, the snap-through force, exerted by application of voltage V_{snap} to the actuators, should remain small.

Thereby, the two-objective optimization problem

$$\text{minimize } f(\mathbf{x}) = \begin{pmatrix} -|u_o(\mathbf{x})| \\ V_{\text{snap}}(\mathbf{x}) \end{pmatrix} \quad (16)$$

is formulated. A detailed FE model is used to carry out the analysis of the morphing action of respective designs. Out-of-plane displacements and snapping voltages are calculated. MOGPS is applied to carry out the optimization.

The results determined for the optimal location of snap-through actuators are illustrated in Figs. 25 and 26. Sampled solutions are displayed as black dots, whereby the Pareto-optimal points are highlighted in red. Non-dominated solutions in the left portion of the frontier shown in Fig. 25 correspond to actuator designs with high displacements up to 6.5 mm as well as high snap-through voltage. As the goal was also to minimize snap-through voltage, the best solutions in terms of snap-through voltage are located in the right portion of the Pareto frontier. The displacement is less than 4 mm, which is unfavorably small.

In Fig. 26, the Pareto-optimal solutions agglomerate mainly in two distinct areas. The points related to small values of the design variable a correspond to designs with high displacements, but high snap-through voltage. The Pareto-optimal points in the second area, comprising

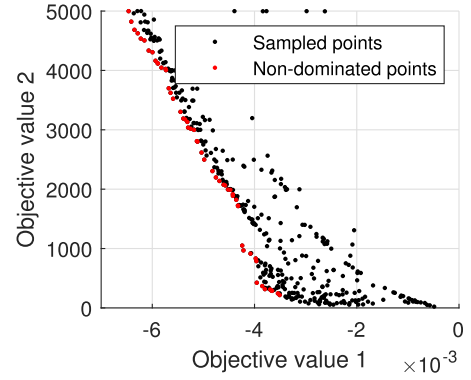


Fig. 25. Objective value space of actuator optimization with MOGPS.

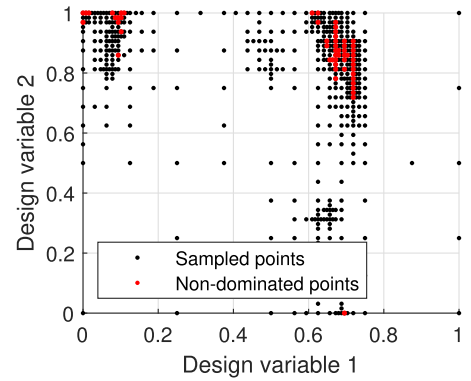


Fig. 26. Design variable space of actuator optimization with MOGPS.

greater values of $0.6 \leq a \leq 0.8$, lead to designs with reduced snapping voltage and smaller maximal displacements. According to expert preferences, the optimal arrangement is found for a displacement of $u_o = 4.2$ mm and snapping voltage of $V_{\text{snap}} = 1050$ V. The related design variables are $a = 5.58$ mm and $b = 49.4$ mm. Since the analyzed laminate has a size of 100×30 mm, this solution corresponds to an installation slightly offset in the middle of the rectangular laminate.

6. Conclusion

In this paper, EngiO – the Engineering Optimization framework – is introduced to facilitate the optimization of practical engineering problems for teaching and research purposes. The key innovation of EngiO is associated with its object-oriented software architecture. The core of the architecture is the optimization class, which inherits methods to derived algorithm classes. It constitutes the unified interface between optimization problem and algorithm and centralizes the main optimization loop. All algorithmic implementations hence follow the same comprehensible pattern of initialization, sampling and processing of results. This handling of derivative-free algorithms in one framework leads to clean concise code that is beneficial both for experienced researchers as well as undergraduated students. Supporting global and local derivative-free optimizers and single- and multi-objective optimization problems with and without constraints, EngiO is perfectly suited to facilitate engineering optimization. To demonstrate this feature in this work, three engineering problems, which greatly differ in terms of objectives, were solved.

The architecture of EngiO is designed for derivative-free algorithms only. Hence, gradient-based algorithms are not compatible with the interface defined by the architecture of EngiO. In favor of a lean code, the integration of optimization packages is not supported in the framework. Using Matlab and GNU Octave, the computation speed is a

drawback compared to other programming languages. Considering optimization of numerically expensive problems, this is insignificant due to the computation time of the model itself.

In the future, we are planning to apply the framework to new optimization problems as well as to implement additional algorithms to further improve the capabilities of EngiO. The current and future versions of the framework are available under GPLv3 license at <https://github.com/isd-luh/EngiO>.

CRedit authorship contribution statement

Ricarda Berger: Conceptualization, Methodology, Software, Writing - original draft. **Marlene Bruns:** Software, Visualization, Writing - review & editing. **Andreas Ehrmann:** Writing - review & editing. **Ayan Haldar:** Software, Visualization. **Jan Häfele:** Conceptualization, Visualization, Software. **Benedikt Hofmeister:** Conceptualization, Methodology, Software, Writing - review & editing. **Clemens**

Appendix A. Test functions

Himmelblau [56,57]

$$f(x) = (x_1^2 + x_2 - 11)^2 + (x_1 + x_2^2 - 7)^2 \quad (\text{A.1})$$

$$\text{s.t. } [-6 \quad -6]^T \leq \mathbf{x} \leq [6 \quad 6]^T$$

$$\begin{aligned} \text{Minima : } & f(3, 2) = 0 \\ & f(-2.805118, 3.131312) = 0 \\ & f(-3.779310, -3.283186) = 0 \\ & f(3.584428, -1.848126) = 0 \end{aligned}$$

Simionescu [58]

$$f(x) = 0.1x_1x_2 \quad (\text{A.2})$$

$$\text{s.t. } [-1.25 \quad -1.25]^T \leq \mathbf{x} \leq [1.25 \quad 1.25]^T$$

$$1.0 + 0.2\cos\left(8.0\arctan\frac{x_1}{x_2}\right)^2 - (x_1^2 + x_2^2) \geq 0$$

Kursawe [59]

$$f(x) = \left(\begin{array}{c} \sum_{i=1}^2 \left[-10\exp\left(-0.2\sqrt{x_i^2 + x_{i+1}^2}\right) \right] \\ \sum_{i=1}^3 \left[|x_i|^{0.8} + 5\sin(x_i^3) \right] \end{array} \right) \quad (\text{A.3})$$

$$\text{s.t. } [-5 \quad -5 \quad -5]^T \leq \mathbf{x} \leq [5 \quad 5 \quad 5]^T$$

$$\begin{aligned} \text{Minima : } & f(+0.84852813, +0.84852813) = -0.072 \\ & f(+0.84852813, -0.84852813) = -0.072 \\ & f(-0.84852813, +0.84852813) = -0.072 \\ & f(-0.84852813, -0.84852813) = -0.072 \end{aligned}$$

References

- [1] Wolpert DH, Macready WG. No free lunch theorems for optimization. *IEEE Trans Evol Comput* 1997;1(1):67–82. <https://doi.org/10.1109/4235.585893>.
- [2] Parejo JA, Ruiz-Cortés A, Lozano S, Fernandez P. Metaheuristic optimization frameworks: a survey and benchmarking. *Soft Comput* 2012;16(3):527–61. <https://doi.org/10.1007/s00500-011-0754-8>.
- [3] Rios LM, Sahinidis NV. Derivative-free optimization: a review of algorithms and comparison of software implementations. *J Global Optim* 2013;56(3):1247–93. <https://doi.org/10.1007/s10898-012-9951-y>.
- [4] Eldred M, Outka D, Bohnhoff W, Witkowski W, Romero V, Ponslet E, et al. Optimization of complex mechanics simulations with object-oriented software design. *Comput Model Simul Eng* 1996;1(3):323–52. <https://doi.org/10.2514/6.1995-1433>.
- [5] Humeau J, Liefoghe A, Talbi E-G, Verel S. ParadisEO-MO: from fitness landscape analysis to efficient local search algorithms. *J Heuristics* 2013;19(6):881–915. <https://doi.org/10.1007/s10732-013-9228-8>.
- [6] Bleuler S, Laumanns M, Thiele L, Zitzler E. PISA — A platform and programming language independent interface for search algorithms. In: Goos G, Hartmanis J, van Leeuwen J, Fonseca CM, Fleming PJ, Zitzler E, et al., editors. *Evolutionary multi-criterion optimization. Lecture Notes in Computer Science*, 2632. Berlin, Heidelberg: Springer Berlin Heidelberg; 2003. ISBN 978-3-540-01869-8. p. 494–508. https://doi.org/10.1007/3-540-36970-8_35.
- [7] Tazowski P, Blachowski B, Lógó J. Functor-oriented topology optimization of elasto-plastic structures. *Adv Eng Softw* 2019;135:102690. <https://doi.org/10.1016/j.advengsoft.2019.102690>.
- [8] Gray JS, Moore KT, Naylor BA. OpenMDAO: an open-source framework for multidisciplinary analysis and optimization. *Proceedings of the 13th AIAA/ISSMO*

Hübler: Supervision, Writing - review & editing. **Raimund Rolfes:** Supervision, Project administration, Funding acquisition.

Declaration of Competing Interest

The authors declare that they have no known competing financial interests or personal relationships that could have appeared to influence the work reported in this paper.

Acknowledgements

This work was funded by the Deutsche Forschungsgemeinschaft (DFG, German Research Foundation) – SFB 871/3 – 119193472. Moreover, we acknowledge the financial support of the German Federal Ministry for Economic Affairs and Energy (BMWi) for the research projects *Multivariate Schadensmonitoring von Rotorblättern* – 0324157A and *SmartBlades2* – 0324032 C that enabled this work.

- multidisciplinary analysis and optimization conference, Fort Worth, TX, AIAA, AIAA-2010-9101. Fort Worth, Texas: AIAA; 2010. <https://doi.org/10.2514/6.2010-9101>.
- [9] Gray JS, Hwang JT, Martins JRRA, Moore KT, Naylor BA. OpenMDAO: an open-source framework for multidisciplinary design, analysis, and optimization. *Struct Multidiscip Optim* 2019;59(4):1075–104. <https://doi.org/10.1007/s00158-019-02211-z>.
- [10] Izzo D. PyGMO and pyKEP: open source tools for massively parallel optimization in astrodynamics (the case of interplanetary trajectory optimization). *Proceedings of the fifth international conference on astrodynamics tools and techniques, ICATT. 2012.*
- [11] Perez RE, Jansen PW, Martins JRRA. pyOpt: a Python-based object-oriented framework for nonlinear constrained optimization. *Struct Multidiscip Optim* 2012; 45(1):101–18. <https://doi.org/10.1007/s00158-011-0666-3>.
- [12] Jones E., Oliphant T., Peterson P., et al. SciPy: open source scientific tools for Python. 2001. <http://www.scipy.org/>.
- [13] Hart WE, Watson J-P, Woodruff DL. Pyomo: modeling and solving mathematical programs in Python. *Math Program Comput* 2011;3(3):219–60. <https://doi.org/10.1007/s12532-011-0026-8>.
- [14] Fortin F-A, Rainville F-MD, Gardner M-A, Parizeau M, Gagné C. DEAP: evolutionary algorithms made easy. *J Mach Learn Res* 2012;13:2171–5.
- [15] Durillo JJ, Nebro AJ. jMetal: a Java framework for multi-objective optimization. *Adv Eng Softw* 2011;42(10):760–71. <https://doi.org/10.1016/j.advengsoft.2011.05.014>.
- [16] Lukasiwycz M, Glaß M, Reimann F, Teich J. Opt4J - A modular framework for meta-heuristic optimization. *Proceedings of the genetic and evolutionary computing conference, GECCO. 2011. p. 1723–30.*Dublin, Ireland
- [17] MATLAB Optimization Toolbox. 2020. The MathWorks, Natick, MA, USA.
- [18] MATLAB Global Optimization Toolbox. 2020. The MathWorks, Natick, MA, USA.
- [19] Marelli S, Sudret B. UQLab: a framework for uncertainty quantification in Matlab. In: Beer, editor. *Vulnerability, uncertainty, and risk*. American Society of Civil Engineers; 2014, ISBN 9780784413609. p. 2554–63. <https://doi.org/10.1061/9780784413609.257>.
- [20] Zuo W. An object-oriented graphics interface design and optimization software for cross-sectional shape of automobile body. *Adv Eng Softw* 2013;64:1–10. <https://doi.org/10.1016/j.advengsoft.2013.04.003>.
- [21] Qin H, Liu Z, Liu Y, Zhong H. An object-oriented matlab toolbox for automotive body conceptual design using distributed parallel optimization. *Adv Eng Softw* 2017;106:19–32. <https://doi.org/10.1016/j.advengsoft.2017.01.003>.
- [22] Patelli E. COSSAN: a multidisciplinary software suite for uncertainty quantification and risk management. Cham: Springer International Publishing; 2017, ISBN 978-3-319-12385-1. p. 1909–77.
- [23] Löfberg J. YALMIP: a toolbox for modeling and optimization in MATLAB. *Proceedings of the CACSD conference. 2004.*Taipei, Taiwan
- [24] Holmström K. The TOMLAB optimization environment in Matlab. *Adv Model Optim* 1999;1(1):47–69.
- [25] Global optimum determination by linking and interchanging kindred evaluators. 2018. <https://github.com/rodyo/FEX-GODLIKE>.
- [26] Jonkman J, Buhl Jr ML. FAST user's guide. Tech. Rep. EL-500-38230. National Renewable Energy Laboratory; 2005.
- [27] ABAQUS Documentation. 2019. Dassault Systèmes, Providence, RI, USA.
- [28] Beume N, Fonseca CM, Lopez-Ibanez N, Paquete L, Vahrenhold J. On the complexity of computing the hypervolume indicator. *IEEE Trans Evol Comput* 2009;13(5):1075–82. <https://doi.org/10.1109/TEVC.2009.2015575>.
- [29] Coello Coello CA. Theoretical and numerical constraint-handling techniques used with evolutionary algorithms: a survey of the state of the art. *Comput Methods Appl MechEng* 2002;191(11–12):1245–87. [https://doi.org/10.1016/S0045-7825\(01\)00323-1](https://doi.org/10.1016/S0045-7825(01)00323-1).
- [30] Wright SJ. Coordinate descent algorithms. *Math Program* 2015;151(1):3–34. <https://doi.org/10.1007/s10107-015-0892-3>.
- [31] Schwefel H-P. *Numerical optimization of computer models*. Chichester: Wiley; 1981, ISBN 0471099880.
- [32] Goldberg DE. *Genetic algorithms in search, optimization and machine learning*. 1st ed. Boston, MA, USA: Addison-Wesley Longman Publishing Co., Inc.; 1989, ISBN 0201157675.
- [33] Kirkpatrick S, Gelatt CD, Vecchi MP. Optimization by simulated annealing. *Science (New York, NY)* 1983;220(4598):671–80. <https://doi.org/10.1126/science.220.4598.671>.
- [34] Kennedy J, Eberhart R. Particle swarm optimization. *Proceedings of ICNN'95 – international conference on neural networks. vol. 4; 1995. p. 1942–8.* <https://doi.org/10.1109/ICNN.1995.488968>.
- [35] Geem ZW, Kim JH, Loganathan GV. A new heuristic optimization algorithm: harmony search. *Simulation* 2016;76(2):60–8. <https://doi.org/10.1177/003754970107600201>.
- [36] Hofmeister B, Bruns M, Rolfes R. Finite element model updating using deterministic optimisation: a global pattern search approach. *Eng Struct* 2019;195: 373–81. <https://doi.org/10.1016/j.engstruct.2019.05.047>.
- [37] Hooke R, Jeeves TA. “Direct Search” solution of numerical and statistical problems. *J ACM* 1961;8(2):212–29. <https://doi.org/10.1145/321062.321069>.
- [38] Yang X-S. *Nature-inspired metaheuristic algorithms*. 2nd ed. Frome: Luniver Press; 2010, ISBN 1905986289.
- [39] Marler RT, Arora JS. Survey of multi-objective optimization methods for engineering. *Struct Multidiscip Optim* 2004;26(6):369–95. <https://doi.org/10.1007/s00158-003-0368-6>.
- [40] Deb K, Agrawal S, Pratap A, Meyarivan T. A fast elitist non-dominated sorting genetic algorithm for multi-objective optimization: NSGA-II. In: Goos G, Hartmanis J, van Leeuwen J, Schoenauer M, Deb K, Rudolph G, et al., editors. *Parallel problem solving from nature PPSN VI. Lecture Notes in Computer Science, vol. 1917*. Berlin, Heidelberg: Springer Berlin Heidelberg; 2000, ISBN 978-3-540-41056-0. p. 849–58. https://doi.org/10.1007/3-540-45356-3_83.
- [41] Deb K, Pratap A, Agarwal S, Meyarivan T. A fast and elitist multiobjective genetic algorithm: NSGA-II. *IEEE Trans Evol Comput* 2002;6(2):182–97. <https://doi.org/10.1109/4235.996017>.
- [42] Brockhoff D, Tran T-D, Hansen N. Benchmarking numerical multiobjective optimizers revisited. In: Esparcia-Alcázar AI, Silva S, Jiménez-Laredo JL, editors. *Proceedings of the 2015 on genetic and evolutionary computation conference - GECCO '15*. New York, New York, USA: ACM Press; 2015, ISBN 9781450334723. p. 639–46. <https://doi.org/10.1145/2739480.2754777>.
- [43] Mottershead JE, Friswell MI. Model updating in structural dynamics: a survey. *J Sound Vib* 1993;167(2):347–75. <https://doi.org/10.1006/jsvi.1993.1340>.
- [44] Simoen E, De Roeck G, Lombaert G. Dealing with uncertainty in model updating for damage assessment: a review. *Mech Syst Signal Process* 2015;56-57:123–49. <https://doi.org/10.1016/j.ymssp.2014.11.001>.
- [45] Bruns M, Hofmeister B, Pache D, Rolfes R. Finite element model updating of a wind turbine blade—a comparative study. *Proceedings of the 6th international conference on engineering optimization*. Springer International Publishing; 2019. p. 569–80. https://doi.org/10.1007/978-3-319-97773-7_51.
- [46] Jonkman J, Butterfield S, Musial W, Scott G. Definition of a 5-MW reference wind turbine for offshore system development. Tech. Rep. NREL/TP-500-38060, 947422. National Renewable Energy Laboratory; 2009. <https://doi.org/10.2172/947422>.
- [47] Allemang RJ, Brown DL. A correlation coefficient for modal vector analysis. *Proceedings of the 1st international modal analysis conference. vol. 1; 1982. p. 110–6.*
- [48] Offshore wind: industry's journey to GBP 100/MWh cost breakdown and technology transition from 2013 to 2020. Tech. Rep. BVGassociates; 2013.
- [49] Häfele J, Gebhardt CG, Rolfes R. A comparison study on jacket substructures for offshore wind turbines based on optimization. *Wind Energy Sci* 2019;4(1):23–40. <https://doi.org/10.5194/wes-4-23-2019>.
- [50] Häfele J, Damiani R, King R, Gebhardt CG, Rolfes R. A systematic approach to offshore wind turbine jacket pre-design and optimization: geometry, cost, and surrogate structural code check models. *Wind Energy Sci Discuss* 2018:1–29. <https://doi.org/10.5194/wes-2018-39>.
- [51] Häfele J, Damiani R., King R., Gebhardt C.G., Rolfes R.. Supplement to a systematic approach to offshore wind turbine jacket pre-design and optimization: geometry, cost, and surrogate structural code check models. 2018b. 10.5194/wes-3-553-2018-supplement.
- [52] Veritas D.N. Fatigue design of offshore steel structures. 2016.
- [53] Standard N.. N-004 Design of steel structures. 2004;Rev. 2.
- [54] Schultz MR, Wilkie WK, Bryant RG. Investigation of self-resetting active multistable laminates. *J Aircr* 2007;44(4):1069–76.
- [55] Haldar A, Reinoso J, Jansen E, Rolfes R. Thermally induced multistable configurations of variable stiffness composite plates: semi-analytical and finite element investigation. *Compos Struct* 2018;183:161–75. <https://doi.org/10.1016/j.compstruct.2017.02.014>.
- [56] Himmelblau DM. *Applied nonlinear programming*. New York, NY: McGraw-Hill; 1972, ISBN 0070289212.
- [57] Jamil M, Yang X-S. A literature survey of benchmark functions for global optimisation problems. *Int J Math ModellNumer Optim* 2013;4(2):150–94.
- [58] Simionescu PA. *Computer-aided graphing and simulation tools for AutoCAD users*. Chapman & Hall / CRC Computer and Information Science Series. Hoboken: Taylor and Francis; 2015, ISBN 9781482252903.
- [59] Kursawe F. A variant of evolution strategies for vector optimization. *Proceedings of the international conference on parallel problem solving from nature*. Springer; 1990. p. 193–7. <https://doi.org/10.1007/BFb0029752>.

4 Optimization of Blend Repairs

4.1 Research Context

Geometric variations of compressor blades have been studied from different scientific perspectives for a long time [62, 27]. In particular, changes of the blade profiles are of interest for the aerodynamic flow around the blade [96] and the blade mechanics [82]. In terms of mechanical properties, sensitivity studies of blade variations are performed with regard to natural frequencies and modes shapes of blades [30], vibration amplitudes [28], mistuning [85] and, endurance limits [83].

Paper B addresses the influence of blade geometry by analyzing changes in natural frequencies and mode shapes of compressor blisk blades. In contrast to other works mentioned, the paper does not consider variances due to manufacturing or operation. The impact of blend repairs on blade frequencies is studied instead, because the blend could be regarded as a special case of geometric change in the blade contour. Unlike other variations, blends are firstly introduced locally and secondly by purpose. Works that also deal specifically with this repair are presented by Day et al. [44] and Karger and Bestle [95]. These works and the work presented in paper B are united in the pursuit of a systematic approach to appropriate repairs. However, the combination of numerical simulation of blend repairs, evaluation of objectives, and optimization strategy is unique for the approach presented by the author of this thesis.

4.2 Methods

In order to evaluate the effect of blend repairs on structural properties, a blend repair model is first developed in paper B. To this end, a parametric description is introduced that specifies the blend repair design by three scalar variables. These design variables define the size and location of an ellipsoidal volume. The final blend contour results from a Boolean operation of the ellipsoid with the nominal blade. According to the blend thus defined, the FE mesh of the nominal model is modified by applying a customized local remeshing procedure. This preserves most of the nominal discretization and allows automated numerical simulation. The second part of paper B deals with the application of numerical optimization to improve blend repairs. A multi-objective approach [114] is adopted to consider two frequency criteria in the decision process. Both objective functions are related to the natural frequencies of blades since the frequency tuning is the structural aspect most affected by blending. The first objective function considers the change in frequencies relative to nominal ones to prevent mistuning. Since in the operating range mainly six vibration modes are relevant, the worst case out of the six relative frequency changes determines the first objective. The second objective function is inspired by frequency criteria also used in the early design phase. It is computed from the minimal relative distance of the six natural frequencies to excitation frequencies. The optimization framework EngiO, which is introduced in paper A, is utilized

to perform multi-objective optimization. In paper B, the Multi-Objective Global Pattern Search [86] approach is used. All modal quantities, which are involved in the evaluation of objective functions of the optimization task, are computed using the commercial FE software Abaqus.

4.3 Results and Outlook

Using the developed blending model the sensitivities of different blend sizes and positions are studied for the first six natural frequencies of the blade. Therewith, the correlation between the mode shapes and the spatial position of the blend repairs is elaborated. The main outcome of paper B is the Pareto optimal set of blend repair solutions presented for two different damage patterns. According to the damage pattern considered, the Pareto frontier has different characteristics. While in the first example the frontier has a continuous course, the second damage pattern shows a discontinuity. By considering related blend shapes, the repair design has to be selected from the set of Pareto optimal solutions according to further engineering preferences.

Since the removed material leads to a detuning of the single blade and a change in the aerodynamic contour, the optimization problem would greatly benefit from the consideration of the mistuning of the entire blisk and the aerodynamic properties.

4.4 Paper B: A Two-Objective Design Optimisation Approach for Blending Repairs of Damaged Compressor Blisks

The following paper is published in *Aerospace Science and Technology*, Volume 105, October 2020, pages 106022 (<https://doi.org/10.1016/j.advengsoft.2020.102959>).

Author Contribution

The main work was done by the author of this thesis. Benedikt Hofmeister contributed with conceptualization and gave technical suggestions on the entire publication. Cristian Gebhardt and Raimund Rolfes contributed with advisory and supporting work.



A two-objective design optimisation approach for blending repairs of damaged compressor blisks

Ricarda Berger*, Benedikt Hofmeister, Cristian G. Gebhardt, Raimund Rolfes

Leibniz Universität Hannover, Institute of Structural Analysis, Germany

ARTICLE INFO

Article history:

Received 1 October 2019
 Received in revised form 24 February 2020
 Accepted 10 April 2020
 Available online 16 June 2020
 Communicated by Saravanos Dimitris

Keywords:

Compressor blisk
 Repair
 Blending
 Multi-objective optimisation
 Vibration

ABSTRACT

The blending of compressor blades leads to a permanent modification of the blade geometry. According to these geometric changes, the modal properties of refurbished blades will generally differ from the nominal blade design. Currently, the structural integrity of refurbished blades is maintained by only allowing blends within predefined geometric limits, where the final geometry of the blend is based on a case-by-case decision made by the technician.

This work contributes to repair decisions by utilising multi-objective optimisation methods to find structurally optimised blend designs. A parameterised blending model is introduced to uniquely specify the repair design for any blade geometry. Blend designs are analysed systematically by linking the blending model with the Finite Element model of a bladed sector. The influence of the blending shape is evaluated by means of blade-alone frequencies and vibration mode shapes. A two-objective optimisation problem is derived from the frequency tuning of blended blades. The first objective results from the deviation of natural frequencies from the nominal ones, the second objective considers the proximity of natural frequencies to resonance frequencies. Moreover, the approach is applied to one bladed sector of a compressor blisk. The sensitivities of the blend geometry regarding the first six vibration modes are studied. Two damage patterns at different positions at the leading edge of the blade are chosen to exemplarily demonstrate the capability of the proposed approach. For both damage patterns, the set of Pareto optimal solutions is found using Global Pattern Search. The courses of the Pareto frontiers clearly differ and are identified to be specific for each damage pattern. Depending on the damage pattern, discontinuous as well as continuous Pareto frontiers are determined. Providing Pareto optimal solutions for repair designs, the developed approach can be understood as a valuable complement to purely experience-based design decisions.

© 2020 Elsevier Masson SAS. All rights reserved.

1. Introduction

The maintenance and repair of jet engine parts is becoming increasingly important with more elaborated and complex part designs. About 80 percent of defect blade integrated disks (blisks) are repaired by blending [1]. The repair technique involves the removal of the blade material around a defect to prevent crack growth [2]. The repair of blades by blending, therefore, leads to permanent changes in the geometry and the resulting contour always deviates from the nominal shape. In most cases, the repairs are carried out manually and appropriate decisions during the maintenance procedure are taken individually by maintenance technicians. The repair design of the blend and the final geometry of the repaired blade is thus the result of subjective assessments.

Several studies on blade geometries have shown that even small geometric deviations from the initial blade geometry significantly impact the structural and aerodynamic properties. Garzon and Darmofal [3] investigated the effect of geometric variances with focus on the aerodynamic performance. They employed the Principal Component Analysis (PCA) to capture the essential geometric information of the blade surface and performed a probabilistic blade passage analysis. The aerodynamic performance as well as the mechanical behaviour of a fan blisk were recently analysed by Schnell et al. [4]. Due to the manufacturing tolerances, variations in frequencies up to a standard deviation of 3 Hz were determined. Performance degradation caused by geometric modifications on the leading edge were proven by Keller et al. [5]. Publications focusing on the structural properties of compressor blades are provided by Brown et al. [6,7]. A forced response analysis was conducted and fatigue strength was evaluated for scattering fan geometries of an integrally bladed rotor. The parametrisation and modelling

* Corresponding author.

E-mail address: r.berger@isd.uni-hannover.de (R. Berger).

of manufacturing tolerances was further addressed by Heinze et al. [8] and Backhaus et al. [9]. Scattering endurance limits and natural frequencies were computed for manufactured compressor blades. In addition to the blade-alone frequencies, the frequency mistuning pattern is considered by Maywald et al. [10]. A model update procedure involving mesh morphing of nominal blades was presented. The amplification of vibrations due to blending was currently emphasised by Beck et al. [11]. They investigated the forced response of small and large blends in the context of a mistuned rotor. The studies demonstrate that not only manufacturing tolerances but also intentionally modified blades have to be considered more precisely. In particular, repair designs should be regarded, because they can be influenced more actively in contrast to the manufacturing tolerances.

So far, there are only few works that deal with the integrity of repaired blades. The challenges involved in high-tech repairs and manufacturing of blisks were summarised by Bussmann et al. [12,2]. Tip and edge blends of blades were systematically evaluated by Day et al. [13], who built up a database of different blending shapes. The crack ignition on circular blending shapes in repaired plates was analysed by Burchil and Heller [14]. The fatigue strength of repaired impeller blades was studied by Xu et al. [15]. The works are usually based on simulation models that are parameterised according to the design, e.g. [16]. Therewith, the models can be integrated in a numerical optimisation approach. A multi-objective problem formulation was proposed by Karger and Bestle [17]. A D-shaped blending was optimised according to blade mass and fatigue strength. Results were presented for designs on the Pareto frontier. Multi-objective optimisation of blends with regard to blade mass and frequencies using a simplified simulation model were conducted by Berger et al. [18]. Furthermore, optimisation methods are extensively used during the aerodynamic and structural design phase in order to find optimal nominal blade shapes [19–22]. Two-objective airfoil shape optimisation is addressed by Lim and Kim [23], who propose a combination of evolutionary and direct search algorithms for efficient optimisation of lift and drag conditions.

In this paper, we focus on the design of repairs by blending from a structural point of view. A new approach is developed to utilise multi-objective optimisation to find individually optimised blending shapes. This enables to consider the susceptibility of the blades to vibration that is defined by two frequency criteria simultaneously. On the one hand, the natural frequencies of the blended blade are supposed to be close to the natural frequencies of the nominal blade design. Therefore, the relative change in all natural frequencies should be small. On the other hand, like in the initial design process, resonance conditions have to be avoided. The susceptibility of the blades to vibration is decreased by maximising the distances between natural and related excitation frequencies. In contrast to existing works, we thus combine criteria of initial design and repair design in our integrated optimisation procedure. Since the two goals may conflict each other, we propose a two-objective optimisation formulation. The calculation of Pareto optimal solutions has the advantage that the weighting of objectives is done a posteriori according to user preferences. Therefore, the optimisation ends up with Pareto optimal solutions that give first guidance to the technicians. The analysis of variations in aerodynamic performance falls outside the scope of the current work and thus is left out.

In the first part, a unified description of blending shapes is introduced, which allows for an automated generation of blends. For the evaluation of repair designs, we further concentrate on natural frequencies of the blade-alone model. The modelling of aerodynamic and mistuning is omitted in favour of fast objective function evaluation. In section 3, the two-objective optimisation problem is derived from the conflicting frequency criteria. Finally, a trade-off

between the objectives is exemplarily shown by computing optimal solutions for different damage patterns. Defects are introduced at two different positions of the leading edge of one compressor blisk sector. Using a Multi-Objective Pattern Search, Pareto optimal blending shapes are successfully determined for both fictional examples. On the basis of the two examples, it is shown that the course of the frontier may differ in individual cases. The final design of the blend can be chosen from the solutions on the Pareto frontier and hence the optimisation results complement experience-based maintenance decisions.

2. Numerical modelling of blend and blade

The optimisation of blend geometries involves the automated generation of numerical models and computation. Therefore, we firstly introduce models and the assumptions made during modelling.

2.1. Parameterised blending shape

For the modelling of blends, we propose a parameterised representation of the blending shape. According to the typical shape of blends, we choose an ellipsoid as illustrated in Fig. 1(a). The geometry of the blade is assumed to be according to the nominal design. The blending shape shown in Fig. 1(b)–(c) results from the intersection of the ellipsoid and the blade, where the intersection of both volumes specifies the material portion removed. The ellipsoid therefore corresponds to the blending contour and not to the actual machining tool used.

The actual portion removed depends on the size and position of the ellipsoid. The size of the ellipsoid in Fig. 1(a) is determined by the length of its three principal axes, r_x , r_y and r_z .

Since blend repairs are mainly performed at the leading and trailing edges, we further locate the ellipsoid relative to the edge of the blade. As shown in Fig. 1(b), a global coordinate frame $\{X, Y, Z\}$ and a local coordinate frame $\{x, y, z\}$ are used to describe the geometry of ellipsoid and blade. The global coordinate frame is oriented such that X points in axial, Y in tangential and Z in radial direction of the blisk. The origin of the local coordinate frame $\{x, y, z\}$ coincides with the centre of the ellipsoid X_C . The principal axes are aligned with the local coordinate frame. The position along the edge is parameterised by the scalar distance to the blade tip e , which is normalised according to the nominal blade height. The distance between the centre of the ellipsoid and the leading edge is specified by r'_x (Fig. 1(c)). The x -axis of the local coordinate frame is parallel to the camber line at the edge. The z -axis of the local coordinate frame is parallel to the global Z -direction. Finally, the y -axis is found orthogonal to the x - and z -axis by the right hand rule.

By the definition of radii r_x , r_y and r_z as well as the local coordinate frame $\{x, y, z\}$, any size and position of ellipsoidal blending shape can be modelled. We parameterise the blend by the machining depth and decompose the first principal axis

$$r_x = d + r'_x, \quad (1)$$

where d denotes the maximum machining depth. This has the main advantage that the parameterisation refers to the final blending shape rather than to the ellipsoid itself. Moreover, the definition of the radius r_x according to Eq. (1), enforces the size of the ellipsoid to always be larger than the machining depth. Parameter combinations, where $d > r_x$, are prevented.

Using the coordinate frames introduced, any point P can be specified in terms of global or local coordinates. Coordinates are mapped using the affine transformation

$$\mathbf{x}_P = \mathbf{R}^T \cdot (\mathbf{X}_P - \mathbf{X}_C), \quad (2)$$

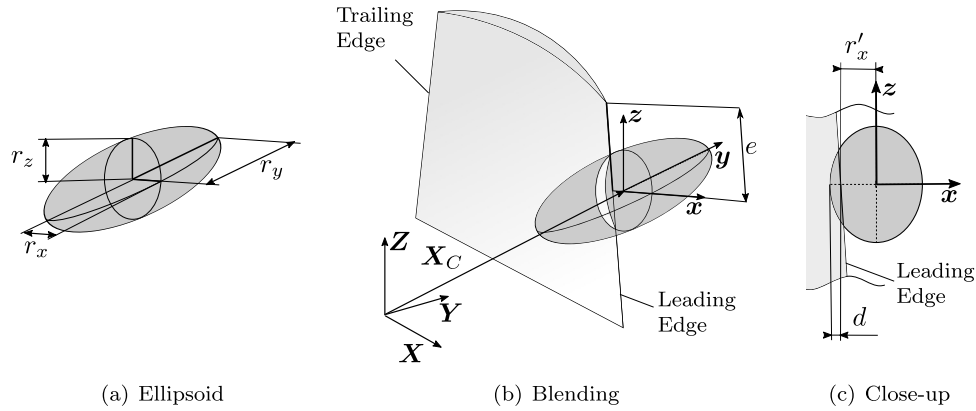


Fig. 1. Ellipsoid (a) and position of the blending shape at the leading edge of a compressor blade (b) and view of $x - z$ plane (c).

where \mathbf{R} is the rotation matrix, \mathbf{x}_p are the local and \mathbf{X}_p the global point coordinates. The rotation matrix \mathbf{R} is an orthogonal matrix and comprises the basis vectors of the local coordinate frame in each of its columns.

In addition to the blending shape, the damaged portion of the blade is modelled. We choose a point cloud to describe the defect of the blade. Depending on the defect, different numbers of points may be necessary to describe the damage pattern sufficiently accurate. In this context, the parameterisation of the blending shape by an ellipsoid is advantageous. Each damaged point is transformed to local coordinates (x_p, y_p, z_p) according to Eq. (2). The evaluation of

$$\frac{x_p}{r_x} + \frac{y_p}{r_y} + \frac{z_p}{r_z} \leq 1 \quad (3)$$

efficiently checks, whether the defect is removed by the blending procedure. If the inequality condition is fulfilled, the blending completely removes the damage. Otherwise, the blending design is not permissible in the case considered.

2.2. Blade-alone model

A compressor blisk designed for a test rig is taken as nominal design to demonstrate the applicability of the blending model. The blisk is made of titanium alloy and installed in a 1.5-stage axial compressor for aerodynamic experiments [24]. The nominal blisk is rotationally symmetric and consists of 24 blades with a blade height of about 70 mm. Following the assumption that manufacturing tolerances can be neglected, all bladed sectors are identical and the whole blisk can be modelled by one periodic sector. The geometry of one periodic sector and the corresponding nominal Finite Element (FE) mesh are shown in Fig. 2.

In the depicted nominal case, the sector is meshed with about 24000 quadratic tetrahedral and hexahedral elements and comprises about 42000 nodes. The type and order of elements is chosen according to the local complexity of the geometry and the non-linear deformation. Following the analytical blending model introduced in the previous section, the geometry of the nominal blade is modified to the blended case. Typically, there are two ways to implement an interface between the analytical expression and numerical simulation. One approach is based on the modification of the nominal CAD data and therefore involves a complete remeshing of the structure [25]. Alternatively, changes may be made on the discretised nominal FE model [26]. We propose a mesh-based preprocess to transfer the structural changes to the FE simulation. The blended region is remeshed locally, while the rest of the mesh is maintained. A pure mesh morphing procedure is not applicable due to complex geometry and large blending shapes.

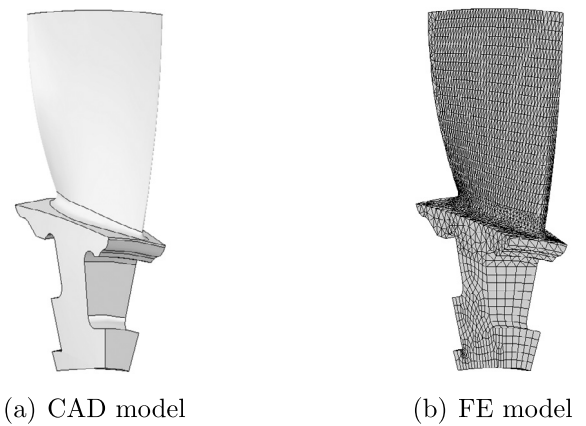


Fig. 2. Blade geometry (a) and FE model (b) of the compressor blisk sector used for numerical studies.

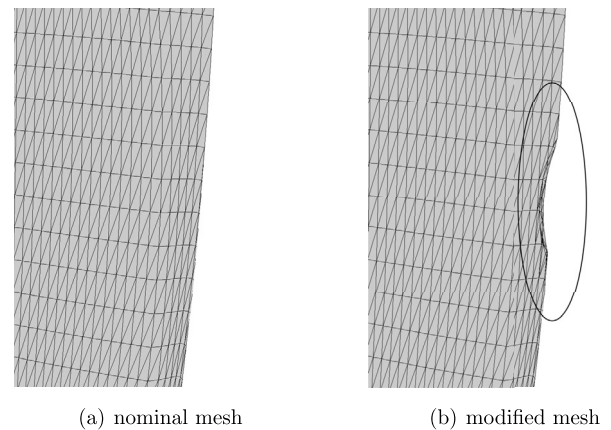


Fig. 3. Close-up of nominal (a) and locally modified FE mesh (b).

Consequently, the local remeshing around the blend is a trade-off between complete new mesh generation and morphing. The resulting mesh without and with blend is shown in Fig. 3. The quality of the inserted FE elements is not as good as that of the initial ones. However, it is sufficient for the modal analysis performed subsequently.

The displacements in axial and radial direction are constrained at appropriate surfaces near the rotor hub. The rotation of the sector is restricted by imposing appropriate displacement constraints on the sector faces. The effect of mistuning is not considered here, because we limit our analysis on a single sector only. For the influence of mistuning, we refer to [27], where we put the emphasis

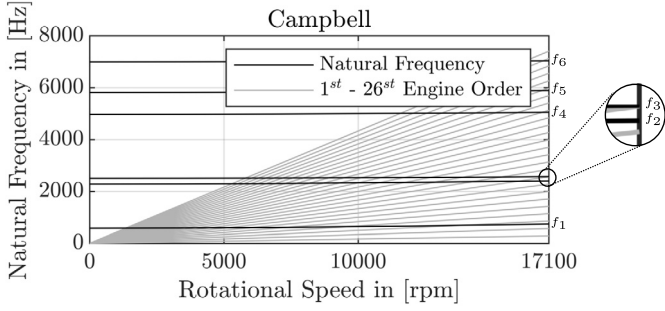


Fig. 4. Campbell diagram of blisk sector covering the operating range up to nominal speed and the first six natural frequencies f_1 - f_6 .

on aerodynamic and structural mistuning. Material properties are specified according to the mechanical properties of Ti-6Al-4V at nominal operating temperature [28]. The vibration behaviour is analysed performing modal analysis, assuming a nodal diameter of twelve, which is $N/2$. The modal analysis includes pre-stresses according to the rotational speed and steady pressure forces. The natural frequencies and vibration modes are evaluated using the commercial FE solver Abaqus. As typical for rotating machinery, we use the Campbell diagram in Fig. 4 to display the natural and excitation frequencies. The intersections of engine order lines and natural frequencies denote resonance conditions, which may lead to high vibration amplitudes and must be avoided especially at nominal operating speed.

The natural frequencies shown in the Campbell diagram vary with rotational speed. Changes in frequencies are quite small, but become apparent, if frequencies at standstill are compared with the frequencies at nominal speed. The first natural frequency for example increases from 579 Hz to 738 Hz. At a nominal rotational speed of 17100 rpm most natural frequencies show no resonances. Only the third natural frequency of the nominal design is relatively close to one engine order line. This has been accepted during the initial design process, as it was primarily driven by aerodynamic interests. The monitoring system of the 1.5-stage axial compressor ensures a safe operation of the blisk in the test rig. Further, we focus on the first six vibration modes only, because the highest excitation considered is the 26th engine order. This excitation results from the upstream stator guide vanes in the rig. Higher excitation orders are not considered.

In case of blend repair, the shape of the blade is modified locally and the blade geometry is changed. Thus, the Campbell diagram of the repaired blade differs from the nominal one, even if the loading conditions are assumed to remain unchanged. Sometimes, even the mode shapes interchange due to larger geometric modifications. Moreover, blending always involves the removal of material which reduces the total mass of the part, and thus natural frequencies consequently tend to increase. In addition, the removed portion of material has an impact on the local stiffness of the blade, where natural frequencies may decrease as a result. The influence on the natural frequency strongly depends on the location of blending and the related mode shape. In general, repairs in regions with high vibration amplitudes mainly reduce the resonating mass and result in higher frequencies. Next to a vibration node, the effect of stiffness reduction is more significant. In order to analyse the impact of blend repairs on the structural behaviour of the single bladed sector more precisely and to quantify frequency deviations, simulations of the modified blade are carried out.

3. Optimal design of blends

In this section, the proposed optimisation setup is illustrated. The two-objective optimisation problem formulation is given and

the optimisation algorithm used to efficiently solve the problem is introduced.

3.1. Evaluation criteria

Based on the blade-alone model and the parameterised blending shape, the structural response of different blade designs can be determined. To quantify the impact of blending on the modal properties, we firstly consider the natural frequencies, which vary due to the blending introduced. To prevent mistuning in the assembly or blisk, the variation from nominal design frequencies should remain small. The quality of the blending is hence assessed by

$$\delta_i^{nom} = |f_i - f_i^{nom}| \quad (4)$$

comparing the modified f_i with the related nominal natural frequency f_i^{nom} for each vibration mode i . The criterion, as it is stated in Eq. (4), is only valid if the order of the blade modes does not change. Since higher frequencies tend to larger variations, relative frequency deviations are considered instead. We define the maximum relative frequency deviation

$$\delta^{nom} = \max_i \frac{\delta_i^{nom}}{f_i^{nom}} \quad (5)$$

over all modes to be the most severe outcome.

However, even if the relative deviation δ^{nom} is small, natural frequencies may shift towards the closest excitation frequency. Especially, if the design frequency is close to the excitation, the risk of meeting resonance conditions increases. Therefore, in addition to the nominal frequencies, we consider the closest excitation frequency

$$f_i^{exc} = \min_j |f_i - f_{j,exc}| \quad (6)$$

of all possible excitation frequencies $f_{j,exc}$ for each vibration mode i at nominal rotational speed. The absolute distance

$$\delta_i^{exc} = |f_i - f_i^{exc}| \quad (7)$$

between the modified natural frequency f_i and the frequency of the closest engine order line is analysed. Only the distance is evaluated, so that the two cases illustrated in Fig. 5(a) and (b) lead to same results.

Again, the relative deviation is used, assuming an unchanged sequence of mode shapes. We focus on the worst case

$$\delta^{exc} = \min_i \frac{\delta_i^{exc}}{f_i^{exc}} \quad (8)$$

as the second criterion. Large values for δ^{exc} are favourable, because they indicate an decreased susceptibility to vibration.

Although small geometric modifications usually do not change the mode shape or their sequence, the mode shapes are analysed as well. The similarity between the modes of the nominal and the modified blade is assessed using the Modal Assurance Criterion (MAC) according to [29]. A MAC value close to one indicates a good agreement between mode shapes, where Heinze et al. [8] assume that mode shapes with MAC values higher than 0.8 are clearly related. Martin and Bestle [30] presented an approach, where modes shapes are identified automatically by a mapping technique. In the present case, the nodes of the FE mesh outside the blending are unchanged. MAC values of modes are directly computed using the modal displacements.

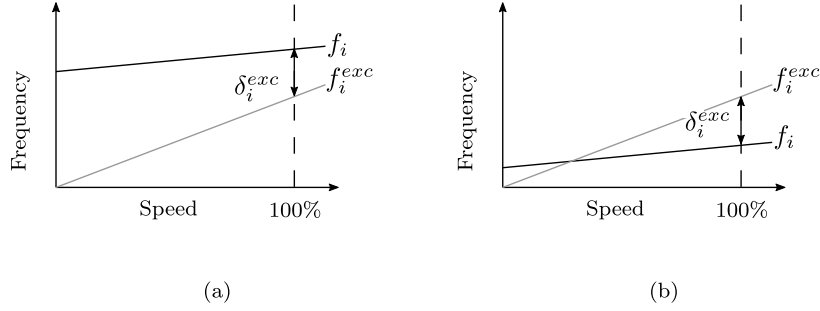


Fig. 5. Different natural frequencies in (a) and (b) with same excitation measure δ_i^{exc} .

3.2. Optimisation problem formulation

The designs of blending shapes can be improved by solving a multi-objective optimisation problem:

$$\begin{aligned} & \min_{\xi} \delta(\xi) \\ & \text{subject to } g(\xi) \leq 0 \\ & \text{and } \xi_{lb} \leq \xi \leq \xi_{ub}, \end{aligned} \quad (9)$$

where $\delta(\xi)$ is the vector-valued objective function, $g(\xi)$ is the constraint equation and ξ_{lb} and ξ_{ub} are the lower and upper boundaries for design variables ξ .

The vector of design variables results from the parameterised blending model described previously:

$$\xi = [e, d, r_z]^T, \quad (10)$$

where e describes the normalised spanwise position, d the machining depth and r_z the ellipsoid radius in z -direction, see Fig. 1. The distance r'_x is set to 5.0 mm and the radius r_y to 50 mm and these values are not used as design variables in the following. This limits the numerical effort and the optimisation concentrates on the dimensions that mainly affect the blend design.

Since the two frequency criteria Eqns. (5) and (8) are conflicting goals, the objective function

$$\delta(\xi) = \begin{pmatrix} \delta^{nom}(\xi) \\ -\delta^{exc}(\xi) \end{pmatrix} \quad (11)$$

is formulated. The negative sign of the second objective is chosen due to the formulation as a minimisation problem. The MAC value computation is not part of the optimisation, since the modes are hardly affected by small blend repairs. At the end of the optimisation process, the MAC values are used to verify that the Pareto optimal designs in fact have mode shapes very close to nominal ones.

The smallest possible blend repair depends on the size true defect in the blade. Only blending shapes that remove the defect completely are valid solutions. This is enforced by the constraint equation

$$g(\xi) = \max_k \left(\frac{x_k}{r_x^2} + \frac{y_k}{r_y^2} + \frac{z_k}{r_z^2} - 1 \right), \quad (12)$$

where (x_k, y_k, z_k) are damaged points. The expression becomes positive, if at least one damaged point is not removed. The constraint equation results from the rearranged ellipsoid equation stated in Eq. (3).

The solution to the optimisation problem stated in Eq. (9) is found using the Multi-Objective Global Pattern Search. This algorithm is based on the pattern search approach, tracks multiple local minima, and thus is a global optimisation method. The single-objective version of this optimisation algorithm has been published

by Hofmeister et al. [31]. It has recently been extended to also handle multi-objective problems using a non-linear scalarisation technique and Pareto sorting. This approach enables the discovery of multiple unconnected partial Pareto frontiers as well as robust convergence. The deterministic algorithm is used due to its high numerical performance. Less objective function evaluations are needed to generate points on the Pareto frontier. The deterministic nature of the algorithm further allows to reproduce optimisation results from a previous optimisation runs. Optimisation constraints are imposed by reformulating Eq. (9) with a penalty approach

$$\min_{\xi} \delta(\xi) + \Phi(g(\xi)), \quad (13)$$

where Φ is the vector-valued penalty function. In this work, we use a linear penalty expression

$$\Phi_i(g(\xi)) = \begin{cases} 0 & g(\xi) \leq 0 \\ r_i \cdot g(\xi) & \text{otherwise,} \end{cases} \quad (14)$$

where r_i are penalty factors and i denotes the objective function index. Designs not fulfilling the constraint $g(\xi)$ are penalised by adding the linear penalty expression to the objective function values. Penalty factors r_i are determined numerically in such a way that no constraint violation is observed in the resulting Pareto frontier.

4. Numerical results

In this section, the results of numerical studies are presented with respect to modal properties. The optimisation of two exemplarily chosen damage patterns demonstrates the defect-specific outcome.

4.1. Sensitivities

Prior to optimisation, the influence of blendings on the natural frequencies is studied in detail. A design of experiments is performed to gain knowledge about correlations between design variables and goals. Depending on the particular interest, various sampling methods are used to determine the design combinations evaluated. Despite the high numerical effort, compared to variance-reducing approaches, a simple grid search approach is used to gather the first information about the system behaviour. Since the blending model is only based on three design variables, the grid-based evaluation of the design space is affordable.

We consider a $19 \times 19 \times 19$ grid, which leads to 6859 realisations in total. The lower and upper limits of the design variables are specified as follows:

$$\begin{aligned} 0.05 & \leq e \leq 0.5, \\ 0.5 \text{ mm} & \leq d \leq 5.0 \text{ mm}, \\ 0.5 \text{ mm} & \leq r_z \leq 25.0 \text{ mm}. \end{aligned} \quad (15)$$

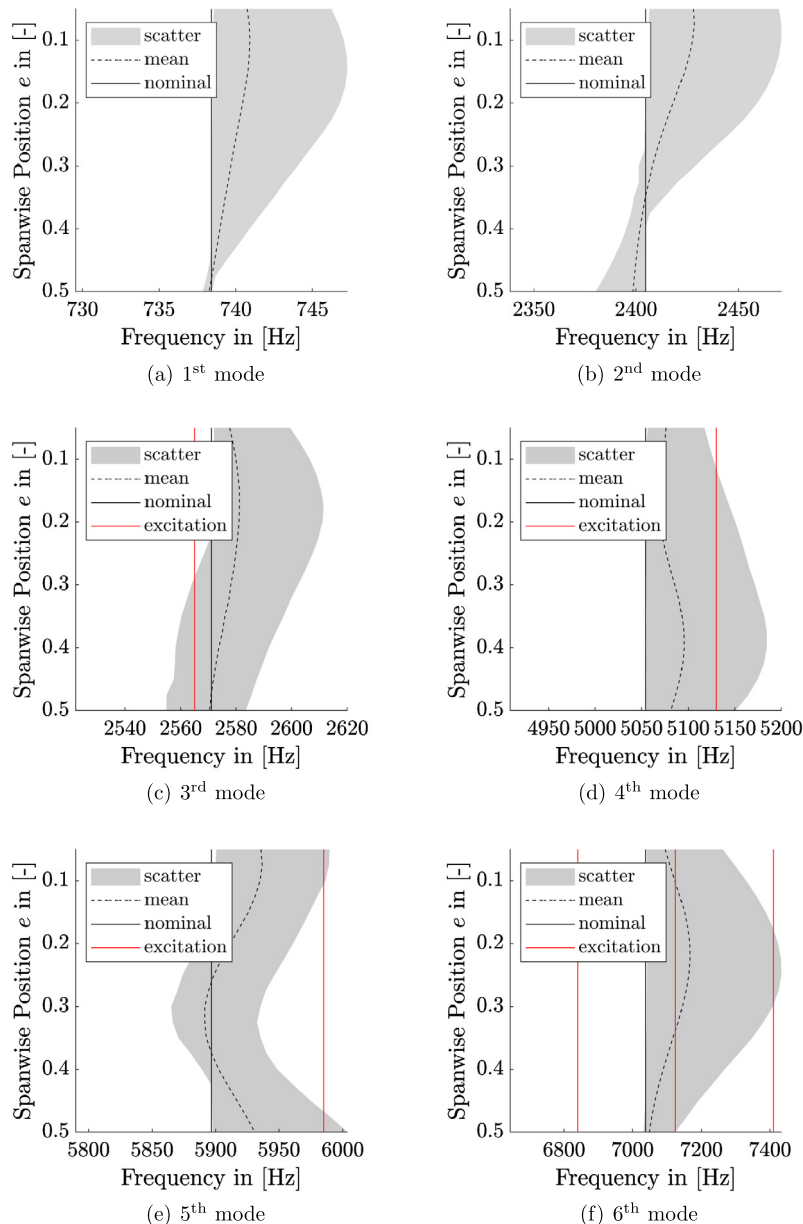


Fig. 6. Scattering of natural frequencies determined for the first six vibration modes of the bladed sector. (For interpretation of the colours in the figure(s), the reader is referred to the web version of this article.)

The sampling thus covers blending repairs of different sizes and depths in the upper half of the blade.

In order to investigate the impact of blend repairs on modal properties, the first six natural frequencies are initially analysed separately. The charts in Fig. 6 illustrate the influence of blend repairs on the absolute values of natural frequencies for each vibration mode, where frequencies are given as a function of the spanwise position of the blend. The vertical black lines indicate the natural frequencies of the nominal blade design. The range between maximum and minimum natural frequencies of all samples is highlighted in grey, where dashed lines mark the averaged frequency variation.

In general, most samples tend to have higher natural frequencies compared to the nominal blade. This shift to higher frequencies is mainly induced by the reduction of the resonating mass caused by removed material. Furthermore, the charts show a correlation between the variation of frequencies and the blending location specified by e . At positions close to the tip of the blade

($e \leq 0.2$), the maximum natural frequencies tend to decrease. In this region, the ellipsoid only partly intersects with the blade, so that the mass reduction is lower. In addition, the dependency of frequency tuning and blending position is clearly mode-specific.

Fig. 7 shows the fifth mode shape of the nominal and two blended blades, where the two blends only differ in the blending position e . If the blend is located in an area with low vibration amplitude or vibration nodes, the frequency slightly reduces. Therefore, the example depicted in Fig. 7(b) has a frequency of 5871.7 Hz being lower than the nominal frequency of 5896.7 Hz. In contrast, Fig. 7(c), corresponds to an increased frequency of 5958.4 Hz.

Moreover, the absolute variance in natural frequencies predominantly increases with higher vibration modes. The nominal frequencies and signed relative frequency deviations are listed in Table 1. In terms of relative frequency deviation, the sixth mode generally shows the greatest variation. Due to the blending position dependency, this cannot be concluded for all blending designs shown in Fig. 6.

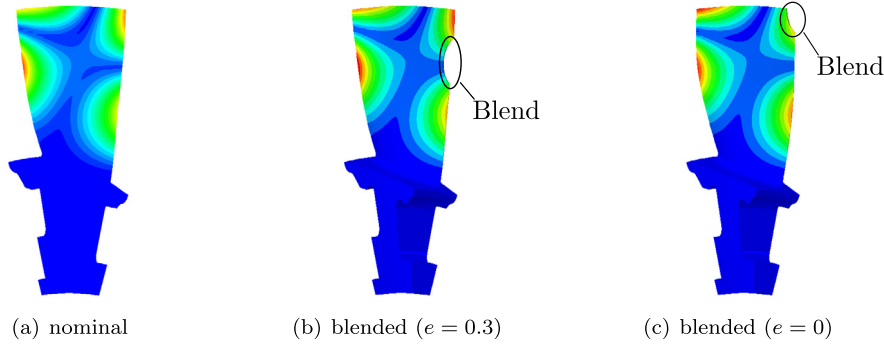


Fig. 7. Fifth vibration mode shape for nominal blade (a) and different modified blades (b) and (c).

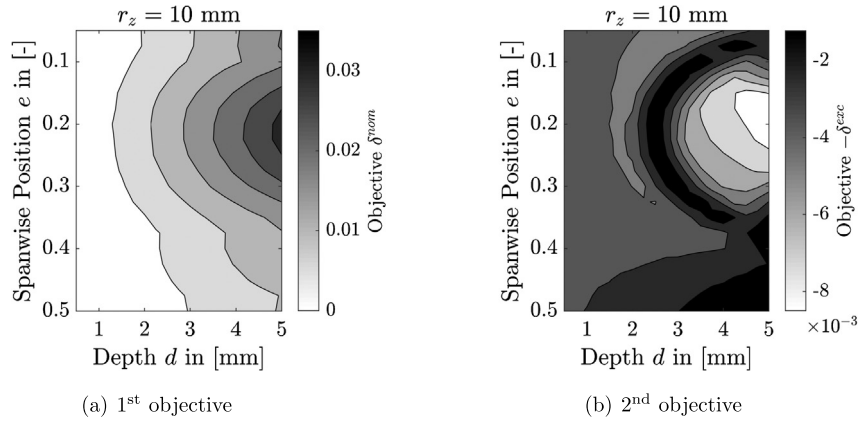


Fig. 8. Illustration of design space for in $d - e$ plane.

Table 1
Nominal natural frequencies f_i^{nom} and minimum and maximum values of relative frequency deviation $\frac{f_i - f_i^{nom}}{f_i^{nom}}$ determined.

Natural Frequency	f_i^{nom} in [Hz]	$\min_i \left(\frac{f_i - f_i^{nom}}{f_i^{nom}} \right)$ in [%]	$\max_i \left(\frac{f_i - f_i^{nom}}{f_i^{nom}} \right)$ in [%]
1st	738.41	-0.08	1.20
2nd	2404.7	-1.01	2.76
3rd	2571.1	-0.63	1.57
4th	5054.3	-0.04	2.57
5th	5896.7	-0.54	1.81
6th	7038.0	-0.08	5.62

Furthermore, all relevant excitation frequencies are marked by red vertical lines in Fig. 6. As illustrated, the design of the blisk was chosen in the way that no resonances occur at rated speed, and even through blending repairs no frequency crossings exist for the first two modes. But with higher vibration modes, the distances to the excitation can become small, which is indicated by the intersection of the red lines with grey coloured areas.

4.2. Design space

For each realisation of the grid sampling, the two objective functions of Eq. (11) are evaluated and the design space is explored for one of the design variables held constant, Fig. 8 and 9.

Fig. 8 shows the objective function values for blend designs with constant radius $r_z = 10$ mm of the ellipsoid, where dark coloured areas denote unfavourable designs. Considering the first objective in Fig. 8(a), the best designs relate to small blends and the objective value enlarges with increasing blend depth d . The contour lines further show that the objective function value is dominated by different modes. In the upper region, where $e < 0.075$, the maximum relative frequency deviation results from the

second mode. At spanwise positions $e \in [0.075, 0.37]$, the maximum relative frequency δ_6^{nom} is caused by the deviation of the sixth vibration frequency δ_6^{nom} . At blade positions closer to the disk, $e > 0.37$, the fourth and fifth mode predominate. The contours of the second objective function values in Fig. 8(b) clearly show circled regions corresponding to the crossing of natural frequencies with the excitation. The best objective values are obtained for relatively large blending shapes at $e = 0.2$.

Exploring the design space for a constant position $e = 0.2$ in Fig. 9(a), a monotonic increase in the first objective function values with larger size and depth of the blending is determined. This effect is mainly caused by the correlation between mass reduction and frequencies. Concerning the second objective, the design space again subdivides into local regions with high and low function values, respectively. Regions with unfavourable properties correspond to crossings of natural frequencies of the sixth and fourth mode with harmonic excitations.

4.3. Example I

For the first example, two-objective optimisation is performed for an artificial damage described by two points. The damage is located at mid-span at the leading edge (Fig. 10(a)). The optimisation is performed by 10000 objective function evaluations using Global Pattern Search. The objective values of solutions sampled during optimisation are displayed in Fig. 10(b).

Solutions that are identified as Pareto optimal solutions are marked in red. In this example, the Pareto frontier is unconnected and the non-dominated solutions can be grouped into two parts. For solutions in the upper left part, the excitation of the third vibration mode is the decisive one. The designs corresponding to the first and last solution, (a) and (b) in Fig. 10(b), are depicted in Fig. 11(a) and (b). Comparing both designs, the most prominent

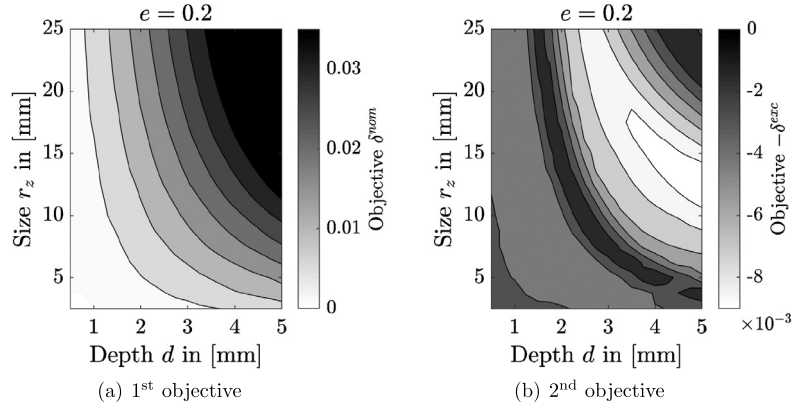


Fig. 9. Illustration of design space for $e = 0.2$ in $d - r$ plane.

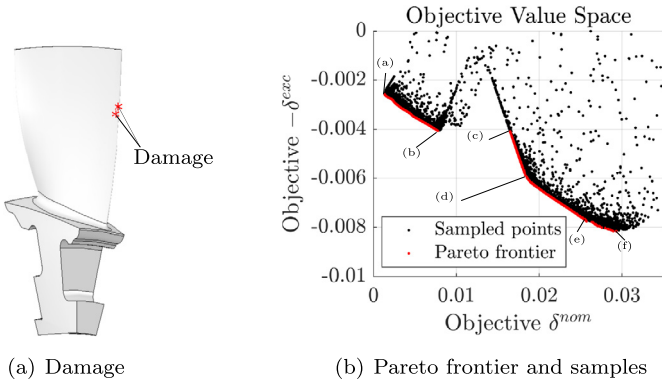


Fig. 10. Damaged blisk sector (a) and Pareto frontier (b) for example 1.

Table 2

Minimum MAC_i values of Pareto optimal solutions of example 1.

MAC_1	MAC_2	MAC_3	MAC_4	MAC_5	MAC_6
0.9999	0.9942	0.9924	0.9988	0.9971	0.9820

The gap between the partial frontiers is caused by the different courses of the objective functions (cf. Sec. 4.2). For designs corresponding to the gap in the frontier, (b) and (c) in Fig. 10(b), the first objective function increases monotonically, while the second objective function has a local maximum. This trend is also indicated by the sampled points in the range between a maximum relative frequency of 0.8% and 1.7% annotated as (b) and (c) in Fig. 10(b).

The sections of the second frontier (c)-(f) are caused by different excited modes. The second objective is driven by the sixth, third and fourth mode. Figs. 11 (c) to (f) show designs corresponding to characteristic solutions of the second partial frontier. The designs in (c) and (d) are located closer to the tip and the depth is increased from about 1 mm to 2-3 mm. The designs (d) and (e) are located around the bend in the partial frontier, where (e) clearly has a higher blending depth compared to the other. All solutions following this design are characterised with a depth greater than 4 mm. Finally, the last design (f) denotes the other end of the Pareto frontier and deviates up to 3% from the nominal natural frequencies. To check whether the mode shapes significantly differ from the nominal ones, the MAC values are calculated for these Pareto optimal solutions (Table 2). Although the natural frequencies are quite different, the minimum MAC values are significantly greater than 0.8. Even in the worst case, a value of $MAC_6 = 0.9820$ is determined, which means that the modes did not change order. Considering all Pareto optimal solutions computed, the final design is supposed to be selected from the middle of the left partial frontier, because these solutions are a good compromise between the objectives and maintain largely the aerodynamic shape.

4.4. Example II

The second example differs from the first one concerning the location of the damage positioned in the tip region of the blade as shown in Fig. 12(a). All other settings for the optimisation are maintained as described for the first case. The Pareto frontier found after 10000 objective function evaluations is shown in Fig. 12(b).

Unlike the first example, the non-dominated solutions form a single connected frontier. Comparing the Pareto frontiers of both examples, it should be noted, that the solutions of the first example (blue) in most cases dominate the solutions of the second one. Considering the first objective, the values in the second example

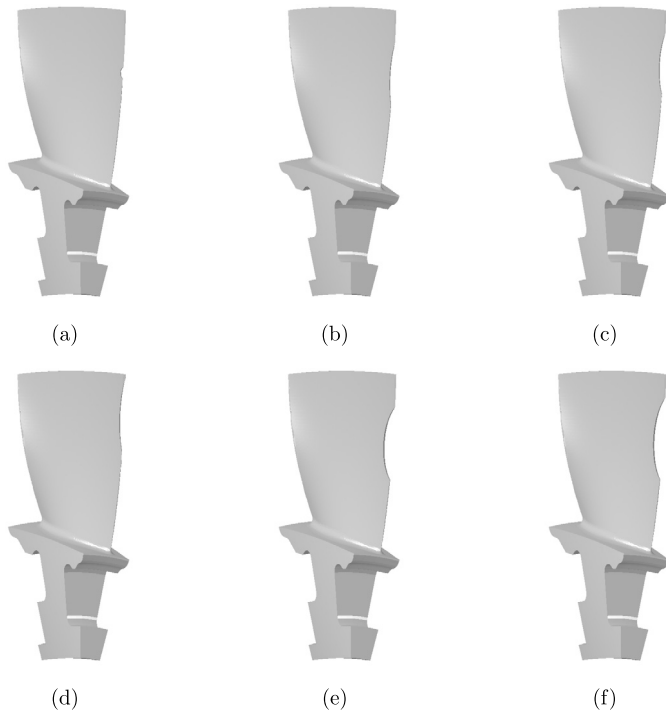


Fig. 11. Blending designs related to non-dominated solutions of example 1.

difference is the width of the shape. In the partial frontier, the radius r_z increases, while the position of the blend remains almost the same.

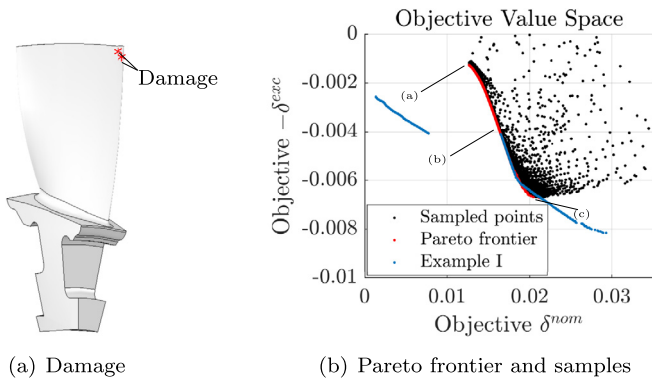


Fig. 12. Damaged blisk sector (a) and Pareto frontier (b) for example II.

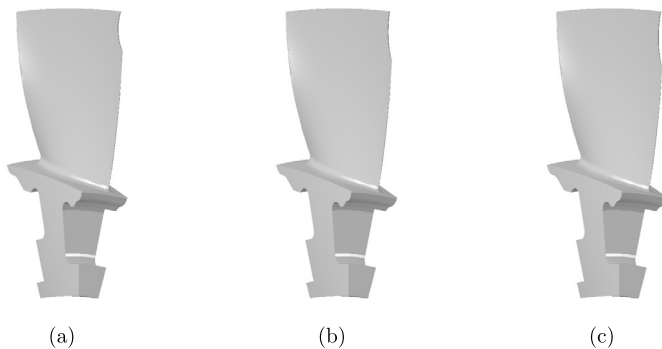


Fig. 13. Blending designs related to non-dominated solutions of example II.

Table 3

Minimum MAC_i values of Pareto optimal solutions of example II.

MAC_1	MAC_2	MAC_3	MAC_4	MAC_5	MAC_6
0.9999	0.9863	0.9862	0.9987	0.9912	0.9646

range from 1.25% to 2.1% which roughly corresponds to the gap shown for the first example (Fig. 10(b)). This indicates that repairs at the tip of the blade impact the frequency tuning more significantly than damages at mid-span position. In this example, the second objective is predominately influenced by the sixth vibration mode. This mode is most susceptible to vibration, because blends at the tip significantly increase the sixth frequency and shift it towards the closest excitation frequency. Almost all non-dominated solutions are related to the excitation of the sixth vibration mode. Only solutions close to (c) are mainly influenced by the excitation of the fifth vibration mode. In total, 2168 solutions are found to be Pareto optimal in the second example. Three blending designs corresponding to the Pareto frontier are illustrated in Fig. 13. As described for the first example, the material removed by blending increases with improved second objective values.

The blending depicted in Fig. 13(a) leading to frequencies close to the nominal frequencies is located next to the defect. But this design has an unfavourable influence on the resonance conditions. The blend repairs shown in Fig. 13(b) and (c) are generally larger but have a smoother shape. Due to the larger width of the blend, the distances to the closest excitation frequencies, described by the second objective function, are positively influenced. The MAC values of all modes listed in Table 3 show that the weakest correlation to nominal modes is determined for the sixth mode. The values are smaller than in the first example, but still indicate a good agreement between nominal and modified mode shapes. In this example, the final repair is supposed to be again one of the designs corresponding to the middle part of the frontier. The size

of the blends remains small and both objectives are met adequately.

5. Benefits and limitations

In the present work, an optimisation process of blending shapes with respect to the tuning of frequencies is proposed. A two-objective optimisation problem is formulated aiming for small variation in natural frequencies and preventing the excitation by harmonic frequencies. A blend and a FE blade-alone model are introduced, to allow for the sufficiently accurate simulation of the blending shapes. The analytical model of blendings together with the pointwise definition of the damaged portion is beneficial, because it allows a fast assessment of blending designs. Applying the approach to one sector of a compressor blisk, it is demonstrated how various blend designs influence the first six natural frequencies of the blade. A two-objective optimisation problem is formulated based on frequency criteria and is efficiently solved by a multi-objective version of Global Pattern Search. Running the optimisation for two different damage patterns, Pareto optimal solutions are found. Interestingly, the optimisation results computed for these defects do not only differ in absolute objective values only, but also show significant differences in the shape of the Pareto frontier. While the damage located at mid-span position leads to a Pareto frontier subdivided into two parts, the defect at the tip leads to a continuous frontier. Decisions have to be made on a case-by-case basis and each individual problem is dominated by different vibration modes.

The presented approach is developed for optimised blade-alone frequencies of compressor sectors. The impact of geometric changes on the aerodynamic flow around the blade and the tuning of the blisk or bladed assembly are not considered in this paper. However, additional computations, like aerodynamic simulations, can also be integrated in the optimisation. An extension to a model including the amplification by mistuning and a lifetime assessment is conceivable in future works. In particular, thinking about automated process chains for blending repairs, the individual optimisation of blending shapes is a promising approach. Numerical studies of repair designs support the repair process and show great potential for future process automation.

Declaration of competing interest

The authors declare that they have no known competing financial interests or personal relationships that could have appeared to influence the work reported in this paper.

Acknowledgements

The authors kindly thank the German Research Foundation (DFG, Deutsche Forschungsgemeinschaft) for financial support to accomplish the research project B4 "Dynamical Behavior and Strength of Structural Elements with Regeneration-induced Imperfections" within the Collaborative Research Center (SFB, Sonderforschungsbereich) 871 - Regeneration of Complex Capital Goods - 119193472.

References

- [1] A. Eberlein, Phases of high-tech repair implementation—definition, development, adaptation, validation and qualification, in case of patch-repair on blisk-blades, in: *Proceedings of the International Symposium on Air Breathing Engines*, 2007.
- [2] M. Bussmann, E. Bayer, Blisk production of the future—technological and logistical aspects of future-oriented construction and manufacturing processes of integrally bladed rotors, in: *Proceedings of the International Symposium on Air Breathing Engines*, Curran, Montreal, Canada, 2009, ISABE-2009-1169.

- [3] V.E. Garzon, D.L. Darmofal, Impact of geometric variability on axial compressor performance, *J. Turbomach.* 125 (2003) 692–703.
- [4] R. Schnell, T. Lengyel-Kampmann, E. Nicke, On the impact of geometric variability on fan aerodynamic performance, unsteady blade row interaction, and its mechanical characteristics, *J. Turbomach.* 136 (2014) 091005.
- [5] C. Keller, A. Kellersmann, J. Friedrichs, J.R. Seume, Influence of geometric imperfections on aerodynamic and aeroelastic behavior of a compressor blisk, in: *Proceedings of ASME Turbo Expo 2017*, Charlotte, North Carolina, USA, ASME, 2017, GT2017-63556.
- [6] J.M. Brown, R.V. Grandhi, in: *Proceedings of ASME Turbo Expo 2004*, Vienna, Austria, ASME, 2004, GT2004-53959.
- [7] J.M. Brown, R.V. Grandhi, Probabilistic high cycle fatigue assessment process for integrally bladed rotors, in: *Proceedings of ASME Turbo Expo 2005*, Reno-Tahoe, Nevada, USA, ASME, 2005, GT2005-69022.
- [8] K. Heinze, S. Schrape, M. Voigt, K. Vogeler, Probabilistic endurance level analyses of compressor blades, *CEAS Aeronaut. J.* 3 (2012) 55–65.
- [9] T. Backhaus, T. Maywald, S. Schrape, M. Voigt, R. Mailach, A parametrization describing blisk airfoil variations referring to modal analysis, in: *Proceedings of ASME Turbo Expo 2017*, Charlotte, North Carolina, USA, ASME, 2017, GT2017-64243.
- [10] T. Maywald, T. Backhaus, S. Schrape, A. Kühhorn, Geometric model update of blisks and its experimental validation for a wide frequency range, in: *Proceedings of ASME Turbo Expo 2017*, Charlotte, North Carolina, USA, ASME, 2017, GT2017-63446.
- [11] J.A. Beck, J.M. Brown, B. Runyon, O.E. Scott-Emuakpor, Probabilistic study of integrally bladed rotor blends using geometric mistuning models, in: *Proceedings of Structures, Structural Dynamics, and Materials Conference 2017*, Grapevine, Texas, USA, AIAA, 2017, AIAA 2017-0860.
- [12] M. Bussmann, J. Kraus, E. Bayer, An integrated cost-effective approach to blisk manufacturing, in: *Proceedings of the International Symposium on Air Breathing Engines*, 2005.
- [13] W.D. Day, S.W. Fiebiger, H.N. Patel, Parametric evaluation of compressor blade blending, in: *Proceedings of ASME Turbo Expo 2012*, Copenhagen, Denmark, ASME, 2012, GT2012-68641.
- [14] M. Burchil, M. Heller, Stress and fracture analysis of circular arc blends for repair of cracked metallic components, in: *Proceedings of Australasian Congress on Applied Mechanics*, Brisbane, Australia, 2007.
- [15] L. Xu, H. Cao, H. Liu, Y. Zhang, Assessment of fatigue life of remanufactured impeller based on fea, *Front. Mech. Eng.* 11 (2016) 219–226.
- [16] L. Högner, M. Voigt, R. Mailach, M. Meyer, U. Gerstberger, Probabilistic fe-analysis of cooled high pressure turbine blades – part a: holistic description of manufacturing variability, in: *Proceedings of ASME Turbo Expo 2019*, Phoenix, Arizona, USA, ASME, 2019, GT2019-91205.
- [17] K. Karger, D. Bestle, Parametric blending and fe-optimisation of a compressor blisk test case, in: D. Greiner, B. Galván, J. Périaux, N. Gauger, K. Giannakoglou, G. Winter (Eds.), *Advances in Evolutionary and Deterministic Methods for Design, Optimization and Control in Engineering and Sciences*, in: *Computational Methods in Applied Sciences*, vol. 36, Springer International Publishing, Cham, 2015, pp. 257–266.
- [18] R. Berger, J. Häfele, B. Hofmeister, R. Rolfes, Blend repair shape optimization for damaged compressor blisks, in: A. Schumacher, T. Vietor, S. Fiebig, K.-U. Bletzinger, K. Maute (Eds.), *Advances in Structural and Multidisciplinary Optimization*, Springer International Publishing, Cham, 2018, pp. 1631–1642.
- [19] J.M. Brown, R. Grandhi, Reliability optimization of three dimensional structures using geometry parameters, *AIAA*, 1999, AIAA 99-1602.
- [20] A. Keskin, D. Bestle, Application of multi-objective optimization to axial compressor preliminary design, *Aerosp. Sci. Technol.* 10 (2006) 581–589.
- [21] P. Hecker, D. Delimar, H. Brandl, M. Lötzerich, Process integration and automated numerical design optimization of an eigenfrequency analysis of a compressor blade, in: *Proceedings of ASME Turbo Expo 2011*, Vancouver, British Columbia, Canada, ASME, 2011, GT2011-45489.
- [22] X. He, J. Li, C.A. Mader, A. Yildirim, J.R. Martins, Robust aerodynamic shape optimization—from a circle to an airfoil, *Aerosp. Sci. Technol.* 87 (2019) 48–61.
- [23] H. Lim, H. Kim, Multi-objective airfoil shape optimization using an adaptive hybrid evolutionary algorithm, *Aerosp. Sci. Technol.* 87 (2019) 141–153.
- [24] C. Keller, T. Willeke, S. Burrafato, J.R. Seume, Design process of a 1.5-stage axial compressor for experimental flutter investigations, in: *Proceedings of the International Gas Turbine Congress 2015*, Tokyo, Japan, Gas Turbine Society of Japan, 2015, IGTC2015-0141.
- [25] W.N. Dawes, P.C. Dhanasekaran, A.A.J. Demargne, W.P. Kellar, A.M. Savill, Reducing bottlenecks in the cad-to-mesh-to-solution cycle time to allow cfd to participate in design, *J. Turbomach.* 123 (2001) 552.
- [26] M.L. Staten, S.J. Owen, S.M. Shontz, A.G. Salinger, T.S. Coffey, A comparison of mesh morphing methods for 3d shape optimization, in: W.R. Quadros (Ed.), *Proceedings of the 20th International Meshing Roundtable*, Springer Berlin Heidelberg, Berlin, Heidelberg, 2012, pp. 293–311.
- [27] L. Schwerdt, T. Hauptmann, A. Kunin, J.R. Seume, J. Wallaschek, P. Wriggers, L. Panning-von Scheidt, S. Loehnert, Aerodynamical and structural analysis of operationally used turbine blades, *CIRP J. Manuf. Sci. Technol.* (2016).
- [28] MIL-HDBK-5J *Metallic Materials and Elements for Aerospace Vehicle Structures*, <http://www.everyspec.com>, 2003.
- [29] J. Allemang, The modal assurance criterion—twenty years of use and abuse, *Sound Vib.* 37 (2003) 14–23.
- [30] I. Martin, D. Bestle, Automated mode identification of airfoil geometries to be used in an optimization process, in: *Proceedings of ASME Turbo Expo 2016*, Seoul, South Korea, ASME, 2016, GT2016-56987.
- [31] B. Hofmeister, M. Bruns, R. Rolfes, Finite element model updating using deterministic optimisation: A global pattern search approach, *Eng. Struct.* 195 (2019) 373–381.

5 Optimization of Patch Repairs

5.1 Research Context

In contrast to other repair techniques in the field of turbomachinery blades, repairs by patching currently receive relatively little attention in scientific publications. The reason for this is the narrow scope of this repair technique [34]. As described in detail in Sec. 1.2.2, the repair by patching is applied only to blisk blades with moderate damage and is demanding in terms of manufacturing. Therefore, not every MRO companies offer this repair method at all [124]. Nonetheless, with further automation [25] and improved process control, repair of blisk blades using a patch could be a reasonable alternative in the future.

The most important works on patch repairs mainly deal with the residual stresses due to the welding process and the evaluation of mechanical integrity [150, 12]. The focus is on measurements as well as numerical simulation of single repair designs. The distinction between long and short patch geometries according to length of the patch can be found in [55].

5.2 Methods

The first part of paper C is concerned with the parametric modeling of patch repairs and the description of the welding trajectory, respectively. A spatial description of the welded region is introduced, which specifies the repair geometry by two scalar variables.

In the second part of the publication, the optimization task is derived from the design goals of patch repairs and solved following the idea of a multi-objective approach [114]. The basic idea behind the objective function formulations is to achieve a patch design where the weld is located in blade regions with minimal HCF loading. HCF fatigue strength is evaluated based on the established metric of amplitude frequency strength. Since multiple load conditions contribute to the fatigue strength of the weld, the five most critical load conditions are analyzed separately. The five corresponding amplitude frequency strength values each contribute to an objective function. To minimize the repair effort, a further objective function is formulated, which includes the length of the weld as a measure for the manufacturing effort. The resulting optimization problem consists of six objective functions. The optimization software EngiO, which is published in paper A, is used to optimize the patch geometry of a damaged blisk blade. The state-of-the-art multi-objective algorithm NSGA-II [46] is utilized to identify the Pareto optimal solutions. The visualization of Pareto optimal solutions in six dimensions is based on a matrix representation [2].

In the last part of the paper, more detailed FE simulations are performed on the residual stress distribution for individual patch designs. The evaluation of residual stresses relies on a decoupled thermomechanical simulation [17] of the welding process. The position of the moving heat source is calculated according to the specified trajectory and the heat flux is described by an analytic model [138] that is implemented in a user-defined subroutine.

5.3 Results and Outlook

In the publication, the multi-objective optimization method is used to identify optimal design alternatives for patch repairs of blisk blades. It is shown that different patch geometries are optimal in terms of manufacturing and fatigue strength aspects. The trade-off between minimum effort for the welding process and optimal strengths of individual load cases is visualized by appropriate Pareto frontiers. The main innovation of the paper is the extension to a six-objective formulation, where five load cases and the weld length are considered simultaneously. The analysis of optimization results and related designs demonstrates that the multi-objective optimization method is suitable to narrow down the number of possible design alternatives. However, the final decision has to be made according to preferences and engineering experience. In the computational example, the presented method is able to find solutions that would not be intuitively selected.

These results suggest that future repair design decisions could be supported by simulations and an optimization approach. To further improve the capabilities of the approach, some work needs to be done on the simulation models of the repair processes. In particular, the simulation of welding processes is still challenging when they need to be automated and performed in an acceptable time. In addition, the real patch repair process consists of several manufacturing steps such as milling, welding, and recontouring. The validity of the results would improve if the entire process chain is included in future simulation models.

5.4 Paper C: A Multi-Objective Approach towards Optimized Patch Repairs of Blisk Blades

The following paper is published online in AIAA Journal, 24 September 2021 (<https://doi.org/10.2514/1.J060723>).

Author Contribution

The main work was done by the author of this thesis. Guido Quaak developed the initial subroutine, which enables the welding simulation in Abaqus, and is part of Sec. 5 of paper C. Benedikt Hofmeister gave technical and editorial suggestions for improvement of the entire publication. Raimund Rolfes contributed with advisory and supporting work.

A Multi-Objective Approach towards Optimized Patch Repairs of Blisk Blades

Ricarda Berger ^{*}, Guido Quaak [†], Benedikt Hofmeister [‡], Cristian G. Gebhardt [§] and Raimund Rolfes [¶]
Leibniz Universität Hannover, 30167 Hannover, Germany

Patching is a high-tech repair to preserve damaged jet engine blisks instead of replacing them. The damaged portion of the blade is restored by welding a patch to the blade. Since the extent of defects varies, the optimal repair is initially unknown. This work contributes to the design of patch repairs by employing multi-objective optimization. A multi-objective function is formulated maximizing High Cycle Fatigue strength and minimizing the length of the weld. An inequality constraint equation ensures the complete removal of the damaged blade area. The geometry of the patch and the position of the defect are described using parametric models. Optimization results are presented for an exemplary damage scenario. The set of Pareto optimal alternatives is computed using the Non-dominated Sorting Genetic Algorithm II and imposing constraints by utilizing a linear penalty approach. The results demonstrate that designs are found by the optimization that would not intuitively be recognized as optimal by maintenance technicians. Individual designs from the Pareto frontier are selected and the welding process is analyzed in more detail using thermomechanical simulations. The distribution of residual stresses in the repaired blade is computed and the influence on fatigue strength is determined. The multi-objective optimization and the FE simulations implemented in the presented approach thus enable a systematic evaluation of design alternatives and support informed engineering decisions in the repair process.

^{*}Scientific Researcher, Institute of Structural Analysis, Appelstraße 9A.

[†]Scientific Researcher, Institute of Structural Analysis, Appelstraße 9A.

[‡]Scientific Researcher, Institute of Structural Analysis, Appelstraße 9A.

[§]Senior Faculty Member, Institute of Structural Analysis, Appelstraße 9A.

[¶]Professor, Institute of Structural Analysis, Appelstraße 9A.

Nomenclature

$\mathcal{A}, \mathcal{B}, \mathcal{C}, \mathcal{D}$	=	labels of representative designs
a, b	=	patch sizes
af	=	amplitude frequency strength
d	=	distance to interface plane, m
e	=	natural exponential function
f	=	vector-valued objective function
g	=	inequality constraint
l	=	weld length, m
p	=	damage point
Q	=	power of heat source, J/s
q	=	power density of heat source, $J/(s\text{ mm}^3)$
r	=	radius of heat source, mm
r_0	=	depth-dependent radius of heat source, mm
r_i	=	interior radius of heat source, mm
r_e	=	exterior radius of heat source, mm
\mathbf{r}	=	position vector of interface plane
\mathbf{n}	=	normal vector of interface plane
\mathbf{x}	=	design variables
x, y, z	=	distances to heat source center in local coordinates, m
z_i	=	depth of heat source corresponding to r_i , mm
z_e	=	depth of heat source corresponding to r_e , mm
σ_e	=	endurance limit, Pa
σ_m	=	mean stress, Pa
σ_v	=	vibratory stress, Pa
σ_y	=	yield strength, Pa
Φ	=	penalty function
Subscripts		
lb	=	lower boundary
ub	=	upper boundary
1, 2, 3, 4, 5	=	load cases 1 up to 5
worst	=	worst case

Superscripts

weld = welding simulation results

I. Introduction

Jet engines are maintained at regular intervals in order to prolong their service life. For this purpose, the engine components are replaced or repaired in special maintenance processes [1]. Since modern engines consist of increasingly more complex components, there is growing interest in repairing rather than replacing these components [2].

Blade integrated disks (blisks), which replace the conventional blade disk assembly to improve the thrust-to-weight ratio, are one prominent example [3, 4]. Compared to their conventional counterpart, compressor blisks have high spare part costs and the integrated design makes them difficult to maintain. Therefore, new repair technologies for blisk blades are investigated. According to Eberlein [5], one repair concept suitable for medium damages is patching. A typical medium damage pattern is shown in Fig 1. During patching, the damaged portion of the blade is removed and the missing blade part is restored with a so-called patch. Subsequently, the aerodynamic profile of the blade is restored by machining operations.

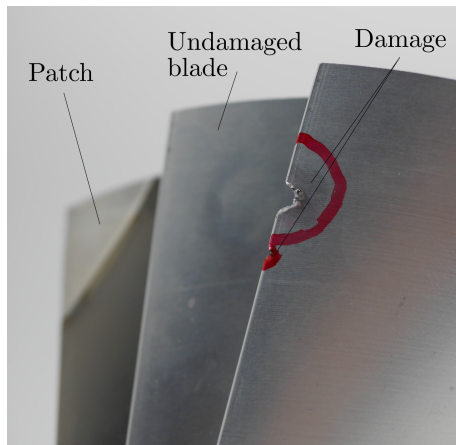


Fig. 1 Blade with damage at the leading edge, without damage and with patch repair.

Challenges involved in blade repairs are reviewed from a manufacturing perspective by Denkena et al. [6]. They discuss the impact of machining, welding and post-treatment steps on the process chain of blade repairs. In particular, Denkena et al. [7, 8] determined the process-related residual stresses in blisk materials and showed that they are greatly influenced by welding techniques. Patching of fan blades using an electron beam welding procedure was studied by Azar et al. [9]. In that work, titanium blades are tested experimentally and residual stresses are computed by Finite Element (FE) simulations. The authors found out that patch repair is a feasible alternative to blade replacement. Further, numerical simulations are performed by Schöneborn and Reile [10], who address the High Cycle Fatigue (HCF) strength of a blade that is patched at the leading edge. Furthermore, decoupled thermal and mechanical simulations are performed

to predict the residual stresses resulting from welding and heat treatment processes. Similar simulations can be found in Berglund et al. [11], who consider the structural stress in a turbine exhaust case and provide valuable information on residual stress levels. FE simulations of a repaired impeller are carried out by Xu et al. [12], who determine the fatigue life of additively manufactured blades. Overall, all contributions highlight that the repair process and design greatly impact the remaining stresses and thus the strength of repaired blades.

To enlarge the safety margin against fatigue failure, increase structural, aerodynamic or aeroacoustic performance, numerical optimization is often applied [13–15]. According to Vicini and Quagliarella [16] especially multi-objective optimization is a powerful tool to determine suitable designs. Design optimization methods were also used, for example, by Hou and Cross [13], who minimize the maximum dynamic magnification factor of a mistuned rotor and therewith improved the vibratory stresses. The mistuning effects caused by blade damage are further studied by Hou [17]. For the investigated blisk, they found that it is insensitive to crack-induced mistuning and the limits for blend repairs could be extended in the future. Since, unlike blending, no geometry change remains after a patch repair, the nominal geometry for the repaired blade is assumed in this study.

Moreover, multi-objective approaches are often employed to enable optimization involving multiple disciplines. Luo et al. [18] as well as Buske et al. [19] combine aerodynamic and structural objectives in their optimization. The objectives comprise isentropic efficiency, maximum von Mises stresses or failure probability. Multi-objective optimization is also widely used in preliminary blade design [20–22]. The approach of Keskin and Bestle [20] goes beyond the formulation as a two-objective problem and the design alternatives are evaluated based on three objective functions. Adjei et al. [23] even include six objectives in their optimization. They optimize a fan geometry considering two blade stresses as well as the efficiency and pressure ratio at two operating points. Optimization results show an improvement relative to the baseline design.

Currently, the optimization approaches mainly focus on the initial design phase of engines and blades. However, Karger and Bestle [24] already showed that there is great potential in the optimization of maintenance procedures as well. In their work, they present a two-objective formulation for the optimization of blending repairs. In an earlier own work [25], the authors demonstrated that multi-objective optimization can support repair decisions related to blend repairs.

Nevertheless, up to now the repair of blisk blades by patching has only been investigated for single exemplary patches. To the authors' knowledge, a systematic analysis of patch designs with respect to generic damage patterns has not yet been performed. Furthermore, existing work does not employ engineering optimization methods to improve patch designs. Therefore, this work aims firstly to develop a systematic analysis procedure for patch repairs and secondly to combine it with state-of-the-art multi-objective optimization.

We propose a multi-objective formulation including objectives resulting from machining effort and HCF. The objective related to the machining effort of the repair is expressed in terms of the length of the weld. A patch design with a short weld is ideal in terms of machining effort, but can result in the welded joint being placed in a highly

stressed region. Especially higher vibration modes lead to local areas with increased vibratory stress and reduced HCF strength. As presented in a previous work [26], this leads to design conflicts between weld length and fatigue. A slightly different weld position therefore would significantly improve HCF properties while leading to only a small increase in the machining effort. To counteract unfavorable positioning of the weld in these regions, the HCF strength of the welded joint serves as further optimization objective. For the HCF evaluation of the repaired blade, the minimum fatigue strength in the corresponding weld-affected region is decisive. The simulation model used to evaluate the associated objective functions is based on a cyclic symmetric simulation of one blisk sector subjected to nominal operational loads. The effect of mistuning due to small changes in blade properties is not considered in this work. By solving the optimization problem and presenting Pareto optimal solutions, a suitable set of repair alternatives can be identified for specific damage patterns. From the optimization results, several representative individual designs are selected and the distribution of thermally induced residual stresses is computed in a welding simulation. Since welding simulations are numerically expensive, require extensive knowledge of welding processes, and often need to be customized to the concrete conditions, they are only conducted for the representative designs to verify the feasibility of the optimization results. Through this new approach towards patch repairs, the effects of different patch designs on competing objectives are systematically assessed and become apparent to the maintenance engineer.

In the first part of the paper, a parametric patching approach is introduced to describe the patch size with regard to the blade dimensions. In the second part, the formulation of the objective functions is introduced. The objectives are the length of the weld between patch and parent material as well as the HCF strength of the joint region. Multiple significant vibration modes are included, which results in a multi-objective optimization problem. The assessment of HCF properties is described and a numerical optimization is performed for a compressor blisk considering five different loading conditions. Individual representative designs of the non-dominated solution set are analyzed in more detail in a subsequent welding simulation.

II. Parametric Patching

The parametric assessment of different patch designs demands for an universal approach to describe the geometry of the applied patch and corresponding weld location. As illustrated in Fig. 2 for a fully repaired blade, all patches considered are described by two design variables.

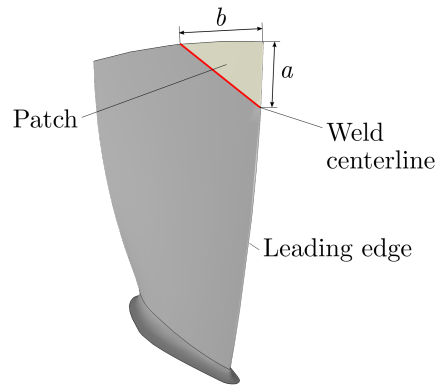


Fig. 2 Parametric representation of the patch geometry at the leading edge of the blade.

The first design variable a specifies the height and the second design variable b specifies the width of the final patch geometry, respectively. Both design variables are defined with regard to the start of the leading edge close to the tip of the blade and describe the size of the patch in chord and spanwise direction. This creates the triangular shape, which is typical for patch repairs. Further, the patch sizes a and b are not given in absolute values, but instead are normalized according to the length of the leading edge and chord, respectively. The design variables a and b are therefore dimensionless.

In Fig. 2, the red line indicates the path of the moving heat source. The joint between the blade and patch material is modeled as a cutting plane. For later fatigue assessment along the weld centerline, a weld-affected region is defined as shown in Fig. 3.

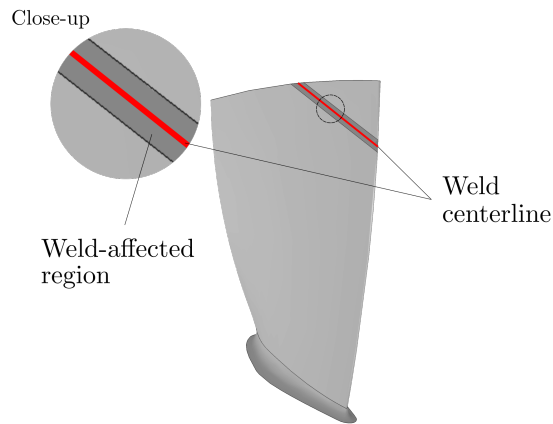


Fig. 3 Weld-affected region (dark gray) around the weld centerline (red).

This region is highlighted in dark gray. It is of constant width and is symmetric with respect to the weld centerline, which marks the center of the moving heat source. The volume is used to analyze stresses in the proximity of the weld and the corresponding strength properties.

The damage of the blade (Fig. 1) can have various shapes and positions. To describe any possible damage pattern, the damaged portion is described by a three-dimensional point cloud p_i with i points as illustrated in Fig. 4. Additionally, the red plane, which partitions patch and blade at the centerline, is used to define the interface between patch and blade. This universal description of the defect and the plane enables automated testing, whether the defect is removed by the patch repair. In the case depicted in Fig. 4, the patch design is suitable to remove the damaged portion completely.

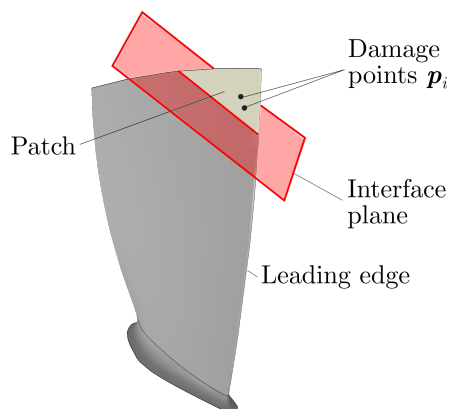


Fig. 4 Generic pointwise damage description p_i .

III. Design Goals and Objectives

The optimal design of a patch repair has to satisfy multiple design goals. One major goal of patching is to preserve the aerodynamic functionality while maintaining mechanical strength of the blisk. The first design criterion is therefore related to the fatigue properties of the repaired blades. Blade vibrations during operation lead to High Cycle Fatigue (HCF) of the blade. The particular fatigue strength of the blisk depends on the stress level and the resistance of the material. The Goodman diagram schematically shown in Fig. 5 illustrates this relation.

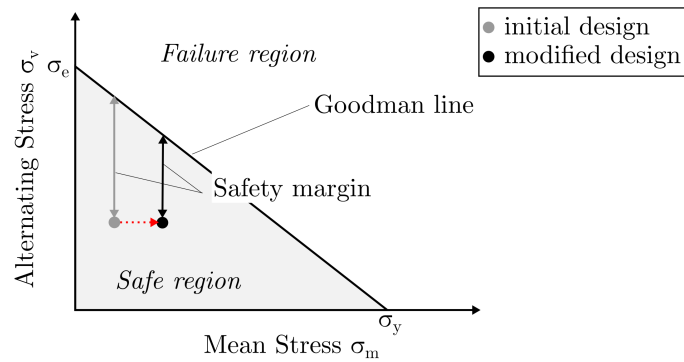


Fig. 5 Goodman relation for evaluation of fatigue strength for initial (gray) and increased (black) stress level.

The fatigue strength is influenced by the mean stresses and the alternating stresses, whereas the Goodman line limits the area of safe operation. For the initial design (gray), the safety margin [10] indicating the distance to the failure region is significantly greater than for the modified design (black). In a rotating component, the mean stresses result from stationary loads and residual stresses and the alternating stresses are caused by vibration. The two states depicted in Fig. 5 are identical in terms of alternating stresses, so that the decrease of fatigue strength results from higher mean stresses.

Considering patch repairs, the mean stresses in the blade change due to the welding process and local heat treatment. The remaining residual stresses increase the mean stresses and hence lead to a lower fatigue strength of the component. Especially, the joint between patch and parent material is prone to fatigue failure. In this region, mean stresses are mainly increased and the microstructure is changed in the heat affected zone around the weld. For this reason, the endurance limit in the proximity of the weld is usually lower than in the parent material.

One common measure to determine the fatigue strength of turbomachinery blades is the dimensionless amplitude frequency strength [27]

$$af = \frac{\sigma_e}{\sigma_v} \left(1 - \frac{\sigma_m}{\sigma_y} \right), \quad (1)$$

where σ_e is the endurance limit in Pa, σ_v is the alternating vibratory stress in Pa, σ_m is the mean stress in Pa and σ_y the yield strength in Pa. The endurance limit σ_e characterizes the failure point and has to be determined experimentally. The amplitude frequency strength (af) can be calculated for each vibration mode and reflects the relation depicted in the Goodman diagram (see Fig. 5). In Equation 1, high af-values indicate a low material loading, while low af-values indicate a high loading. Hence, the location with the minimum af-strength is crucial for the fatigue life of the whole component. Assuming that fatigue failure occurs in the weld-affected region, the spatial position of the weld centerline greatly influences the prevailing vibratory and mean stress level in the weld and thus the strength of the repaired blade. For this reason, the minimum strength of the weld-affected region is a design goal and thus selected as an objective value for the optimization.

A further design criterion is related to the machining effort involved in the patching process. The repair costs and the portion of the initial blade, which is replaced by the patch, are of interest. Since the length of the weld corresponds to the welding time, tool paths and processing costs, the weld length l in m is a suitable measure of the repair effort. Shorter welds are also preferable from a structural-mechanical perspective because of the lower risk of introducing welding imperfections. Patch designs with shorter welds correspond to smaller patches, whereby more of the original blade material is retained and less excess patch material has to be machined away to restore the original blade profile.

Finally, there has to be a constraint in place to ensure that the damaged portion of the blade is fully removed prior to welding. This is implemented using the pointwise description of the defect introduced in the previous section.

IV. Multi-Objective Formulation

Based on the design goals for patch repairs, an optimization problem is formulated such that

$$\begin{aligned} & \min_{\mathbf{x}} f(\mathbf{x}) \\ & \text{subject to} \quad g(\mathbf{x}) \leq 0 \\ & \text{and} \quad \mathbf{x}_{lb} \leq \mathbf{x} \leq \mathbf{x}_{ub}, \end{aligned} \quad (2)$$

where $f(\mathbf{x})$ is the objective function, $g(\mathbf{x})$ is the inequality constraint equation and \mathbf{x}_{lb} and \mathbf{x}_{ub} are the lower and upper boundaries for design variables \mathbf{x} . Since the expression in Eq. (2) is a multi-objective formulation, the objective is a vector-valued function, which represents multiple design goals.

In particular, the objectives considered for optimized patch geometries comprise the weld length and fatigue properties

$$\mathbf{f}(\mathbf{x}) = \begin{pmatrix} l \\ -af_1 \\ \vdots \\ -af_n \end{pmatrix}, \quad (3)$$

where l is the weld length, af indicates the fatigue strength and index n is related to the number of considered load cases. As the optimization problem is formulated as a minimization, a negative sign is added to the af -values. Depending on the number of load cases and vibration modes considered in Eq. (3), this results in an $(n + 1)$ -objective optimization problem.

Besides the objective function, the multi-objective problem in Eq. (2) involves a constraint that limits the design variable space to feasible designs only. For this purpose, the pointwise description of the defect introduced in Sec. II is used. The signed Euclidean distances between i damaged points and the plane specifying the interface between parent material and patch region are determined

$$d_i = (\mathbf{p}_i - \mathbf{r}) \cdot \mathbf{n}, \quad (4)$$

where \mathbf{n} is the normal vector and \mathbf{r} the position vector of the interface plane. Equation (4) assigns a positive value in meters to d_i , if the damage point \mathbf{p}_i lies outside the patch, and a negative sign otherwise if it lies inside the patched region.

Since the goal is to completely eliminate the defect from the blade by the patch repair, the inequality equation

$$g(\mathbf{x}) = \left(\max_i d_i \right) \leq 0 \quad (5)$$

has to be fulfilled. Equation 5 therefore constitutes a constraint for the optimization problem and $g(\mathbf{x})$ is in the unit meter. According to the parametric approach, the design variable set is specified by

$$\mathbf{x} = \begin{pmatrix} a \\ b \end{pmatrix}, \quad (6)$$

where the design variable space is bounded to $[0, 0]^T \leq \mathbf{x} \leq [1, 1]^T$.

To ensure that the constraint given in Eq. (5) is fulfilled, the optimization problem stated in Eq. (2) is further reformulated using a penalized objective function

$$\begin{aligned} \min_{\mathbf{x}} f(\mathbf{x}) + \Phi(g(\mathbf{x})) \\ \text{subject to } \mathbf{x}_{lb} \leq \mathbf{x} \leq \mathbf{x}_{ub}, \end{aligned} \quad (7)$$

which converts the constrained problem to an unconstrained problem. Designs, which are related to non-feasible solutions, are penalized by adding penalty values to the objective function according to a vector-valued penalty function Φ . The penalty function is vector-valued to make it compatible with the vector-valued objective function.

V. Simulation Model and Finite Element Analysis

In order to compute the objectives of the multi-objective optimization problem, a simulation model is established. As shown in Fig. 6, the simulation model links the parametric patching approach with the design goals of the multi-objective formulation.

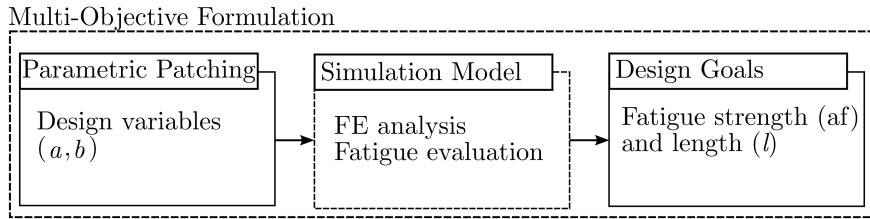


Fig. 6 Flowchart of multi-objective optimization.

The simulation model firstly includes a FE analysis to predict blade stresses, secondly evaluates the mean and alternating stresses in the weld-affected region and thirdly calculates the minimum fatigue strength according to the Goodman relation. The mean stresses in the blade are mainly dominated by centrifugal forces as well as by residual stress resulting from manufacturing processes. Determining the residual stress level resulting from welding requires time-consuming thermomechanical simulations. Due to the complexity of these welding simulations, modifications of the FE meshes or adjustments of the solver settings are usually unavoidable when analyzing different repair designs. A completely automated computation of the thermally induced stress field therefore becomes almost impossible. Furthermore, an extension of the simulation model would also imply that the welding parameters have to be included as additional design variables in the optimization problem formulation. Instead of just finding the optimal spatial positions of the weld, this approach would therefore lead to a vastly more complex problem which encompasses tuning of the welding process parameters. However, the welding process modeling is not the focus of this work and is thus considered as a complement to multi-objective optimization. Therefore, a two-step procedure is proposed.

In the first step, the multi-objective optimization is performed using the mean stresses according to the nominal blade loading while disregarding residual stresses. Subsequent to the optimization, individual Pareto optimal solutions are selected and analyzed further. In this second step, numerically expensive welding simulations are performed that consider welding process parameters.

The proposed two-step approach has advantages especially with respect to the computation time. Since the simulation model is repeatably used during the optimization in each objective function evaluation, the approach leads to feasible computation times for the optimization. In addition, the alternating and mean stresses in the blade need to be computed only once, because the geometry and stiffness of the patch-repaired blade are identical with the original design. The fatigue strength of the weld, contributing to the objective values, is calculated purely from the stresses in the spatial location of the weld. The weld-affected region is specified by the design variables of the parametric patching approach. The fatigue evaluation is based on von Mises stresses, while the minimum fatigue strength in the weld-affected region is significant.

The compressor blisk geometry utilized for the numerical examples of the proposed multi-objective approach is depicted in Fig. 7. The blisk is designed for a 1.5-stage axial compressor that is used for aerodynamic experiments [28]. The blisk is made out of titanium alloy Ti-6Al-4V and comprises 24 blades.

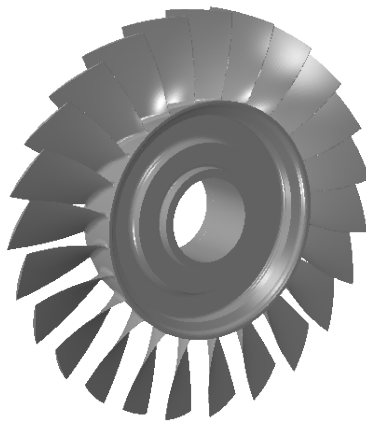


Fig. 7 Geometry of the compressor blisk analyzed.

In the following subsections, the static and modal analysis used in the optimization and the welding simulation are described. All FE simulations are performed using the commercial software Abaqus.

A. Static and Modal Analysis

The FE simulations are carried out using one periodic section of the blisk, because the repaired blade is assumed to have identical stiffness, mass and geometry to the nominal sector. Mistuning of the rotor, as modeled by Hou [17] or Beck et al. [29], is not considered in this work. The cyclic blisk sector geometry with the associated FE mesh is

shown in Fig. 8. Except for the blade fillet, the blade sector is meshed with hexahedral elements. In the fillet region, tetrahedral elements are used due to the irregular geometry. Further, the blade region has a finer mesh compared to the disk region, because the blade is the area of interest for patch repair optimization. In total, the FE mesh of the sector used for mechanical simulation comprises 268 563 nodes and 56 814 elements with quadratic shape functions.

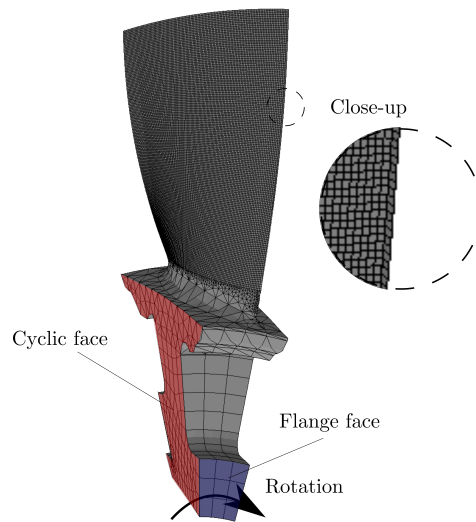


Fig. 8 FE mesh of the compressor blisk sector.

Rotational symmetry is enforced for the blisk sector by cyclic displacement constraints imposed on the cyclic faces of the sector. The displacement in axial and tangential direction is constrained at the flange face near the rotor hub in accordance with the mechanical boundary conditions of the installed blisk. Material parameters are defined using the material properties of Ti-6Al-4V at an operating temperature of 70 °C (see Fig. 11).

During operation, the blade is subjected to centrifugal and pressure forces. At the nominal operating point, the blisk rotates at a speed of 17 100 rpm. Stresses due to the rotation of the blisk are determined by performing a geometrically nonlinear, quasi-static analysis and imposing constant rotational velocity around the rotor axis. Additionally, static uniform pressure loads determined in CFD simulations are applied to the blade. The combination of quasi-static loads provides the mean stress level, which is subsequently used for fatigue evaluation.

Stresses resulting from blade vibrations are determined by a modal analysis which takes into account the mean stress level. Mode shapes and natural frequencies are computed for the undamped system, because structural damping is relatively small in the case of blisks. The mode shapes analyzed in detail are selected according to resonance conditions. For the determination of the resonances, the nodal diameter and the rotational speed are considered according to Singh et al. [30]. In this context, the nodal diameters refer to the number of nodal lines in the global vibration mode of the whole cyclic blisk. The vibratory stresses of the sector mode shapes are scaled to an amplitude frequency level of 1 m Hz to compute af-strength [27]. For absolute lifetime prediction, the actual excitation and thus the true vibration amplitude

must be determined in tip-timing tests. Furthermore, the endurance limit in welded structures is typically much lower than in the parent material [31]. In this work, it is therefore assumed that, due to the degradation of the material, the failure always occurs in the area of the weld. In the following, the endurance limit of 590×10^6 Pa is used [32].

B. Welding Analysis

The FE model described in the previous subsection does not capture residual stresses caused by the welding process. However, these induced stresses further contribute to the mean stress level and therefore impact the fatigue properties. For a more detailed evaluation, the thermally induced stresses are computed in a decoupled thermomechanical simulation [11]. First, a transient heat transfer analysis is carried out. The propagating heat source of the welding process is modeled using an analytic heat source model. In this case, an electron beam process is modeled. Since the heat input of electron beam welding is concentrated locally, a conical heat source model is suitable [9]. The related volume of the conical heat source is shown in Fig. 9.

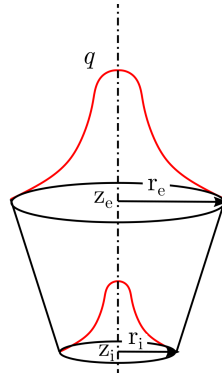


Fig. 9 Conical heat source volume.

The heat input in the truncated cone is analytically defined by

$$q = \frac{9Qe^3}{\pi(e^3 - 1)} \frac{1}{(z_e - z_i) \left(\frac{r_e^2}{r_e r_i} + \frac{r_i^2}{r_i^2} \right)} e^{-\frac{3r^2}{r_0^2}}, \quad (8)$$

where q is the power per unit volume in $J/(s \text{ mm}^3)$, Q is the total thermal power in J/s , z_e and z_i are the start and end depth of the cone in mm, r_e and r_i are exterior and interior radii of the cone in mm, z is the distance to the center in local coordinates in mm and e is the natural exponential function.

The radii

$$r_0(z) = r_e - \frac{r_e - r_i}{z_e - z_i} (z_e - z)$$

and

$$r = \sqrt{x^2 + y^2}$$

(9)

define the depth-dependent radius of the cone r_0 (in mm) and the distance r (in mm) in terms of distances to the center in local coordinates x , y and z .

During the welding process, the torch moves along the interface between the blade and the patch. This movement of the torch is simulated by a three-dimensional trajectory, as shown in Fig. 10.

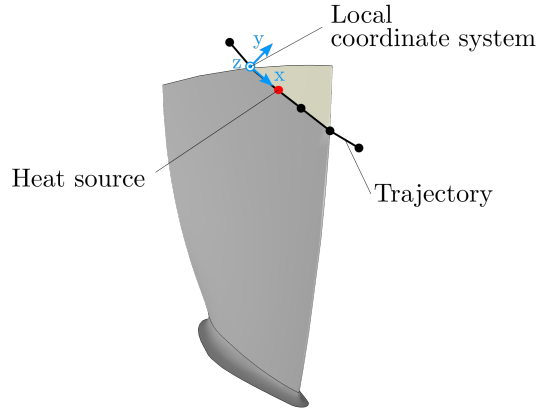


Fig. 10 Blisk blade with welding trajectory.

The trajectory is a piecewise linear path expressed in global coordinates. For the computation of heat flux in the proximity of the heat source, the trajectory is further used to define a local orthogonal coordinate system (light blue). The local coordinate system originates at the starting point of the section on which the heat source moves at that time. As the welding process continues, the position of the local coordinate system is updated. The first local axis (x) is aligned with the welding path, while the z -axis is orthogonal to the blade surface. The welding process including the heat input and torch movement is implemented in a user-defined DFLUX subroutine for the Abaqus solver.

The topology of the mesh used for the computation of temperatures equals the mesh shown before in Fig. 8, but linear heat transfer elements are used instead of quadratic mechanical elements. This results in a mesh with 70 725 nodes and 56 814 elements. The temperature-dependent thermal properties of Ti-6Al-4V used in the simulation are shown in Fig. 11. The film coefficient at the blade surface is assigned to $25 \frac{\text{W}}{\text{m}^2\text{K}}$ and the latent heat is specified as $3.6 \times 10^5 \frac{\text{J}}{\text{kg}}$ according to [33].

Subsequent to the thermal analysis, the transient temperature field is transferred to the mechanical model. A mechanical analysis is performed using an elasto-plastic material law with linear isotropic hardening. The temperature-dependent structural properties of Ti-6Al-4V are also shown in Fig. 11. The FE mesh of the mechanical model is compatible with the mesh topology used for thermal simulation. The geometry of the patch before recontouring to aerodynamic shape is not modeled, therefore the nominal blade geometry is used for the thermo-mechanical simulation. The blisk is clamped in the disk region. No displacement constraints are imposed at the blade region to allow the blade to deform freely during welding. In addition to the welding process, a heat treatment procedure is simulated. During reheating, the repaired blade stresses are relieved by plastic creep deformation. The patch joint is heated up to 600 °C in two hours and the dwell time is one hour [36]. The heating process is followed by furnace cooling, where the component is cooled down to room temperature. The residual stress in the blade contributes to a change in mean stress level and hence to a deterioration of the fatigue strength compared to the original part.

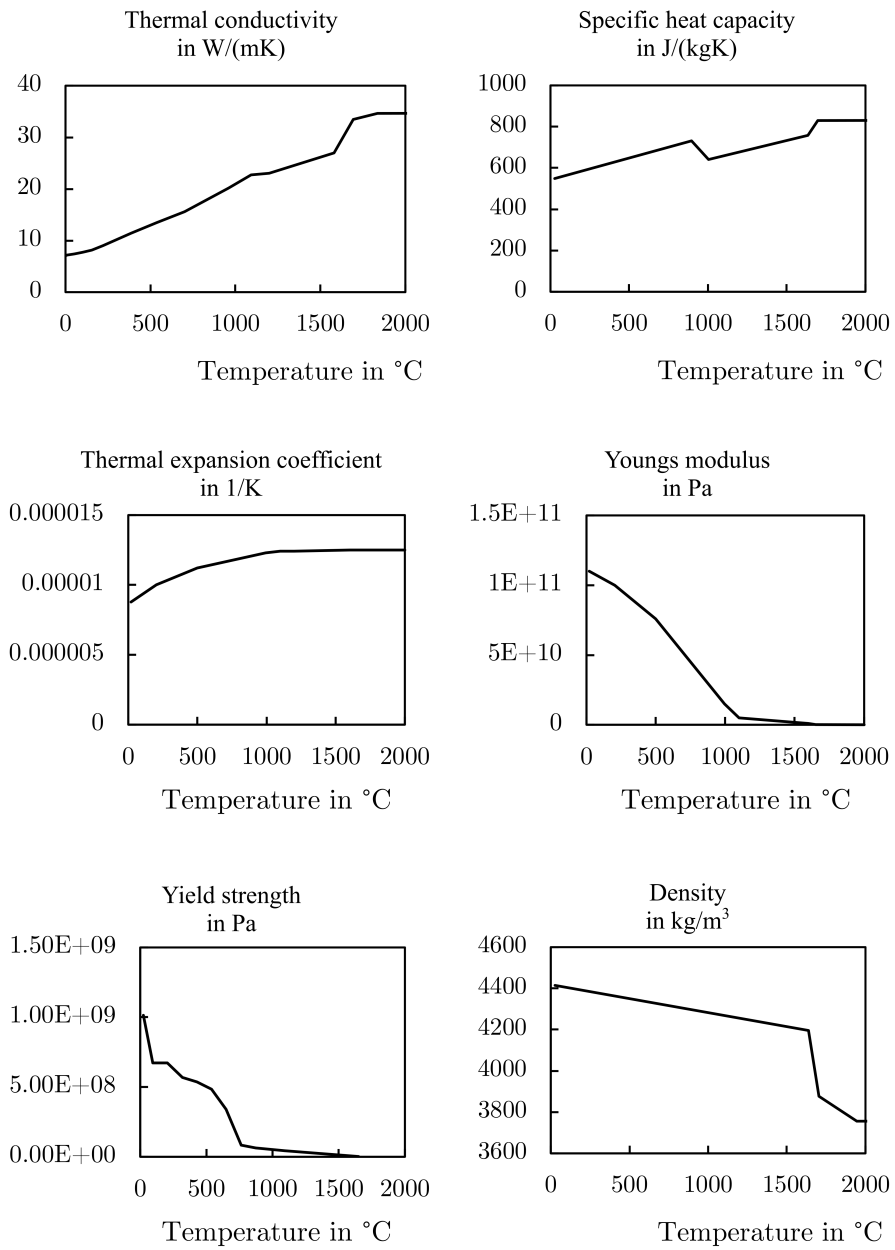


Fig. 11 Material properties of Ti-6Al-4V for FE simulations. [33–35]

VI. Multi-Objective Optimization

In the following section, the multi-objective approach is applied to a blisk blade with an exemplary damage pattern. First, optimization results for optimization formulations with only two objectives are shown to provide first insights into the interaction of optimization goals. Then, the complexity is increased by expanding the formulation to six objectives. The optimization results are compared to results determined in the two-objective case and discussed using a matrix visualization. Finally, welding simulations for characteristic Pareto optimal designs are performed.

A. Optimization Process and Settings

The damage pattern considered in the optimization example is depicted in Fig. 12. The damaged portion is shaped to resemble foreign object damage as it is depicted in Fig. 1. In this case, it is described by a set of three points, which are located close to the leading edge of the blade.

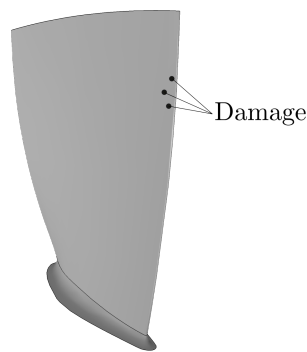


Fig. 12 Defect at the leading edge of the blade.

The relevant load cases, which are taken from the design documentation [37] of the considered compressor blisk, are listed in Tab. 1. These load cases take critical resonance transitions into account. The first load case associated with the first bending mode and third nodal diameter is studied, because the third engine order (EO) is the lowest EO crossing the first frequency in the operating range of the compressor. The excitation of the second load case refers to the difference between up- and downstream stator vane excitation (30 vanes - 26 vanes). Finally, the excitation considered for higher modes in load case three to five corresponds to the upstream stator vane excitation (26th EO).

It should be noted that load cases are labeled with Latin numbers and indices, while Roman numbers are used to indicate blade modes.

Table 1 Load cases taken from the design documentation of the compressor blisk [37] and associated undamped natural frequencies.

Load case	Mode number	Nodal diameter	Operating speed	Frequency
1	I	3	80%	682 Hz
2	I	4	60%	639 Hz
3	V	2	75%	5556 Hz
4	VI	2	85%	6179 Hz
5	VII	2	100%	7429 Hz

For the evaluation of fatigue strength of patch repairs, the af -values in the joint are analyzed according to the parametric model (Sec. II). All optimization problems are solved using the Non-dominated Sorting Genetic Algorithm II (NSGA-II), which is a state-of-the-art optimizer for gradient-free multi-objective optimization. In particular, the implementation in the optimization framework EngiO [38] is used. The algorithm-specific operators are set in accordance with the range of settings used by Deb et al. [39]. The crossover probability was set to 0.9, the mutation probability was set to 0.33 and distribution indexes for crossover as well as for mutation operators were set to 10. These settings were applied for all optimization problems presented in this paper. The population size of NSGA-II is adjusted according to the complexity of the optimization problem. The population size selected in the two- and six-objective case are stated in the corresponding paragraphs. The population size and number of evaluations carried out result from preliminary convergence studies using the hypervolume metric [40].

B. Two-Objective Optimization

First, the patch geometry is optimized considering the length of the weld and the first load case from Tab. 1 in a two-objective function

$$\mathbf{f}(\mathbf{x}) = \begin{pmatrix} l \\ -af_1 \end{pmatrix}. \quad (10)$$

In preliminary studies, different population sizes of NSGA-II were tested. In the two-objective case, a population size of 52 and 10 000 objective function evaluations are sufficient to recover the Pareto frontier. The results of one representative optimization run are shown in Fig. 13. The af -values are further normalized with the lowest fatigue strength af_{worst} found in the optimization run, which represents the worst case.

Samples generated during the optimization are marked using black dots. Solutions that are non-dominated are highlighted in red and indicate the Pareto frontier of the problem. In this case, 235 non-dominated solutions are found that form a continuous convex frontier. The start and end points indicated by \mathcal{A} and \mathcal{B} correspond to the solutions of the single-objective problems formed by the minimization of the individual objectives.

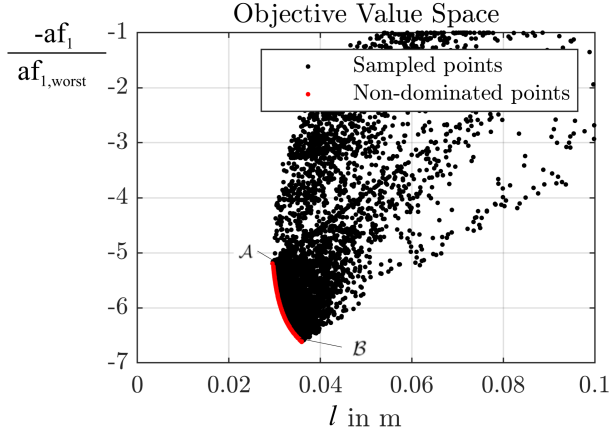


Fig. 13 Pareto frontier for length and normalized fatigue strength related to first mode (load case 1).

For further evaluation of the optimization results, the patch designs related to individual Pareto optimal solutions are shown in Fig. 14. In this visualization, the welding trajectories indicating the interface between patch and blade material are highlighted. The damage pattern introduced in Sec. VI.A is marked in black.

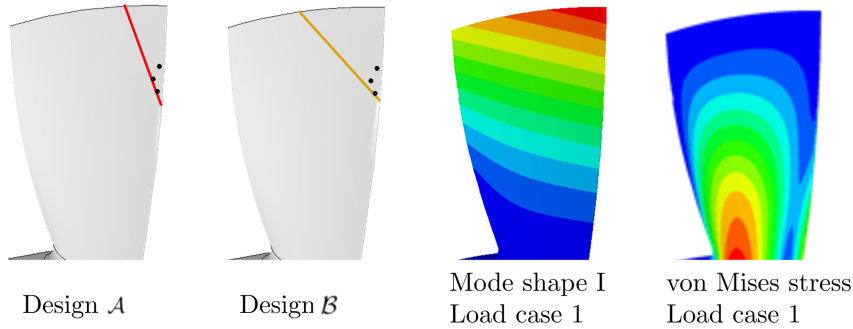


Fig. 14 Designs, mode shape and vibratory stress related to the two-objective optimization results in Fig. 13. Damage points are marked in black.

The first plot visualizes the design labeled with \mathcal{A} . It is the patch design with the shortest possible weld length, which leads to an objective value of $l = 29.55$ mm. The trajectory is located in the upper part of the blade and the patch has a height of $a = 0.35$ with respect to the length of the leading edge (see Fig. 2). The width of the patch is about one quarter of the blade width. The design \mathcal{B} , which has an optimal fatigue strength with respect to the first vibration mode, is shown in the second plot. The patch has a longer weld and is of larger width ($b = 0.48$), while the spanwise dimensions are comparable. All other designs associated with the Pareto frontier in Fig. 13 have similar patch heights a and the widths b range between Design \mathcal{A} and \mathcal{B} . Therefore, only short patch designs, which only remove a small portion of the blade tip region, should be used with regard to the first mode. This is reasonable, because the first mode as shown in Fig. 14 is a bending mode, where the highest stress amplitudes due to vibration occur close to the fil-

let. Patch designs that place the joint into the lower portion of the blade are thus unfavorable regarding the fatigue strength.

Second, the vector-valued objective function stated in Eq. 10 is modified such that another load case is analyzed. The second objective is hence exchanged and replaced by the objective function related to the fatigue strength of the fifth load case of Tab. 1. The first objective, the damage definitions, optimization and algorithm settings are the same as in the previous example. The two-objectives

$$f(\mathbf{x}) = \begin{pmatrix} l \\ -af_5 \end{pmatrix} \quad (11)$$

are optimized. After 10 000 objective function evaluations, the Pareto frontier shown in Fig. 15 is found. In total, 150 non-dominated solutions are determined. Analogous to the results shown previously, the solutions on the left and right end of the frontier refers to the patches with shortest and longest welding length. The corresponding two designs \mathcal{A} and \mathcal{C} are depicted in Fig. 16. Since the design with shortest weld length equals the patch design shown in the last paragraph, the solution is again labeled with \mathcal{A} . However, design \mathcal{C} , which is optimal with regard to the fatigue strength of the seventh vibration mode (mode VII) differs from the design \mathcal{B} found in the previous example.

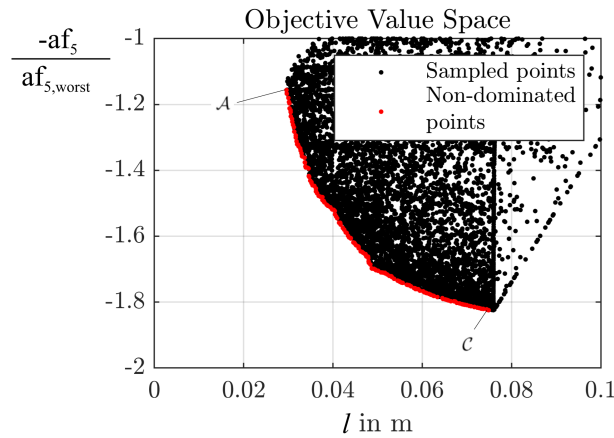


Fig. 15 Pareto frontier for weld length and normalized fatigue strength related to seventh mode (load case 5).

This time, the Pareto optimal set includes designs, which can be described as long patches. These long patches are characterized by a weld, which runs along the leading edge of the blade. The last point on the frontier labeled with \mathcal{C} corresponds to such a long narrow patch geometry. It is favorable in terms of fatigue properties of the seventh vibration mode, which is shown in Fig. 16. The depicted mode shape leads to low vibratory stresses in a narrow region close to the leading edge, which makes long patches favorable. The other Pareto optimal solutions are found for designs located in between the two extreme solutions \mathcal{A} and \mathcal{C} . They are characterized by small widths ($b \leq 0.23$) and heights up to the length of the leading edge ($a = 1$).

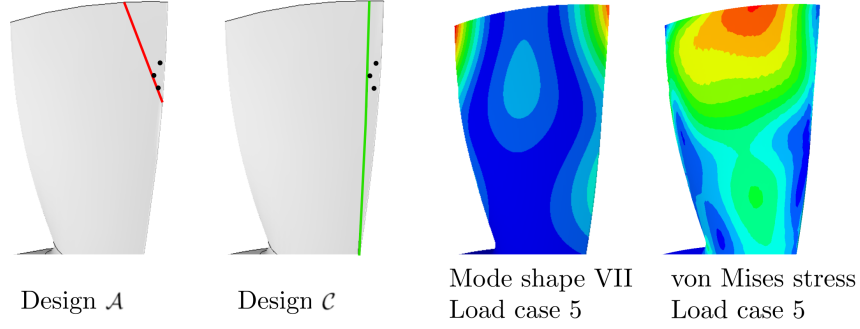


Fig. 16 Designs, mode shape and vibratory stress related to the two-objective optimization results in Fig. 15. Damage points are marked in red.

C. Six-Objective Optimization

The two-objective design procedures showed optimal design alternatives for two load cases separately. However, the patch repair should meet all design requirements at the same time. Hence, the optimization problem is formulated including all load cases specified in Tab. 1. Combined with the weld length, this results in a six-objective optimization

$$f(\mathbf{x}) = \begin{pmatrix} l \\ -af_1 \\ -af_2 \\ -af_3 \\ -af_4 \\ -af_5 \end{pmatrix}. \quad (12)$$

Following the definition of Pareto dominance, Pareto optimal solutions can be determined in the same way as in the two-objective case. However, the non-dominated solutions lie on a hyper-dimensional plane and can therefore not be visualized in a two-dimensional plot. To analyze the optimization results calculated for this extended problem, a matrix representation similar to the visualization of Adjei et al. [23] is used.

Fig. 17 shows the multi-objective results using NSGA-II with a population size of 100. Since the complexity of the problem increases, the population size is increased compared to the two-objective case and the number of function evaluations is raised to 20 000 to ensure converged results. All further algorithm settings are the same as in the two-objective cases. As in the two-objective case, the Pareto frontier shown in Fig. 17 refers to a single optimization run, but is representative of multiple optimization runs. Each row and column in the depicted matrix corresponds to one objective such that each of the plots shows the combination of two objective functions. The first row e.g. visualizes the dependency between different fatigue properties shown on the abscissa and the weld length shown on the ordinate of the

plots. The depicted solutions (blue and red markers) result from the projection of the six-objective optimization results onto the respective two-dimensional objective plane. Moreover, each sub-figure shows the Pareto optimal solutions, which are also Pareto optimal with respect to the two associated objectives, using red highlighting.

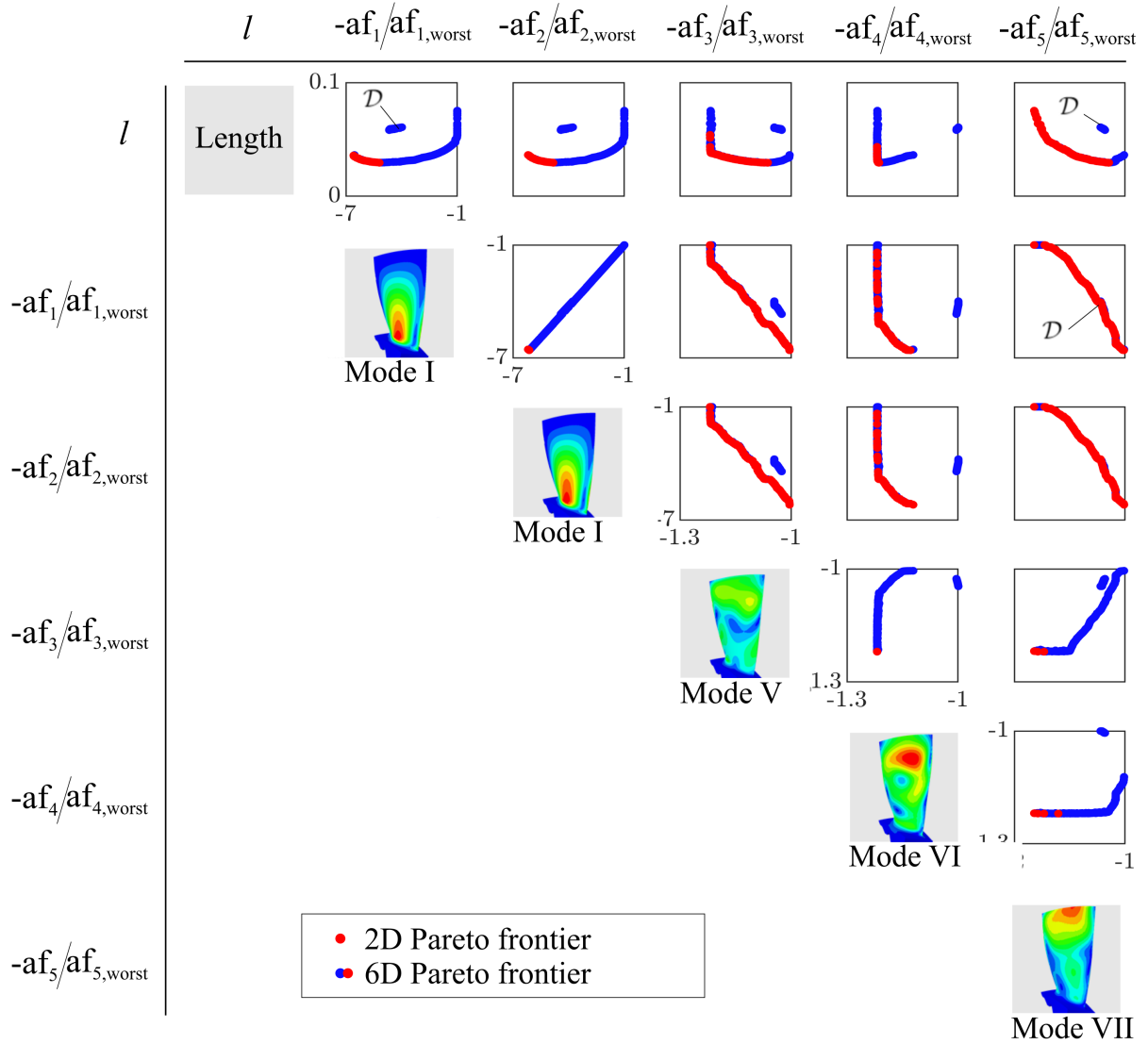


Fig. 17 Pareto frontiers for combinations of objectives. Von Mises stresses of the blade's mode shapes are depicted in the diagonal.

Depending on the combination of objectives, different courses of frontiers become visible using this highlighting scheme. By analyzing the first and last plot in the first row, the same Pareto frontiers as calculated in the two-objective case (Fig. 13 and 15) are recovered. However, due to the combination with additional objectives, further Pareto optimal solutions are found in the six-objective case.

With regard to the combinations of objectives in the matrix, it can be observed that the objectives of the optimization have different correlations. The linear correlation between $-af_1$ and $-af_2$ shows that these two objectives are not contradicting each other. The two load cases refer similar vibration modes and the Pareto frontier thus converges to a singular solution. In contrast, e.g the combination of $-af_1$ and $-af_3$ shows a clear trade-off between design alternatives. These differences result from the related load cases. For further interpretation of results, the diagonal of the matrix depicts the von Mises stresses of the corresponding vibration modes. From the comparison of the stress plots, it can be concluded that the higher modes lead to relatively high stress amplitudes in the center of the upper part of the blade, whereas the first bending mode leads to maximum amplitudes near the fillet. Hence, narrow long patches as well as short patches are favorable depending on fatigue preferences. Moreover, in the sub-plots showing the dependencies between $-af_3$, $-af_4$ and $-af_5$, only a few solutions are highlighted in red. This means that no improvement in one objective is achieved even if a deterioration in the other goal is accepted. In the sub-plot of $-af_3$ and $-af_4$, it becomes particularly clear that there are hardly any design alternatives that are Pareto optimal with respect to the two objectives. This effect is caused by similar distribution of the vibratory stress of mode V and VI which drive the respective fatigue strength.

The effect of mode-specific fatigue properties is also discernible in the design space of the non-dominated solutions. Designs, which are characteristic for the six-objective case are depicted in Fig. 18. In addition to designs \mathcal{A} , \mathcal{B} and \mathcal{C} discussed in the previous section, there are Pareto optimal designs that are characterized by a large width of the patch as in Design \mathcal{D} .

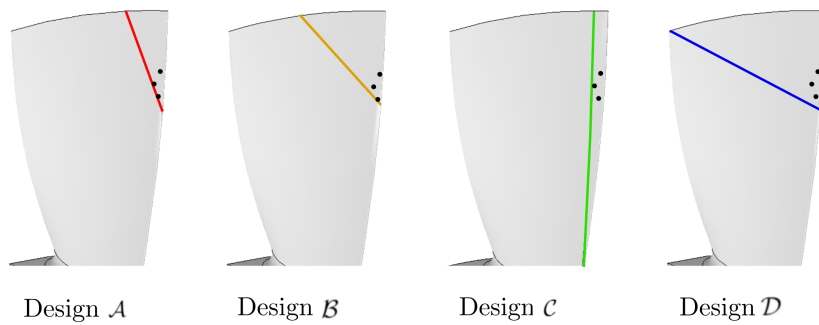


Fig. 18 Designs related to the six-objective optimization results in Fig. 17.

Overall, the Pareto optimal designs can be subdivided into two groups. The first group refers to designs with relatively narrow patches ($b < 0.5$). The patterns of this group are equal to results presented in the previous section and include Designs \mathcal{A} , \mathcal{B} and \mathcal{C} . The patch geometries related to this group thus merge the designs found in the two-objective cases.

The second group of designs corresponds to patches with large width ($b \approx 1$) and short height, which clearly differ from the designs analyzed previously. Design \mathcal{D} also shown in Fig. 18 represents one solution out of this second

group. The related objective values are marked in three sub-plots of Fig. 17 for the combination of the objectives l , $-af_1$ and $-af_5$. The visualization in objective values space shows that the correlation between $-af_1$ and $-af_5$ causes Pareto optimality for the design. With regard to the vibration modes, high vibration amplitudes of the first mode (load case 1 and 2) at the fillet and high stresses of the seventh mode (load case 5) in the center close to the tip are avoided simultaneously by designs similar to design \mathcal{D} . In contrast to previous results, this design is not intuitive and would therefore not be considered to be an optimal solution prior to the optimization.

Another interesting aspect resulting from the six-objective optimization is that most feasible designs are excluded for the positioning of the weld. The white regions of the blade shown in Fig. 19 indicate regions where the weld should not be placed. Gray colored regions refer to regions where Pareto optimal weld trajectories can be found. Given the Pareto optimal designs, an engineer tasked with the blisk repair thus needs to consider only a few design alternatives to pick the final design.

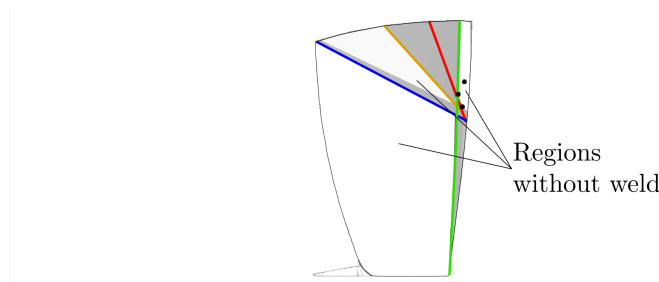


Fig. 19 Blade with representative designs and regions referring to optimal welding trajectories (gray).

D. Results of Welding Analysis

According to the modeling approach introduced in Sec. V, residual stresses resulting from the welding process are evaluated for Pareto optimal designs. This detailed evaluation of thermally induced stresses is done for the four characteristic design alternatives \mathcal{A} , \mathcal{B} , \mathcal{C} and \mathcal{D} identified from optimization in the previous section. The welding process parameters [7] and heat source dimensions used for the simulation are specified by the parameters listed in Tab. 2.

Table 2 Parameters used for the welding simulation.

Parameter	
Heat input	50 J/mm
Speed	5 mm/s
Exterior radius	2.0 mm
Interior radius	0.5 mm
Penetration depth	3.0 mm

Utilizing the thermal and mechanical FE analyzes, the temperature distribution during welding and the resulting stresses are calculated. In Fig. 20 a), the temperature distribution is exemplarily shown for the welding process of Design \mathcal{B} (see Fig. 13) at a time step of $t = 2\text{ s}$. The heat is introduced localized close to the center of the heat source. The weld pool temperature reaches about $1900\text{ }^\circ\text{C}$, which is above the melting temperature of the alloy at $1650\text{ }^\circ\text{C}$ [33].

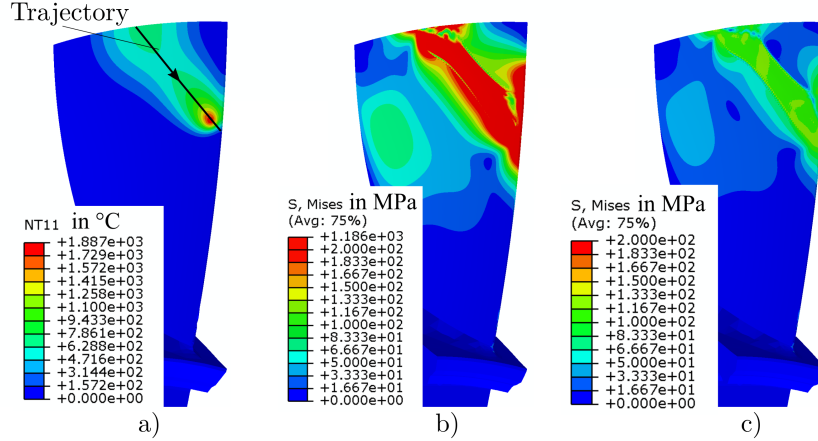


Fig. 20 Sector with a) temperatures during welding, b) von Mises stresses right after welding and c) after heat treatment for Design \mathcal{B} .

The von Mises stresses caused by the transient temperature field, which are computed in the subsequent mechanical analysis using the nominal blade geometry, are visualized in Fig. 20 b). In the whole joint region, a stress level of more than 200 MPa is computed. This high residual stress level is decreased in the heat treatment process, such that the remaining stresses depicted in Fig. 20 c) diminish to about 100 MPa . Changes in the residual stress state due to contouring processes are not considered. Well-adjusted machining leads to an improvement of surface strength. Neglecting the mechanical influence of machining is therefore the conservative approach.

Finally, the remaining residual stresses in the weld region are analyzed for each of the four designs \mathcal{A} , \mathcal{B} , \mathcal{C} and \mathcal{D} and the fatigue properties are calculated. As the weld of design \mathcal{C} is very close to the leading edge, where the blade becomes thin, less power is needed to melt the material. The welding process power is reduced by 20% to meet the melt pool temperature of $1900\text{ }^\circ\text{C}$. The fatigue strength properties including residual stresses af_i^{weld} are compared with the fatigue strength properties computed during optimization af_i . The relative reduction of fatigue strength values $\frac{af_i^{\text{weld}} - af_i}{af_i}$ caused by increased mean stresses are shown in Tab. 3 for all load cases i .

Table 3 Relative fatigue strength deviation $\frac{af_i^{\text{weld}} - af_i}{af_i}$ of design alternatives \mathcal{A} , \mathcal{B} , \mathcal{C} and \mathcal{D} for each load case i .

Load case	Design \mathcal{A}	Design \mathcal{B}	Design \mathcal{C}	Design \mathcal{D}
1	-12.75 %	-11.13 %	-9.97 %	-11.07 %
2	-12.70 %	-11.01 %	-10.06 %	-10.91 %
3	-11.09 %	-11.22 %	-9.61 %	-11.54 %
4	-11.07 %	-11.25 %	-10.44 %	-12.57 %
5	-8.66 %	-12.24 %	-8.57 %	-14.47 %

In general, the residual stresses from the welding process reduce the HCF properties of the weld by about 10 %. The smallest deviations are determined for the longest patch (Design \mathcal{C}). This is mainly caused by the reduced welding power of the design alternative, which decreases thermally induced stresses. Even though the residual stresses generally lead to a reduction in strength, the previous qualitative conclusion about the fatigue behavior of different patch designs remains valid. Furthermore, it is shown that the residual stresses are sensitive to changes in welding parameters and an appropriate choice of welding process and heat treatment parameters positively influence the strength. Thermomechanical simulations are therefore required to determine the fatigue properties of the joint between blade and patch more precisely.

VII. Conclusion

In this paper, multi-objective optimization is used to find optimal patch repair designs for compressor blisks. The multi-objective formulation included the maximization of fatigue strength properties in terms of af -values and the minimization of the weld length of the patch repair. Design alternatives were modeled using a parameterized patching model. For the calculation of the objective function values, a simulation model is proposed that utilizes FE simulations to analyze the stresses and evaluates the HCF properties of the weld-affected region.

For a typical damage scenario, Pareto optimal solutions were found using NSGA-II and patch designs were subsequently analyzed in terms of their fatigue performance considering different load cases. It was demonstrated that the patch geometries to be preferred are strongly influenced by the considered load cases. In the studied example, the two-objective optimization reflecting the first bending mode and the weld length showed that only short patch designs were favorable. In contrast, for the seventh vibration mode, long patches proved to have the best fatigue behavior. New insights into patch designs were provided in particular by the six-objective optimization formulation, which combines five fatigue load cases and the weld length. While the results of the two-objective problem may have been predicted using engineering knowledge, the six-objective results showed Pareto optimal designs that are not intuitive.

In favor of an automated evaluation and computational efficiency, simplifications were made with regard to the FE model used for the optimization runs. Subsequent thermomechanical analyses of manually selected Pareto optimal

designs enabled a more detailed analysis of actual residual stresses. Residual blade stresses are computed considering purely thermally induced stresses. Changes in blade geometry and other stress contributions induced by the repair process were not considered. In this paper, four characteristic patch designs were used as a basis for welding process simulation. These simulations yielded a fatigue strength reduction of about 10 % compared to the nominal strength.

Overall, the multi-objective approach presented in this paper thus contributes to the initial selection of patch geometries and supports the design process. The advantages offered by multi-objective optimization can be fully exploited by the approach where the Pareto optimal solutions effectively narrow down the number of designs to be considered by the engineer. Finally, the design alternatives can then be further studied to adjust weld parameters and improve the strength of patched blades. In future work, it is conceivable to optimize patch repairs on the basis of fast surrogate models and thus to integrate numerically complex welding simulations into the optimization.

Funding Sources

This work was funded by the Deutsche Forschungsgemeinschaft (DFG, German Research Foundation) – SFB 871/3 – 119 193 472.

References

- [1] Aschenbruck, J., Adamczuk, R., and Seume, J. R., “Recent Progress in Turbine Blade and Compressor Blisk Regeneration,” *Procedia CIRP*, Vol. 22, 2014, pp. 256–262. <https://doi.org/10.1016/j.procir.2014.07.016>.
- [2] Bremer, C., “Automated Repair and Overhaul of Aero-Engine and Industrial Gas Turbine Components,” *Proceedings of the ASME Turbo Expo 2005*, ASME, New York, NY, 2005, pp. 841–846. <https://doi.org/10.1115/GT2005-68193>.
- [3] Bussmann, M., Kraus, J., and Bayer, E., “An Integrated Cost-Effective Approach to Blisk Manufacturing,” *Proceedings of the International Symposium on Air Breathing Engines*, American Inst. of Aeronautics and Astronautics, Munich, Germany, 2005.
- [4] Bussmann, M., and Bayer, E., “Blisk production of the future—technological and logistical aspects of future-oriented construction and manufacturing processes of integrally bladed rotors,” *Proceedings of the International Symposium on Air Breathing Engines*, Curran, Montreal, Canada, 2009.
- [5] Eberlein, A., “Phases of high-tech repair implementation—Definition, Development, Adaptation, Validation and Qualification, in Case of Patch-Repair on Blisk-Blades,” *Proceedings of the International Symposium on Air Breathing Engines*, American Inst. of Aeronautics and Astronautics, Beijing, China, 2007.
- [6] Denkena, B., Boess, V., Nesper, D., Floeter, F., and Rust, F., “Engine blade regeneration: A literature review on common technologies in terms of machining,” *The International Journal of Advanced Manufacturing Technology*, Vol. 81, No. 5-8, 2015, pp. 917–924. <https://doi.org/10.1007/s00170-015-7256-2>.

- [7] Denkena, B., Nespör, D., Böß, V., and Köhler, J., "Residual stresses formation after re-contouring of welded Ti-6Al-4V parts by means of 5-axis ball nose end milling," *CIRP Journal of Manufacturing Science and Technology*, Vol. 7, No. 4, 2014, pp. 347–360. <https://doi.org/10.1016/j.cirpj.2014.07.001>.
- [8] Denkena, B., Grove, T., Mücke, A., Langen, D., Nespör, D., and Hassel, T., "Residual stress formation after re-contouring of micro-plasma welded Ti-6Al-4V parts by means of ball end milling," *Materialwissenschaft und Werkstofftechnik*, Vol. 48, No. 11, 2017, pp. 1034–1039. <https://doi.org/10.1002/mawe.201600743>.
- [9] Azar, P., Li, P., Patnaik, P., Thamburaj, R., and Immarrigeon, J., "Electron beam weld repair and qualification of titanium fan blades for military gas turbine engines," *RTO AVT Specialsits' Meeting on " Cost Effective Application of Titanium Alloys in Military Platforms*, 2001.
- [10] Schoenenborn, H., and Reile, E., "Analytical analysis of the welding and heat treatment of a compressor blisk leading edge repair process," *Meeting Proceedings of RDP*, RTO, Montreal, Canada, 2005, pp. 17–1 –17–9.
- [11] Berglund, D., Alberg, H., and Runnemalm, H., "Simulation of welding and stress relief heat treatment of an aero engine component," *Finite Elements in Analysis and Design*, Vol. 39, No. 9, 2003, pp. 865–881. [https://doi.org/10.1016/S0168-874X\(02\)00136-1](https://doi.org/10.1016/S0168-874X(02)00136-1).
- [12] Xu, L., Cao, H., Liu, H., and Zhang, Y., "Assessment of fatigue life of remanufactured impeller based on FEA," *Frontiers of Mechanical Engineering*, Vol. 11, No. 3, 2016, pp. 219–226. <https://doi.org/10.1007/s11465-016-0394-x>.
- [13] Hou, J., and Cross, C., "Minimizing Blade Dynamic Response in a Bladed Disk Through Design Optimization," *AIAA Journal*, Vol. 43, No. 2, 2005, pp. 406–412. <https://doi.org/10.2514/1.11526>.
- [14] Kim, J.-H., Ovgor, B., Cha, K.-H., Kim, J.-H., Lee, S., and Kim, K.-Y., "Optimization of the aerodynamic and aeroacoustic performance of an axial-flow fan," *AIAA Journal*, Vol. 52, No. 9, 2014, pp. 2032–2044.
- [15] Keskin, A., "Application of Numerical Optimisation to Support Engineering Design," *Proceedings of the 58th AIAA/ASCE/AHS/ASC Structures, Structural Dynamics, and Materials Conference*, 2017. <https://doi.org/10.2514/6.2017-1545>.
- [16] Vicini, A., and Quagliarella, D., "Inverse and direct airfoil design using a multiobjective genetic algorithm," *AIAA journal*, Vol. 35, No. 9, 1997, pp. 1499–1505.
- [17] Hou, J., et al., "Assessment of allowable blade damage size for a blisk," *AIAC16: 16th Australian International Aerospace Congress*, Engineers Australia, 2015, p. 243.
- [18] Luo, C., Song, L., Li, J., and Feng, Z., "A Study on Multidisciplinary Optimization of an Axial Compressor Blade Based on Evolutionary Algorithms," *Journal of Turbomachinery*, Vol. 134, No. 5, 2012, p. 054501. <https://doi.org/10.1115/1.4003817>.
- [19] Buske, C., Krumme, A., Schmidt, T., Dresbach C., and Zur, S. and Tiefers, R., "Distributed Multidisciplinary Optimization of a Turbine Blade Regarding Performance, Reliability and Castability," *Proceedings of the ASME Turbo Expo 2016*, ASME, South Korea, 2016. <https://doi.org/10.1115/GT2016-56079>.

- [20] Keskin, A., and Bestle, D., "Application of multi-objective optimization to axial compressor preliminary design," *Aerospace Science and Technology*, Vol. 10, No. 7, 2006, pp. 581–589. <https://doi.org/10.1016/j.ast.2006.03.007>.
- [21] Kupijai, P., Bestle, D., Flassig, P. M., and Kickenweitz, D., "Automated Multi-Objective Optimization Process for Preliminary Engine Design," *Proceedings of the ASME Turbo Expo 2012*, ASME, 2012, p. 87. <https://doi.org/10.1115/GT2012-68612>.
- [22] Poehlmann, F., and Bestle, D., "Multi-Objective Compressor Design Optimization Using Multi-Design Transfer Between Codes of Different Fidelity," *Proceedings of the ASME Turbo Expo 2012*, ASME, New York, N.Y, 2012, pp. 2001–2010. <https://doi.org/10.1115/GT2012-68577>.
- [23] Adjei, R. A., Fan, C., Wang, W. Z., and Liu, Y., "Multidisciplinary Design Optimization for Performance Improvement of an Axial Flow Fan using Free-form Deformation," *Journal of Turbomachinery*, 2020, pp. 1–25. <https://doi.org/10.1115/1.4048793>.
- [24] Karger, K., and Bestle, D., "Parametric Blending and FE-Optimisation of a Compressor Blisk Test Case," *Advances in Evolutionary and Deterministic Methods for Design, Optimization and Control in Engineering and Sciences*, Computational Methods in Applied Sciences, Vol. 36, edited by D. Greiner, B. Galván, J. Périaux, N. Gauger, K. Giannakoglou, and G. Winter, Springer International Publishing, Cham, 2015, pp. 257–266. <https://doi.org/10.1007/978-3-319-11541-2{ }16>.
- [25] Berger, R., Hofmeister, B., Gebhardt, C. G., and Rolfes, R., "A two-objective design optimisation approach for blending repairs of damaged compressor blisks," *Aerospace Science and Technology*, Vol. 105, 2020, p. 106022. <https://doi.org/10.1016/j.ast.2020.106022>.
- [26] Berger, R., Hofmeister, B., Gebhardt, C. G., and Rolfes, R., "Parametric Design of Blisk Repairs by Patching Considering High Cycle Fatigue," *PRINT PROCEEDINGS OF THE ASME TURBO EXPO 2019*, edited by ASME, AMER SOC OF MECH ENGINEER, [S.l.], 2019. <https://doi.org/10.1115/GT2019-90351>.
- [27] Hanschke, B., Klauke, T., and Kühhorn, A., "The Effect of Foreign Object Damage on Compressor Blade High Cycle Fatigue Strength," *Proceedings of the ASME Turbo Expo 2017*, ASME, 2017, p. V07AT31A005. <https://doi.org/10.1115/GT2017-63599>.
- [28] Keller, C., Willeke, T., Burrafato, S., and Seume, J. R., "Design Process of a 1.5-Stage Axial Compressor for Experimental Flutter Investigations," 2015.
- [29] Beck, J. A., Brown, J. M., Runyon, B., and Scott-Emuakpor, O. E., "Probabilistic study of integrally bladed rotor blends using geometric mistuning models," *Proceedings of the 58th AIAA/ASCE/AHS/ASC Structures, Structural Dynamics, and Materials Conference*, 2017, p. 0860.
- [30] Singh, M. P., Vargo, J. J., Schiffer, D. M., and Dello, J. D., "SAFE Diagram-A Design and Reliability Tool for Turbine Blading," 1988.
- [31] Fomin, F., Horstmann, M., Huber, N., and Kashaev, N., "Probabilistic fatigue-life assessment model for laser-welded Ti-6Al-4V butt joints in the high-cycle fatigue regime," *International Journal of Fatigue*, Vol. 116, 2018, pp. 22–35. <https://doi.org/https://doi.org/10.1016/j.ijfatigue.2018.06.012>, URL <https://www.sciencedirect.com/science/article/pii/S0142112318302305>.

- [32] Shen, M., "Reliability assessment of high cycle fatigue design of gas turbine blades using the probabilistic Goodman Diagram," *International Journal of Fatigue*, Vol. 21, No. 7, 1999, pp. 699–708. [https://doi.org/10.1016/S0142-1123\(99\)00033-X](https://doi.org/10.1016/S0142-1123(99)00033-X).
- [33] Baruah, M., and Bag, S., "Influence of heat input in microwelding of titanium alloy by micro plasma arc," *Journal of Materials Processing Technology*, Vol. 231, 2016, pp. 100–112. <https://doi.org/10.1016/j.jmatprotec.2015.12.014>.
- [34] "MIL-HDBK-5J Metallic Materials and Elements for Aerospace Vehicle Structures," , 2003. URL <http://www.everyspec.com>.
- [35] Lu, X., Lin, X., Chiumenti, M., Cervera, M., Hu, Y., Ji, X., Ma, L., Yang, H., and Huang, W., "Residual stress and distortion of rectangular and S-shaped Ti-6Al-4V parts by Directed Energy Deposition: Modelling and experimental calibration," *Additive Manufacturing*, Vol. 26, 2019, pp. 166–179. <https://doi.org/10.1016/j.addma.2019.02.001>.
- [36] MacDonald, D., Rapuano, B., Deo, N., Stranick, M., Somasundaran, P., and Boskey, A., "Thermal and chemical modification of titanium–aluminum–vanadium implant materials: effects on surface properties, glycoprotein adsorption, and MG63 cell attachment," *Biomaterials*, Vol. 25, No. 16, 2004, pp. 3135–3146. <https://doi.org/https://doi.org/10.1016/j.biomaterials.2003.10.029>.
- [37] "Internal Report Anecom Aerotest: Technischer Bericht - Analyse," , 2016.
- [38] Berger, R., Bruns, M., Ehrmann, A., Haldar, A., Häfele, J., Hofmeister, B., Hübler, C., and Rolfes, R., "EngiO — Object-oriented framework for engineering optimization," *Advances in Engineering Software*, Vol. 153, 2021, p. 102959. <https://doi.org/https://doi.org/10.1016/j.advengsoft.2020.102959>.
- [39] Deb, K., Pratap, A., Agarwal, S., and Meyarivan, T., "A fast and elitist multiobjective genetic algorithm: NSGA-II," *IEEE Transactions on Evolutionary Computation*, Vol. 6, No. 2, 2002, pp. 182–197. <https://doi.org/10.1109/4235.996017>.
- [40] Zitzler, E., Deb, K., and Thiele, L., "Comparison of multiobjective evolutionary algorithms: empirical results," *Evolutionary computation*, Vol. 8, No. 2, 2000, pp. 173–195. <https://doi.org/10.1162/106365600568202>.

6 Application of EngiO to Multi-Objective Optimization of Blade Repairs

In engineering practice, the selection of the optimization algorithm and the choice of the algorithm-specific parameters usually happens subsequent to the formulation of the engineering optimization problem. The most suitable optimization algorithm to solve the practical problem is initially unknown. The variety of different optimization approaches used in aerospace [158], automotive [136], or structural design [101, 77] indicate that each algorithm has its specific strengths. In fact, according to the *no free lunch theorems* elaborated by Wolpert and Rupert [174], there is no universal approach to efficiently solve any kind of optimization problem. Therefore, the choice of the appropriate algorithm is related to the optimization task.

To get a general impression of the performance of algorithms and to compare their properties with respect to optimization problems, test functions are used. The comparison of algorithms applied to the same analytical function gives an indication of the relative performance. Such benchmark results were presented by the COCO project [26]. However, to evaluate the performance with respect to the real problem, a good knowledge of the characteristics of objective functions is required. This is usually not the case prior to the exploration of the objective value space. The selection of an algorithm remains a case-by-case decision.

In the following, a comparison of the performance of optimization algorithms is exemplified by the optimization task formulated in the context of patch repairs (paper C). An indicator for performance of multi-objective optimization results is introduced in Sec. 6.1 and utilized in Sec. 6.2. The comparison is performed using the optimization framework EngiO and thus also demonstrates one of the benefits of the developed framework.

6.1 Quality Indicators in Multi-Objective Optimization

To compare different settings and algorithms, e.g. in benchmark studies, optimization results are evaluated using quality indicators. Such quality indicators describe the performance of the algorithm by calculating a scalar value based on the optimization results.

In single-objective optimization, it is intuitive to compare the deviation of numerically calculated optimum to expected optimum, numbers of iterations needed, or convergence characteristics of best objective values. In contrast, in the case of multi-objective optimization, there is no single scalar optimal value, which could be used as a reference. One way to compare optimization results (at least in the two-objective case) is the visual inspection of non-dominated solutions in the objective value space and the propagation of the Pareto frontier depending on the number of evaluations. However, a quantitative ranking of the algorithms is not possible in this way.

Performance metrics are therefore used to indicate the quality of different sets of non-dominated solutions. One common metric is the hypervolume metric [18], which is also known as hypervolume indicator or S-metric⁸. Custódio et al. [43] provide the following definition:

Definition. *Hypervolume Metric:* For a approximation set $A \subset \mathbb{R}^m$ and a reference point $\mathbf{r} \in \mathbb{R}^m$ the hypervolume is defined as m -dimensional volume of a hole-free orthogonal polytope

$$\text{HV}(A) = \lambda(\cup_{\mathbf{a} \in A} [\mathbf{a}, \mathbf{r}]), \quad (6.1)$$

where λ is the Lebesgue measure and $[\mathbf{a}, \mathbf{r}]$ the interval between lower and upper corner of the volume.

A graphical example, visualizing the definition of the hypervolume in Eq. (6.1) in two dimensions, is shown in Fig. 6-1.

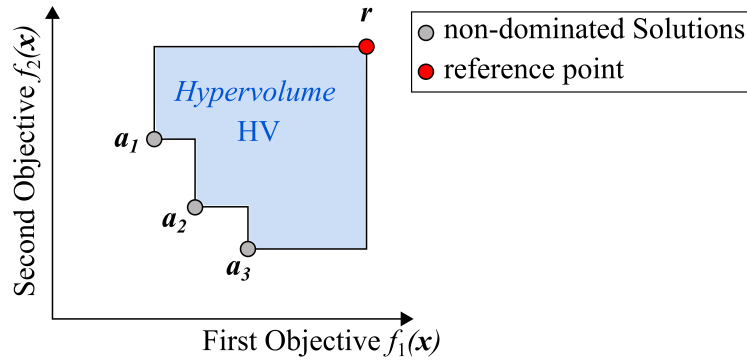


Figure 6-1: Visualization of the hypervolume metric for a two-dimensional example.

In the schematic example, the non-dominated set A found during optimization comprises of three solutions \mathbf{a}_1 , \mathbf{a}_2 , and \mathbf{a}_3 . Further, an arbitrary point, which has to be dominated by all points on the Pareto frontier, is selected as a reference. The corresponding hypervolume, which degenerates to an area in the two-dimensional case, is highlighted in blue. The size of this area depends on the position of all identified Pareto optimal solutions. When the results of an optimization relate to better objectives and the points are located closer to the origin of the objective value space, this area increases. A high value, therefore, denotes maximal hypervolume and indicates a good quality of results.

6.2 Optimization Algorithms and Parameters

As each algorithm performs differently for a given problem, two different optimization algorithms are compared in the following using one practical example. The chosen example is taken from the third paper of this thesis and refers to a two-objective problem, where the patch length and the fatigue strength related to the fifth load case are optimized for an

⁸S-metric is the abbreviation of Size of space covered.

optimal patch repair. For more information on the problem formulation and optimization result, it is referred to part B of paper C (see Sec. 5).

In EngiO, two algorithms are implemented which are able to handle multi-objective optimization problems. The first one is probably the most frequently used multi-objective algorithm known as Non-dominated Sorting Genetic Algorithm-II (NSGA-II) [46] and the second one is an in-house version of a deterministic approach named Multi-Objective Global Pattern Search (MOGPS) [86]. The optimization example is computed using both algorithms with default settings and allowing a maximum number of 10 000 objective function evaluations. During the optimization process, the values of the hypervolume metric are tracked. The obtained normalized values are shown in Fig. 6-2.

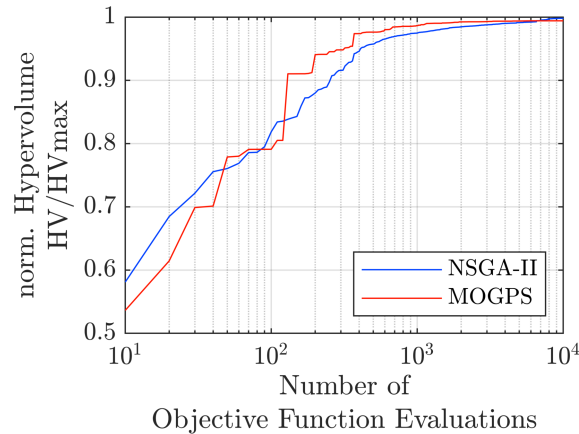


Figure 6-2: Visualization of the hypervolume metric for the second two-dimensional example in paper C for different algorithms.

The hypervolume metric is evaluated according to Eq. (6.1) with a reference point of $(0.1|0)$.⁹ Since the area referred to by the hypervolume metric has no physical meaning, the hypervolume is normalized according to the maximum hypervolume HV_{max} found in all optimization runs. Hence, the diagram in Fig. 6-2 illustrates the relative improvement in Pareto optimal solutions as a function of objective function evaluations.

Moreover, NSGA-II is a metaheuristic approach, which means that optimization results may vary from run to run. The data presented in Fig. 6-2 are therefore the mean values of 10 optimization runs. As MOGPS has a deterministic nature, the results are the same for each optimization run. In general, the value of the hypervolume indicator increases for a larger number of function evaluations. This is to be expected since a larger number of samples generated and evaluated by the algorithms should improve the quality of the results. At the beginning of the optimization, the improvement in hypervolume is relatively large. Later during the optimization, the improvement stagnates for both algorithms and the value converges to the maximum hypervolume. Depending on the number of solutions observed so far, one or the other algorithm performs slightly better. In particular, for a higher number of evaluations MOGPS shows better performance. Nevertheless, after 10 000 evaluations the HV indicators are almost the same for both algorithms. Therefore, it can be concluded that both algorithms are suitable to solve the problem considered in this example.

⁹This reference point was specified, because it refers to maximal (worst case) objective values in the feasible design space. Qualitative similar results could also be calculated with slightly different reference points.

In paper C, NSGA-II is selected to solve the optimization problems defined. The main reason for this decision is the fact that NSGA-II is known as a state-of-the-art optimization approach for multi-objective problems, while MOGPS for higher dimensions was still under development.

Further, not only the choice of the algorithm affects the performance of the optimization. Normally, the behavior of algorithms can be adjusted with algorithm-specific parameters. NSGA-II e.g is based on a genetic algorithm and hence the crossover and mutation properties, as well as the population size, can be changed by corresponding parameters [46]. Since the population size has the greatest effect of all parameters [172], the hypervolume of so-far-observed solutions is evaluated for five different population sizes. In Fig. 6-3, the results are shown for 10 000 objective function evaluation carried out with NSGA-II using the same optimization example as in Fig. 6-2.

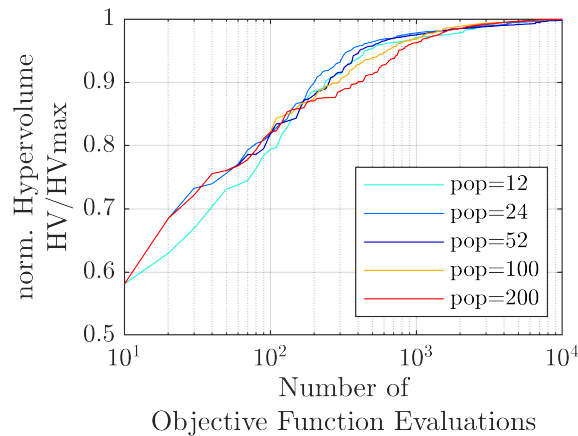


Figure 6-3: Visualization of the hypervolume metric for the second two-dimensional example in paper C for different population sizes.

Firstly, it should be noted that the graph corresponding to a population size of 52 is the same as in the previous diagram (Fig. 6-2), because it represents the initial settings. The graphs of different population sizes indicate that the best performance of the algorithm for about 100 up to 1000 evaluations is achieved by a population size of 24 particles or less. Larger population sizes of 100 or even 200 individuals mainly result in lower performance. However, all optimization results converge to the same hypervolume after about 1000 to 5000 evaluations, as is expected for a properly parameterized global optimization approach. In paper C, a medium population size of 52 is selected as a sufficient number of objective function evaluations was performed.

The hypervolume metric introduced in Sec. 6.1 is implemented in the parent class (optimizer class) of the optimization framework EngiO. Hence, the assessment and graphics, which are shown in Fig. 6-2 and 6-3, can be generated with very little coding effort. Switching between different optimization algorithms (e.g. MOGPS and NSGA-II) is also possible quickly, as the syntax of all algorithms is standardized due to the class definitions of EngiO. In this particular case, the optimization algorithm can be changed by exchanging a single line of code in the main script, which shows the benefits of EngiO for the engineering user.

7 Summary and Outlook

7.1 Summary

In this doctoral thesis, a computational scheme for multi-objective optimization of the design of blade repairs is developed. Engineering optimization techniques are used to identify the best design alternatives for the repair of damaged blades of compressor blisks. The main focus is on optimizing the structural properties of the repaired blades, such as natural blade frequencies or fatigue life. The presented approach relies on multi-objective optimization, which allows a posteriori weighting of design alternatives. Repair-specific FE simulations and user-defined routines form the basis for the automated evaluation in the optimization process. In particular, the blade repair technologies known as blending and patching are analyzed.

In accordance with the objectives formulated in Sec. 1.4, the first outcome of this thesis refers to the **design of an engineering optimization framework**. The design of the framework, which is published in paper A, is chosen in such a way that it features easy integration and an efficient solution to the optimization task. The main innovation of the developed software named EngiO is the object-oriented architecture, which allows implementing the optimization problem and algorithm in a clear concise fashion. The interface definition of EngiO enables single/multi-objective, global/local, and constrained/unconstrained optimization using derivative-free optimization methods. Therefore, the architecture of EngiO is well suited to solve the multi-objective optimization formulations derived for blisk repairs but also shows to be adapted to other engineering tasks with little programming effort. It is demonstrated that the designed software architecture has great benefits for the implementation and usage of optimization algorithms in engineering research.

Subsequent to the development of the engineering optimization framework, the optimization of blend repairs is addressed in paper B of this thesis. To show the potential of multi-objective optimization for improved blend repair shapes, the primary focus is on appropriate **modeling of blend repairs**. The result is a parametric model, which allows describing the geometric shape of blend repairs by the depth, width, and spanwise position of an ellipsoidal blending shape. This analytical approach is complemented by a custom remeshing routine that incorporates the blend into the FE model of one blisk sector. The **vibration properties are evaluated** by modal analysis using the FE model of the geometrically modified compressor blade. The relation between natural frequencies of the repaired blade and nominal blade frequencies as well as excitation frequencies are assessed in user-defined routines. It is found that the resulting natural frequencies of repaired blades are sensitive to the actual blend shape and some blendings even lead to crossings of natural blade frequencies with frequencies of harmonic excitation sources. These findings are further studied in the context of a two-objective optimization using two exemplary damage patterns. An optimization problem is formulated considering the tuning of the first six natural frequencies with respect to the nominal blade frequencies as the first and the proximity of natural frequencies to the harmonic excitation frequencies as the second objective.

The objective of this thesis, which is related to the **modeling of patch repairs**, constitutes a major part of paper C. Since the structural integrity of a blade with an applied patch is primarily threatened by the weld between patch and blade material, the position of the weld is of great interest. To describe the geometry of the patch and therewith the location of the weld a parametric model is developed, where the width and length of the patch are defined with regard to the leading edge and the chord length of the blade. The welding path along the interface between patch and blade is specified by a piece-wise linear trajectory. The vibratory stresses in the weld region are analyzed by performing a modal analysis of the blade and thermally induced residual stresses are computed in a decoupled thermomechanical welding simulation. The results of the corresponding FE simulations reveal, that a significant amount of residual stresses remains in the repaired blade and that the spatial distribution of the vibratory stresses varies for the different load cases. The **evaluation of fatigue properties** in the welded region clearly shows the influence of the different stress levels on the HCF properties of the weld. The automated evaluation of the HCF behavior of repaired blades is based on the well-established amplitude frequency concept and is part of user-implemented routines. The simulation model is, therefore, able to systematically evaluate different patch designs. This capability is further exploited by combining the objectives corresponding to the fatigue strength of five load cases and the objective of minimum machining effort in a multi-objective optimization task.

Thus, in the case of both blend and patch repairs, mathematical optimization problems are derived from the specific technical design criteria. These problems, containing multiple objectives, are solved using the optimization framework EngiO presented in paper A of this thesis. The final findings achieved in papers B and C are hence **Pareto optimal designs for blisk repairs**. Concerning the optimization of blend repairs, two different damage patterns are analyzed. Depending on the damage considered, the Pareto frontiers thereby have a very different appearance. It is shown that, depending on the damage pattern, the frontier can have a continuous course or may consist of several parts. In both examples, the two frequency criteria, which are represented by two objective functions, compete with each other and can not be achieved simultaneously. However, the plot of Pareto optimal solutions in the objective value space visualizes the effects of different alternatives on the frequency tuning of the repaired blade. The final repair decision can be made on based on further engineering (e.g aerodynamic) preferences.

In the case of patch repair optimization, the number of objectives included in the multi-objective problem formulation is increased to six objectives. This six-objective approach, whereas all load cases being relevant for the HCF strength and the weld length are considered, lead to Pareto optimal solutions forming a six-dimensional hyperplane. The main findings of this work, become apparent in terms of repair designs that correspond to the set of optimal solutions. It is demonstrated that the number of design alternatives can be narrowed down considerably by the optimization procedure and the decision for the final design is hence facilitated. Moreover, depending on the significance of load cases different patch designs are conceivable. However, the results obtained by applying the approach on the specific blisk geometry show a predominant tendency towards 'short' patches characterized by a small patch length.

Overall, in this thesis, a scheme is devised to model, evaluate and finally optimize the structural design of typical repairs of blisk blades. The results determined in the reported examples provide evidence, that the multi-objective approach is able to support the engineering design decision in future repair processes of blisk blades.

7.2 Outlook

This doctoral thesis suggests that real maintenance processes for blisk repairs benefit from numerical simulations and multi-objective optimization. In particular, two repair technologies are studied. Since the optimization of these two repairs showed great potential to improve the maintenance of blisk blades, further repair processes should be investigated in the future. Regarding blade repair of blisks, the complete blade replacement should be studied. The numerical analysis of this repair technology is especially interesting from a structural point of view, as the joint area between the attached blade and the disk is located at the blade fillet¹⁰. This area is typically also known as the region with maximum stresses due to blade bending and is therefore prone to failure.

All computation examples presented in this thesis are based on the compressor blisk model designed for the aerodynamic experiments in the Collaborative Research Center 871. To ensure safe operation in the test facility, the design is far too conservative compared to actual blisk designs. Therefore, the application of the developed approach should be extended to other and especially more practical blisk designs in future work. It would be of great interest if the presented results could be generalized and the findings could be transferred to other blisk designs.

In addition, further damage patterns should be analyzed. In this context, a classification of typical defects of blisk blades would be preferable to avoid numerous calculations. It is also conceivable that the point-based description of the damage used in the computational scheme is extracted directly from an optical measurement.

Since the focus of this work is on evaluating the structural aspects of blade repairs, other disciplines such as aerodynamics or manufacturing are given little or no consideration in the optimization. However, especially for the evaluation of blend repairs, the influences of the changed blade geometry on the flow field in the engine are important. Changes in the flow could yield to a massive loss in performance and should be taken into account in future multidisciplinary optimization approaches.

Moreover, the blades of blisks are usually close together, leaving little space for manufacturing tools. According to the space requirements of the manufacturing tools used, this could result in additional restrictions that must be followed in the decision process.

For industrial use of the presented approach or comparable approaches, it is further inevitable to include costs in the optimization tasks. Only if the economic aspects of repairs are captured in the optimization, the life cycle costs [153] can be reduced.

Another aspect from the field of mechanics that has not been considered in this work relates to the tuning of all integrated blisk blades. Variations from blade to blade, e.g. due to repairs, would result in a mistuned system, which could lead to an amplification of the vibration amplitudes of single blades. To avoid these potentially high vibration amplitudes, a model of the entire blisk should be used in addition to the cyclic sector model. In total, it can be concluded, that there are multiple aspects from mechanics, aerodynamics, manufacturing, and economy, which should be addressed in future optimization processes of blisk repairs.

¹⁰The blade fillet denotes the region between blade and blade platform or root. In blisk design, this is the interface region between blade and disk.

Including further technical aspects in the optimization problem usually requires additional or more detailed simulations. These simulations lead to the fact that the evaluation of the objective function also takes up more and more computation time. In this thesis, the objectives and the corresponding models are chosen to be computable in an acceptable time. Thus, the optimization problems are solvable by conventional optimization algorithms. However, since the evaluation of objective functions can become extremely time-consuming and conventional methods reach their limits, it may be necessary to use surrogate optimization methods [137]. The basic idea of these methods is to speed up the optimization process by combining metamodeling techniques with conventional optimization approaches. In the future, such a surrogate-based approach allows the integration of aerodynamic quantities, which can only be determined with complex CFD simulation, and improve the validity of the optimization results.

On a wider level, further research is needed to plan and accompany real processes with computational models and numerical simulations. At the latest, since the planning uncertainties in the aerospace industry caused by the Covid-19 pandemic, fixed overhaul schedules are no longer appropriate. Current developments are thus condition-based methods [142] or digital twins [47]. Smart tools such as numerical optimization or artificial intelligence are therefore needed to make MRO processes sustainable for the future.

Bibliography

- [1] ABBOTT, I. H., VON DOENHOFF, A. E., AND STIVERS, L. NACA Report No. 824–Summary of Airfoil Data. *National Advisory Committee for Aeronautics* (1945).
- [2] ADJEI, R. A., FAN, C., WANG, W., AND LIU, Y. Multidisciplinary Design Optimization for Performance Improvement of an Axial Flow Fan Using Free-Form Deformation. *Journal of Turbomachinery* 143, 1 (2020).
- [3] ADVANCED TURBINE SUPPORT. Advanced Turbine Support Website. URL <https://www.advancedturbinesupport.com/blending-services/>.
- [4] ALBA, E., LUQUE, G., AND NESMACHNOW, S. Parallel metaheuristics: Recent advances and new trends. *International Transactions in Operational Research* 20, 1 (2013), 1–48.
- [5] AMEDEI, A., MELI, E., RINDI, A., ROMANI, B., PINELLI, L., VANTI, F., ARNONE, A., BENVENUTI, G., FABBRINI, M., AND MORGANTI, N. Innovative Design, Structural Optimization and Additive Manufacturing of New-Generation Turbine Blades. In *Proceedings of the ASME Turbo Expo 2020* (2020).
- [6] ARASH, B., EXNER, W., AND ROLFES, R. Viscoelastic damage behavior of fiber reinforced nanoparticle-filled epoxy nanocomposites: Multiscale modeling and experimental validation. *Composites Part B: Engineering* 174 (2019), 107005.
- [7] ARMSTRONG, E. K., AND STEVENSON, R. E. Some practical aspects of compressor blade vibration. *The Journal of the Royal Aeronautical Society* 64, 591 (1960), 117–130.
- [8] ASCHENBRUCK, J., ADAMCZUK, R., AND SEUME, J. R. Recent progress in turbine blade and compressor blisk regeneration. In *Procedia CIRP* (2014), vol. 22, pp. 256–262.
- [9] AUDET, C., AND KOKKOLARAS, M. Blackbox and derivative-free optimization: theory, algorithms and applications. *Optimization and Engineering* 17, 1 (2016), 1–2.
- [10] AUSTRALIEN TRANSPORT SAFETY BUREAU. Technical Analysis Report No:39/01 Examination of a Failed Compressor Blisk, 2001. URL https://www.atsb.gov.au/media/1552997/tr200102263_001.pdf.
- [11] AZAR, P. *Electron Beam Weld Repair and Qualification of Titanium Gas Turbine Engine Fan Blades*. Dissertation, Carleton University, 1995.
- [12] AZAR, P., LI, P., PATNAIK, P., THAMBURAJ, R., AND IMMARIGEON, J. Electron beam weld repair and qualification of titanium fan blades for military gas turbine engines. In *RTO AVT Specialists’ Meeting on Cost Effective Application of Titanium Alloys in Military Platforms* (2001).
- [13] BACKHAUS, T., MAYWALD, T., SCHRAPE, S., VOIGT, M., AND MAILACH, R. A parametrization describing blisk airfoil variations referring to modal analysis. In *Proceedings of the ASME Turbo Expo 2017* (2016), ASME.

- [14] BECK, J. A., BROWN, J. M., RUNYON, B., AND SCOTT-EMUAKPOR, O. E. Probabilistic study of integrally bladed rotor blends using geometric mistuning models. In *58th AIAA/ASCE/AHS/ASC Structures, Structural Dynamics, and Materials Conference* (2017), p. 0860.
- [15] BERGER, R., HÄFELE, J., HOFMEISTER, B., AND ROLFES, R. Blend repair shape optimization for damaged compressor blisks. In *Advances in Structural and Multidisciplinary Optimization* (2018), A. Schumacher, T. Vietor, S. Fiebig, K.-U. Bletzinger, and K. Maute, Eds., Springer International Publishing, pp. 1631–1642.
- [16] BERGER, R., HOFMEISTER, B., GEBHARDT, C. G., AND ROLFES, R. Parametric design of blisk repairs by patching considering high cycle fatigue. In *Proceedings of the ASME Turbo Expo 2019* (2019), ASME.
- [17] BERGLUND, D., ALBERG, H., AND RUNNEMALM, H. Simulation of welding and stress relief heat treatment of an aero engine component. *Finite Elements in Analysis and Design* 39, 9 (2003), 865–881.
- [18] BEUME, N., FONSECA, C. M., LOPEZ-IBANEZ, M., PAQUETE, L., AND VAHRENHOLD, J. On the complexity of computing the hypervolume indicator. *IEEE Transactions on Evolutionary Computation* 13, 5 (2009), 1075–1082.
- [19] BLETZINGER, K.-U., FIRL, M., AND DAUD, F. Techniken der Formoptimierung. In *Weimarer Optimierungs- und Stochastiktag* (2005).
- [20] BLEULER, S., LAUMANN, M., THIELE, L., AND ZITZLER, E. PISA — A Platform and Programming Language Independent Interface for Search Algorithms. In *Evolutionary Multi-Criterion Optimization*, G. Goos, J. Hartmanis, J. van Leeuwen, C. M. Fonseca, P. J. Fleming, E. Zitzler, L. Thiele, and K. Deb, Eds., vol. 2632 of *Lecture Notes in Computer Science*. Springer Berlin Heidelberg, Berlin, Heidelberg, 2003, pp. 494–508.
- [21] BOCCINI, E., MELI, E., RINDI, A., CORBÒ, S., FALOMI, S., AND IURISCI, G. Structural topology optimization of turbomachinery components using new manufacturing techniques and innovative materials. In *Proceedings of the ASME Turbo Expo 2017* (2017), ASME.
- [22] BOCCINI, E., MELI, E., RINDI, A., PINELLI, L., PERUZZI, L., AND ARNONE, A. Towards structural topology optimization of rotor blisks. In *Proceedings of the ASME Turbo Expo 2018* (2018), vol. 51135, ASME.
- [23] BÖSS, V., NESPOR, D., SAMP, A., AND DENKENA, B. Numerical simulation of process forces during re-contouring of welded parts considering different material properties. *CIRP Journal of Manufacturing Science and Technology* 6, 3 (2013), 167–174.
- [24] BRAUN, M. Deap: Evolutionary algorithms made easy. *Journal of Machine Learning Research*, 13 (2012), 2171–2175.
- [25] BREMER, C. Automated repair and overhaul of aero-engine and industrial gas turbine components. In *Proceedings of the ASME Turbo Expo 2005* (2005), ASME.
- [26] BROCKHOFF, D., TRAN, T.-D., AND HANSEN, N. Benchmarking numerical multiobjective optimizers revisited. In *Proceedings of the 2015 on Genetic and Evolutionary Computation Conference - GECCO '15* (New York, New York, USA, 2015), A. I. Esparcia-Alcázar, S. Silva, and J. L. Jiménez-Laredo, Eds., ACM Press, pp. 639–646.

- [27] BROWN, J., AND GRANDHI, R. Reliability optimization of three dimensional structures using geometry parameters. In *40th Structures, Structural Dynamics, and Materials Conference and Exhibit* (1999), p. 1602.
- [28] BROWN, J. M., AND GRANDHI, R. V. Probabilistic analysis of geometric uncertainty effects on blade-alone forced response. In *Proceedings of the ASME Turbo Expo 2004* (2004), ASME.
- [29] BROWN, J. M., AND GRANDHI, R. V. Probabilistic high cycle fatigue assessment process for integrally bladed rotors. In *Proceedings of the ASME Turbo Expo 2005* (2005), ASME.
- [30] BROWN, J. M., SLATER, J., AND GRANDHI, R. V. Probabilistic analysis of geometric uncertainty effects on blade modal response. In *Proceedings of the ASME Turbo Expo 2003* (2003), ASME.
- [31] BRUNS, M., HOFMEISTER, B., PACHE, D., AND ROLFES, R. Finite element model updating of a wind turbine blade—a comparative study. In *Proceedings of EngOpt 2018 Proceedings of the 6th International Conference on Engineering Optimization* (2019).
- [32] BUSKE, C., KRUMME, A., SCHMIDT, T., DRESBACH, C., ZUR, S., AND TIEFERS, R. Distributed multidisciplinary optimization of a turbine blade regarding performance, reliability and castability. In *Proceedings of the ASME Turbo Expo 2002* (2016), ASME.
- [33] BUSSMANN, M., AND BAYER, E. Market-oriented blisk manufacturing—a challenge for production engineering. In *Proceedings of the 1st European Air and Space Conference* (Berlin, Germany, 2007), DGLR.
- [34] BUSSMANN, M., AND BAYER, E. Blisk production of the future—technological and logistical aspects of future-oriented construction and manufacturing processes of integrally bladed rotors. In *Proceedings of the International Symposium on Air Breathing Engines* (Montreal, Canada, 2009), Curran.
- [35] BUSSMANN, M., KRAUS, J., AND BAYER, E. An integrated cost-effective approach to blisk manufacturing. In *Proceedings of the International Symposium on Air Breathing Engines* (Munich, Germany, 2005), American Inst. of Aeronautics and Astronautics.
- [36] CAMPBELL, W. Protection of steam turbine disk wheels from axial vibration. *Transactions of the ASME* (1924).
- [37] CHACHURSKI, R., GŁOWACKI, P., AND SZCZECIŃSKI, S. Methods of counting aircraft turbine engines operating cycles. *Transactions of the Institute of Aviation* (2011), 5–13.
- [38] CHRISTENSEN, P. W., AND KLARBRING, A. *An introduction to structural optimization*, vol. 153. Springer Science & Business Media, 2008.
- [39] COELLO COELLO, C. A. Theoretical and numerical constraint-handling techniques used with evolutionary algorithms: A survey of the state of the art. *Computer Methods in Applied Mechanics and Engineering* 191, 11-12 (2002), 1245–1287.
- [40] CONN, A. R., SCHEINBERG, K., AND VICENTE, L. N. *Introduction to Derivative-Free Optimization*. Society for Industrial and Applied Mathematics, 2009.

- [41] COPPINGER, R. MTU Aero Engines claims blisk repair first, 2008. URL <https://www.flightglobal.com/mtu-aero-engines-claims-blisk-repair-first/78166.article>.
- [42] COWLES, B. A. High cycle fatigue in aircraft gas turbines—an industry perspective. *International Journal of Fracture* 80, 2-3 (1996), 147–163.
- [43] CUSTÓDIO, A., EMMERICH, M., AND MADEIRA, J. Recent developments in derivative-free multiobjective optimisation. *Computational Technology Reviews* 5 (09 2012), 1–30.
- [44] DAY, W. D., FIEBIGER, S. W., AND PATEL, H. N. Parametric evaluation of compressor blade blending. In *Proceedings of the ASME Turbo Expo 2012* (2012), ASME.
- [45] DEB, K., AGRAWAL, S., PRATAP, A., AND MEYARIVAN, T. A Fast Elitist Non-dominated Sorting Genetic Algorithm for Multi-objective Optimization: NSGA-II. In *Parallel Problem Solving from Nature PPSN VI*, G. Goos, J. Hartmanis, J. van Leeuwen, M. Schoenauer, K. Deb, G. Rudolph, X. Yao, E. Lutton, J. J. Merelo, and H.-P. Schwefel, Eds., vol. 1917 of *Lecture Notes in Computer Science*. Springer Berlin Heidelberg, Berlin, Heidelberg, 2000, pp. 849–858.
- [46] DEB, K., PRATAP, A., AGARWAL, S., AND MEYARIVAN, T. A fast and elitist multiobjective genetic algorithm: NSGA-II. *IEEE Transactions on Evolutionary Computation* 6, 2 (2002), 182–197.
- [47] DENKENA, B., BOESS, V., NESPOR, D., FLOETER, F., AND RUST, F. Engine blade regeneration: A literature review on common technologies in terms of machining. *The International Journal of Advanced Manufacturing Technology* 81, 5-8 (2015), 917–924.
- [48] DENKENA, B., GROVE, T., MÜCKE, A., LANGEN, D., NESPOR, D., AND HASSEL, T. Residual stress formation after re-contouring of micro-plasma welded Ti–6Al–4 V parts by means of ball end milling. *Materialwissenschaft und Werkstofftechnik* 48, 11 (2017), 1034–1039.
- [49] DENKENA, B., NESPOR, D., BÖSS, V., AND KÖHLER, J. Residual stresses formation after re-contouring of welded Ti-6Al-4V parts by means of 5-axis ball nose end milling. *CIRP Journal of Manufacturing Science and Technology* 7, 4 (2014), 347–360.
- [50] DI GASPERO, L., AND SCHAER, A. Easylocal: An object-oriented framework for flexible design of local search algorithms. In *Metaheuristics International Conference* (2001), pp. 287–292.
- [51] DORNBERGER, R., STOLL, P., BÜCHE, D., AND NEU, A. Multidisciplinary turbomachinery blade design optimization. In *38th Aerospace Sciences Meeting and Exhibit* (2000), p. 838.
- [52] DURILLO, J. J., AND NEBRO, A. J. jMetal: A Java framework for multi-objective optimization. *Advances in Engineering Software* 42, 10 (2011), 760–771.
- [53] DUTTA, A. K., FLASSIG, P. M., AND BESTLE, D. A Non-Dimensional Quasi-3D Blade Design Approach With Respect to Aerodynamic Criteria. In *Proceedings of the ASME Turbo Expo 2008* (2008), ASME.
- [54] DYNAMIC SOFTWARE AND ENGINEERING GMBH. OPTISLANG - The Optimizing Structural Language, 2009. URL <https://www.ansys.com/products/platform/ansys-optislang>.

- [55] EBERLEIN, A. Phases of high-tech repair implementation. In *Proceedings of the International Symposium on Air Breathing Engines* (2007).
- [56] ELDRÉD, M., OUTKA, D., BOHNHOFF, W., WITKOWSKI, W., ROMERO, V., PONSLET, E., AND CHEN, K. Optimization of Complex Mechanics Simulations with Object-Oriented Software Design. *Computer Modeling and Simulation in Engineering* 1, 3 (1996), 323–352.
- [57] ERNST, B., SEUME, J. R., AND HERBST, F. Probabilistic CFD-Analysis of Regeneration-Induced Geometry Variances in a Low-Pressure Turbine. *AIAA Journal* (2016).
- [58] ERRERA, L. Bombardier CRJ-200LR (LCL) Lufthansa D-ACJJ - MSN 7298 - Now in UTair fleet as VQ-BGU, 2009. URL <https://www.flickr.com/photos/30949611@N03/3238726666/>.
- [59] FRISCHBIER, J. Application of structural optimization in the design of jet engine turbine blades. *WIT Transactions on The Built Environment* 14 (1970).
- [60] FÜRST, M., BERTOLINO, A., CUOCI, A., FARAVELLI, T., FRASSOLDATI, A., AND PARENTE, A. Optismoke++: A toolbox for optimization of chemical kinetic mechanisms. *Computer Physics Communications* 264 (2021), 107940.
- [61] GAMMA, E., HELM, R., JOHNSON, R., AND VLISSIDES, J. Design patterns: Abstraction and reuse of object-oriented design. In *Pioneers and Their Contributions to Software Engineering*. Springer, 2001, pp. 361–388.
- [62] GARZON, V. E., AND DARMOFAL, D. L. Impact of geometric variability on axial compressor performance. *Journal of Turbomachinery* 125, 4 (2003), 692–703.
- [63] GEZORK, T., AND VÖLKER, S. Applicability of Quasi-3D Blade Design Methods to Profile Shape Optimizatón of Turbine Blades. In *Proceedings of the ASME Turbo Expo 2013* (2013), ASME.
- [64] GHIOCEL, D., AND RIEGER, N. Probabilistic high cycle fatigue life prediction for gas turbine engine blades. In *40th Structures, Structural Dynamics, and Materials Conference and Exhibit* (Reston, Virigina, 1999), American Institute of Aeronautics and Astronautics.
- [65] GMBH, M. M. B.-B. Borescope blending for CF34-10 engines.
- [66] GOLDBERG, D. E. *Genetic Algorithms in Search, Optimization and Machine Learning*, 1st ed. Addison-Wesley Longman Publishing Co., Inc., Boston, MA, USA, 1989.
- [67] GOOS, G., HARTMANIS, J., BARSTOW, D., BRAUER, W., BRINCH HANSEN, P., GRIES, D., LUCKHAM, D., MOLER, C., PNUELI, A., SEEGMÜLLER, G., STOER, J., WIRTH, N., FLOUDAS, C. A., AND PARDALOS, P. M. *A Collection of Test Problems for Constrained Global Optimization Algorithms*, vol. 455. Springer Berlin Heidelberg, Berlin, Heidelberg, 1990.
- [68] GRANDHI, R. Structural optimization with frequency constraints - a review. *AIAA Journal* 31, 12 (1993), 2296–2303.
- [69] GRAY, J., HWANG, J. T., MARTINS, J. R. R. A., MOORE, K. T., AND NAYLOR, B. A. Openmdao: An open-source framework for multidisciplinary design, analysis, and optimization. *Structural and Multidisciplinary Optimization* 59, 4 (2019), 1075–1104.

- [70] GRAY, J., MOORE, K., AND NAYLOR, B. OpenMDAO: An Open Source Framework for Multidisciplinary Analysis and Optimization. In *13th AIAA/ISSMO Multidisciplinary Analysis Optimization Conference* (Reston, Virginia, 2010), American Institute of Aeronautics and Astronautics.
- [71] GRÄSEL, J., KESKIN, A., SWOBODA, M., PRZEWOZNY, H., AND SAXER, A. A Full Parametric Model for Turbomachinery Blade Design and Optimisation. In *International Design Engineering Technical Conferences and Computers and Information in Engineering Conference* (09 2004), pp. 907–914.
- [72] GUTZWILLER, D. P., AND TURNER, M. G. Rapid low fidelity turbomachinery disk optimization. *Advances in Engineering Software* 41, 5 (2010), 779–791.
- [73] HALDAR, A., P. M., A., JANSEN, E., RAO, B. N., AND ROLFES, R. Semi-analytical investigations on bistable cross-ply laminates with MFC actuators. *Smart Materials and Structures* (2021).
- [74] HALDAR, A., REINOSO, J., JANSEN, E., AND ROLFES, R. Thermally induced multistable configurations of variable stiffness composite plates: Semi-analytical and finite element investigation. *Composite Structures* 183 (2018), 161–175.
- [75] HANSCHKE, B., KLAUKE, T., AND KÜHHORN, A. The effect of foreign object damage on compressor blade high cycle fatigue strength. In *Proceedings of the ASME Turbo Expo 2017* (2017), ASME.
- [76] HANUMANTHAN, H., STITT, A., LASKARIDIS, P., AND SINGH, R. Severity estimation and effect of operational parameters for civil aircraft jet engines. *Proceedings of the Institution of Mechanical Engineers, Part G: Journal of Aerospace Engineering* 226, 12 (2011), 1544–1561.
- [77] HARE, W., NUTINI, J., AND TEFAMARIAM, S. A survey of non-gradient optimization methods in structural engineering. *Advances in Engineering Software* 59, 7–10 (2013), 19–28.
- [78] HART, W. E., LAIRD, C., WATSON, J.-P., AND WOODRUFF, D. L. *Pyomo – Optimization Modeling in Python*, vol. 67. Springer US, Boston, MA, 2012.
- [79] HART, W. E., WATSON, J.-P., AND WOODRUFF, D. L. Pyomo: Modeling and solving mathematical programs in python. *Mathematical Programming Computation* 3, 3 (2011), 219–260.
- [80] HECKER, P., DELIMAR, D., BRANDL, H., AND LÖTZERICH, M. Process integration and automated numerical design optimization of an eigenfrequency analysis of a compressor blade. In *Proceedings of the ASME Turbo Expo 2011* (2011), ASME, pp. 791–800.
- [81] HECKER, P., AND MÜCKE, R. Robustheitsanalyse und Optimierung von Kompressorschaukeln.
- [82] HEINZE, K. *Probabilistische Simulation des strukturmechanischen Verhaltens von Turbinenschaukeln*. Dissertation, 2010.
- [83] HEINZE, K. *Eine Methode für probabilistische Untersuchungen zum Einfluss von Fertigungsstreuungen auf die hochzyklische Ermüdung von Verdichterschaukeln*. Dissertation, 2015.

- [84] HEINZE, K., MEYER, M., SCHARFENSTEIN, J., VOIGT, M., AND VOGELER, K. A parametric model for probabilistic analysis of turbine blades considering real geometric effects. *CEAS Aeronautical Journal* 5, 1 (2014), 41–51.
- [85] HENRY, E. B., BROWN, J. M., AND SLATER, J. C. A fleet risk prediction methodology for mistuned ibrs using geometric mistuning models. In *17th AIAA Non-Deterministic Approaches Conference*.
- [86] HOFMEISTER, B., BRUNS, M., HÜBLER, C., AND ROLFES, R. Multi-Objective Global Pattern Search: Effective numerical optimisation in structural dynamics. URL <https://www.repo.uni-hannover.de/handle/123456789/11106>.
- [87] HOFMEISTER, B., BRUNS, M., AND ROLFES, R. Finite element model updating using deterministic optimisation: A global pattern search approach. *Engineering Structures* 195 (2019), 373–381.
- [88] HOLMSTRÖM, K., EDVALL, M. M., AND GÖRAN, A. O. TOMLAB for large-scale robust optimization. In *Proceedings, Nordic MATLAB Conference* (2003).
- [89] HOOKE, R., AND JEEVES, T. A. “Direct Search” Solution of Numerical and Statistical Problems. *Journal of the ACM (JACM)* 8, 2 (1961), 212–229.
- [90] HUMEAU, J., LIEFOOGHE, A., TALBI, E.-G., AND VEREL, S. ParadisEO-MO: From fitness landscape analysis to efficient local search algorithms. *Journal of Heuristics* 19, 6 (2013), 881–915.
- [91] IZZO, D. PyGMO and pyKEP: Open Source Tools for Massively Parallel Optimization in Astrodynamics (The Case of Interplanetary Trajectory Optimization). In *Proceedings of the Fifth International Conference on Astrodynamics Tools and Techniques, ICATT* (2012).
- [92] JACOBS, E. N., WARD, K. E., AND PINKERTON, R. M. *The Characteristics of 78 related airfoil section from tests in the Variable-Density Wind Tunnel*. No. 460. US Government Printing Office, 1933.
- [93] JAMIL, M., AND YANG, X.-S. A literature survey of benchmark functions for global optimization problems. *International Journal of Mathematical Modelling and Numerical Optimisation* 4, 2 (2013), 150.
- [94] KANPUR GENETIC ALGORITHM LABORATORY. Multi-objective NSGA-II code in C, 2002. URL <https://www.iitk.ac.in/kangal/codes.shtml>.
- [95] KARGER, K., AND BESTLE, D. Parametric Blending and FE-Optimisation of a Compressor Blisk Test Case. In *Advances in Evolutionary and Deterministic Methods for Design, Optimization and Control in Engineering and Sciences*, D. Greiner, B. Galván, J. Périaux, N. Gauger, K. Giannakoglou, and G. Winter, Eds., vol. 36 of *Computational Methods in Applied Sciences*. Springer International Publishing, Cham, 2015, pp. 257–266.
- [96] KELLER, C., KELLERSMANN, A., FRIEDRICH, J., AND SEUME, J. R. Influence of geometric imperfections on aerodynamic and aeroelastic behavior of a compressor blisk. In *Proceedings of the ASME Turbo Expo 2017* (2017), ASME.
- [97] KENNEDY, G. J., AND MARTINS, J. R. A parallel aerostructural optimization framework for aircraft design studies. *Structural and Multidisciplinary Optimization* 50, 6 (2014), 1079–1101.

- [98] KENNEDY, J., AND EBERHART, R. Particle swarm optimization. In *Proceedings of ICNN'95 - International Conference on Neural Networks* (1995), IEEE, pp. 1942–1948.
- [99] KESKIN, A. *Process integration and automated multi-objective optimization supporting aerodynamic compressor design*. Dissertation, BTU Cottbus - Senftenberg, 2007.
- [100] KESKIN, A., AND BESTLE, D. Application of multi-objective optimization to axial compressor preliminary design. *Aerospace Science and Technology* 10, 7 (2006), 581–589.
- [101] KICINGER, R., ARCISZEWSKI, T., AND JONG, K. D. Evolutionary computation and structural design: A survey of the state-of-the-art. *Computers & Structures* 83, 23-24 (2005), 1943–1978.
- [102] KOCHENDERFER, M. J., AND WHEELER, T. A. *Algorithms for optimization*. MIT Press, 2019.
- [103] KURSAWE, F. A variant of evolution strategies for vector optimization. In *Proceedings of the International Conference on Parallel Problem Solving from Nature* (1990), Springer, pp. 193–197.
- [104] LAMB, C. M. *Probabilistic performance-based geometric tolerancing of compressor blades*. Dissertation, Massachusetts Institute of Technology, 2005.
- [105] LANGE, A., VOGELER, K., GÜMMER, V., SCHRAPP, H., AND CLEMEN, C. Introduction of a Parameter Based Compressor Blade Model for Considering Measured Geometry Uncertainties in Numerical Simulation. In *Proceedings of the ASME Turbo Expo 2009* (2009).
- [106] LANGE, A., VOIGT, M., VOGELER, K., SCHRAPP, H., JOHANN, E., AND GÜMMER, V. Impact of manufacturing variability on multistage high-pressure compressor performance. *Journal of engineering for gas turbines and power* 134, 11 (2012).
- [107] LEWIS, R. M., TORCZON, V., AND TROSSET, M. W. Why pattern search works. Tech. rep., Institute for computer applications in Science and engineering, Hampton, VA, 1998.
- [108] LI, Z., AND ZHENG, X. Review of design optimization methods for turbomachinery aerodynamics. *Progress in Aerospace Sciences* 93 (2017), 1–23.
- [109] LÖFBERG, J. YALMIP : A Toolbox for Modeling and Optimization in MATLAB. In *Proceedings of the CACSD Conference* (Taipei, Taiwan, 2004).
- [110] LUKASIEWYCZ, M., GLASS, M., REIMANN, F., AND TEICH, J. Opt4J - A Modular Framework for Meta-heuristic Optimization. In *Proceedings of the Genetic and Evolutionary Computing Conference, GECCO* (2011), pp. 1723–1730.
- [111] LUO, C., SONG, L., LI, J., AND FENG, Z. Multiobjective optimization approach to multidisciplinary design of a three-dimensional transonic compressor blade. In *Proceedings of the ASME Turbo Expo 2009* (2009), ASME, pp. 599–608.
- [112] LUO, C., SONG, L., LI, J., AND FENG, Z. A study on multidisciplinary optimization of an axial compressor blade based on evolutionary algorithms. *Journal of Turbomachinery* 134, 5 (2012), 054501.
- [113] MARELLI, S., AND SUDRET, B. UQLab: A Framework for Uncertainty Quantification in Matlab. In *Vulnerability, Uncertainty, and Risk* (2014), Beer, Ed., American Society of Civil Engineers, pp. 2554–2563.

- [114] MARLER, R. T., AND ARORA, J. S. Survey of multi-objective optimization methods for engineering. *Structural and Multidisciplinary Optimization* 26, 6 (2004), 369–395.
- [115] MARTIN, I. *Automated Process for Robust Airfoil Design-Optimization Incorporating Critical Eigenmode Identification and Production-Tolerance Evaluation*. Dissertation, 2018.
- [116] MARTIN, I., AND BESTLE, D. Automated mode identification of airfoil geometries to be used in an optimization process. In *Proceedings of the ASME Turbo Expo 2016* (2016), ASME.
- [117] MARTIN, I., HARTWIG, L., AND BESTLE, D. A multi-objective optimization framework for robust axial compressor airfoil design. *Structural and Multidisciplinary Optimization* 59, 6 (2019), 1935–1947.
- [118] MARTINS, J. R. R. A., AND LAMBE, A. B. Multidisciplinary design optimization: A survey of architectures. *AIAA Journal* 51, 9 (2013), 2049–2075.
- [119] MARTINS, J. R. R. A., AND NING, A. *Engineering Design Optimization*, 1 ed. University of Michigan, Michigan, 2021.
- [120] MATLAB Global Optimization Toolbox, 2020. The MathWorks, Natick, MA, USA.
- [121] MATLAB Optimization Toolbox, 2020. The MathWorks, Natick, MA, USA.
- [122] MIRJALILI, S. Whale Optimization Algorithm. URL <https://seyedalimirjalili.com/woa>.
- [123] MIRJALILI, S., AND A., L. The whale optimization algorithm. *Advances in Engineering Software* 95 (2016), 51–67.
- [124] MTU. Spitzentechnologie made by MTU, 2005. URL https://www.mtu.de/e-papers/MTU_ePaper/Marketing/Spitzentechnologie_made_by_mtu/epaper/ausgabe.pdf.
- [125] NICHOLAS, T. *High cycle fatigue: A mechanics of materials perspective*, 1. ed. ed. Elsevier, Amsterdam, 2006.
- [126] NYSSSEN, F. *Numerical Modeling and Experimental Identification of Mistuned Multi-Stage Bladed Assemblies*. Dissertation, Université de Liège, Liège, Belgique, 2016.
- [127] ÖKSÜZ, Ö., AND AKMANDOR, İ. S. Multi-objective aerodynamic optimization of axial turbine blades using a novel multilevel genetic algorithm. *Journal of Propulsion and Power* 132, 4 (2010), 397.
- [128] OTTO, D. *Ein Beitrag zur interdisziplinären Prozessintegration und automatischen Mehrzieloptimierung am Beispiel einer Verdichtertrottschaufel*. Dissertation, Brandenburgische Technische Universität Cottbus, Cottbus, 2009.
- [129] PANCHENKO, V., MOUSTAPHA, H., MAH, S., PATEL, K., AND DOWHAN, M. Preliminary multi-disciplinary optimization in turbomachinery design. In *RTO AVT Symposium on “Reduction of Military Vehicle Acquisition Time and Cost through Advanced Modelling and Virtual Simulation”* (2003).
- [130] PAREJO, J. A., RACERO, J., GUERRERO, F., KWOK, T., AND SMITH, K. A. Fom: A framework for metaheuristic optimization. In *International Conference on Computational Science* (2003), Springer, pp. 886–895.

- [131] PAREJO, J. A., RUIZ-CORTÉS, A., LOZANO, S., AND FERNANDEZ, P. Metaheuristic optimization frameworks: A survey and benchmarking. *Soft Computing* 16, 3 (2012), 527–561.
- [132] PARETO, V. *Manual of political economy (manuale di economia politica)*. Kelley, New York, 1971 (1906). Translated by Ann S. Schwier and Alfred N. Page.
- [133] PATELLI, E. *COSSAN: A Multidisciplinary Software Suite for Uncertainty Quantification and Risk Management*. Springer International Publishing, Cham, 2017, pp. 1909–1977.
- [134] PEREZ, R. E., JANSEN, P. W., AND MARTINS, J. R. R. A. pyOpt: A Python-based object-oriented framework for nonlinear constrained optimization. *Structural and Multidisciplinary Optimization* 45, 1 (2012), 101–118.
- [135] PINELLI, L., AMEDEI, A., MELI, E., VANTI, F., ROMANI, B., BENVENUTI, G., FABBRINI, M., MORGANTI, N., RINDI, A., AND ARNONE, A. Innovative design, structural optimization, and additive manufacturing of new-generation turbine blades. *Journal of Turbomachinery* 144, 1 (2021), 011006.
- [136] QIN, H., LIU, Z., LIU, Y., AND ZHONG, H. An object-oriented matlab toolbox for automotive body conceptual design using distributed parallel optimization. *Advances in Engineering Software* 106 (2017), 19–32.
- [137] QUEIPO, N. V., HAFTKA, R. T., SHYY, W., GOEL, T., VAIDYANATHAN, R., AND TUCKER, P. K. Surrogate-based analysis and optimization. *Progress in aerospace sciences* 41, 1 (2005), 1–28.
- [138] RADAJ, D. *Welding residual stresses and distortion*, 1. ed. ed. DVS-Verlag, Düsseldorf, 2003.
- [139] RADAJ, D., AND VORMWALD, M. *Ermüdungsfestigkeit*. Springer Berlin Heidelberg, Berlin, Heidelberg, 2007.
- [140] RAO, J. S., PATHAK, A., AND CHAWLA, A. Blade life: A comparison by cumulative damage theories. *Journal of Engineering for Gas Turbines and Power* 123, 4 (2001), 886.
- [141] RIOS, L. M., AND SAHINIDIS, N. V. Derivative-free optimization: A review of algorithms and comparison of software implementations. *Journal of Global Optimization* 56, 3 (2013), 1247–1293.
- [142] ROEMERMANN, S. Historical trend data can't help mro during unprecedented times. *Aerospace - Manufacturing and Design* (2021), 38–39.
- [143] ROOS, D., CREMANN, K., AND JASPER, T. Probability an variance-based stochastic design optimization of a radial compressor concerning fluid-structure interaction, 2013.
- [144] ROSSMANN, A. *Die Sicherheit von Turbo-Flugtriebwerken, Band 3*. Turbo Consult, 2002.
- [145] ROTTWINKEL, B., NÖLKE, C., KAIERLE, S., AND WESLING, V. Crack repair of single crystal turbine blades using laser cladding technology. In *Procedia CIRP* (2014), vol. 22, pp. 263–267.
- [146] ROY, R., HINDUJA, S., AND TETI, R. Recent advances in engineering design optimisation: Challenges and future trends. *CIRP Annals* 57, 2 (2008), 697–715.

- [147] RUPP, O. Instandhaltungskosten bei zivilien Strahltriebwerken. In *DGLR Workshops "Maintenance von Flugzeugen und Triebwerken"* (2001).
- [148] SALUNKE, N. P., JUNED AHAMAD, R., AND CHANNIWALA, S. Airfoil parameterization techniques: A review. *American Journal of Mechanical Engineering* 2, 4 (2014), 99–102.
- [149] SCHÄLTE, Y., STAPOR, P., AND HASENAUER, J. Evaluation of derivative-free optimizers for parameter estimation in systems biology. *IFAC-PapersOnLine* 51, 19 (2018), 98–101.
- [150] SCHOENENBORN, H., AND REILE, E. Analytical analysis of the welding and heat treatment of a compressor blisk leading edge repair process. In *Meeting Proceedings of RDP* (Montreal, Canada, 2005), RTO, pp. 17–1 –17–9.
- [151] SCHWERDT, L., BERGER, R., PANNING-VON SCHEIDT, L., GEBHARDT, C. G., WALLASCHEK, J., AND ROLFES, R. Probabilistic study of blend repairs on an axial compressor blisk using the subset of nominal modes method. In *Proceedings of International Gas Turbine Congress 2019* (Tokyo, Japan, 2019), Gas Turbine Society of Japan.
- [152] SCHWERDT, L., PANNING-VON SCHEIDT, L., WALLASCHEK, J., BERGER, R., ROLFES, R., KELLER, C., AND SEUME, J. Influence of blade repairs on compressor blisk vibration considering aerodynamic damping and mistuning. In *Proceedings of Shanghai 2017 Global Power and Propulsion Forum* (Shanghai, China, 2017), GPPS.
- [153] SEEMANN, R., LANGHANS, S., SCHILLING, T., AND GOLLNICK, V. Modeling the life cycle cost of jet engine maintenance. In *Proceedings of DLRK 2011* (09 2011), DLRK.
- [154] SESHADRI, A. NSGA - II: A multi-objective optimization algorithm, 2021. URL <https://www.mathworks.com/matlabcentral/fileexchange/10429-nsga-ii-a-multi-objective-optimization-algorithm>, MATLAB Central File Exchange.
- [155] SIMPSON, A., KIM, S. I., PARK, J., KWON, S., AND YOO, S. HCF Optimization of a High Speed Variable Geometry Turbine. In *Proceedings of the ASME Turbo Expo 2021* (2021), ASME.
- [156] SINGH, M. P., AND LUCAS, G. M. *Blade design and analysis for steam turbines*. McGraw-Hill, New York, 2011.
- [157] SINGH, M. P., VARGO, J. J., SCHIFFER, D. M., AND DELLO, J. D. Safe diagram-a design and reliability tool for turbine blading. In *Proceedings of the 17th Turbomachinery Symposium* (1988), Texas A&M University. Turbomachinery Laboratories.
- [158] SOBIESZCZANSKI-SOBIESKI, J., AND HAFTKA, R. T. Multidisciplinary aerospace design optimization: survey of recent developments. *Structural Optimization* 14, 1 (1997), 1–23.
- [159] SONG, L.-K., FEI, C.-W., WEN, J., AND BAI, G.-C. Multi-objective reliability-based design optimization approach of complex structure with multi-failure modes. *Aerospace Science and Technology* 64 (2017), 52–62.
- [160] SONG, W., KEANE, A., REES, J., BHASKAR, A., AND BAGNALL, S. Turbine blade fir-tree root design optimisation using intelligent CAD and finite element analysis. *Computers & Structures* 80, 24 (2002), 1853–1867.

- [161] SONG, W., AND KEANE, A. J. An efficient evolutionary optimisation framework applied to turbine blade firtree root local profiles. *Structural and Multidisciplinary Optimization* 29, 5 (2005), 382–390.
- [162] STAFFORD, D. New tool provides Offutt AFB maintainers with just the right blend, 2014. URL <https://www.af.mil/News/Article-Display/Article/475084/new-tool-provides-offutt-afb-maintainers-with-just-the-right-blend/>, US Airforce.
- [163] TALISCHI, C., PAULINO, G. H., PEREIRA, A., AND MENEZES, I. F. Polytop: a matlab implementation of a general topology optimization framework using unstructured polygonal finite element meshes. *Structural and Multidisciplinary Optimization* 45, 3 (2012), 329–357.
- [164] THOMSON, A., AND ANDERTON, D. A. Development in gas turbine repairs. In *Proceedings of the ASME Turbo Expo 2010* (2010), ASME, pp. 645–652.
- [165] TRAUPEL, W. *Thermische Turbomaschinen: Geänderte Betriebsbedingungen, Regelung, Mechanische Probleme, Temperaturprobleme*, 4. Auflage ed. Klassiker der Technik. Springer, Berlin and Heidelberg, 2001.
- [166] UNGER, R., ARASH, B., EXNER, W., AND ROLFES, R. Effect of temperature on the viscoelastic damage behaviour of nanoparticle/epoxy nanocomposites: Constitutive modelling and experimental validation. *Polymer* 191 (2020), 122265.
- [167] VIRTANEN, P., GOMMERS, R., OLIPHANT, T. E., HABERLAND, M., REDDY, T., COURNAPEAU, D., BUROVSKI, E., PETERSON, P., WECKESSER, W., BRIGHT, J., ET AL. Scipy 1.0: fundamental algorithms for scientific computing in python. *Nature methods* 17, 3 (2020), 261–272.
- [168] VOSS, C., AND NICKE, E. Automatische Optimierung von Verdichterstufen. Tech. rep., AG Turbo COOREFF-T, 2008.
- [169] WAGNER, F., KÜHHORN, A., WEISS, T., AND OTTO, D. Influence of different parametrizations on the optimum design of a high pressure turbine blade firtree. In *Proceedings of the ASME Turbo Expo 2016* (2016), ASME.
- [170] WANG, B., WANG, G., TIAN, K., SHI, Y., ZHOU, C., LIU, H., AND XU, S. A preliminary design method for axisymmetric turbomachinery disks based on topology optimization. In *Proceedings of the Institution of Mechanical Engineers, Part C: Journal of Mechanical Engineering Science* (2021), p. 09544062211039529.
- [171] WANG, G. G., AND SHAN, S. Review of metamodelling techniques in support of engineering design optimization. *Journal of Mechanical Design* 129, 4 (2007), 370.
- [172] WANG, Q., WANG, L., HUANG, W., WANG, Z., LIU, S., AND SAVIĆ, D. A. Parameterization of NSGA-II for the Optimal Design of Water Distribution Systems. *Water* 11, 5 (2019).
- [173] WILDHEIM, S. Excitation of rotationally periodic structures. *Journal of Applied Mechanics* 46 (1979).
- [174] WOLPERT, D. H., AND MACREADY, W. G. No free lunch theorems for optimization. *IEEE Transactions on Evolutionary Computation* 1, 1 (1997), 67–82.

-
- [175] YANG, X. S. Metaheuristic optimization: algorithm analysis and open problems. In *Proceedings of 10th International Symposium on Experimental Algorithms (SEA 2011)* (Kolimpari, Chania, Greece,, 2011), P. M. Pardalos and S. Rebennack, Eds., vol. 6630, pp. 21–32.
- [176] YANG, X.-S. Chapter 1 - introduction to algorithms. In *Nature-Inspired Optimization Algorithms*, X.-S. Yang, Ed. Elsevier, Oxford, 2014, pp. 1–21.
- [177] YILMAZ, O., GINDY, N., AND GAO, J. A repair and overhaul methodology for aeroengine components. *Robotics and Computer-Integrated Manufacturing* 26, 2 (2010), 190–201.
- [178] YILMAZ, O., NOBLE, D., GINDY, N. N., AND GAO, J. A study of turbomachinery components machining and repairing methodologies. *Aircraft Engineering and Aerospace Technology* 77, 6 (2005), 455–466.
- [179] ZHU, S.-P., YUE, P., YU, Z.-Y., AND WANG, Q. A combined high and low cycle fatigue model for life prediction of turbine blades. *Materials* 10, 7 (2017).
- [180] ZUO, W. An object-oriented graphics interface design and optimization software for cross-sectional shape of automobile body. *Advances in Engineering Software* 64 (2013), 1–10.

Formal declaration

I hereby declare that

- I know the Regulations for doctoral candidates at the Faculty of Civil Engineering and Geodetic Science (Promotionsordnung)
- I have completed the thesis independently and have listed materials by others in the references
- I did not pay any monetary benefits for regards to content
- the dissertation has not been used as a M.Sc. or similar thesis before, and that the thesis has not been published before
- I have never applied for an exam as a doctoral candidate at another academic institution

Hannover, February 12, 2022

.....
Signature

Curriculum vitae

Personal details

Name: Ricarda Berger
Date of birth: 19.08.1991
Place of birth: Viersen
Nationality: German

Education

1997-2010: School education
2010-2013: Bachelor of Science in “Mechanical engineering”, Leibniz Universität Hannover, Germany
2011-2014: Bachelor of Science in “Civil engineering”, Leibniz Universität Hannover, Germany
2013-2015: Master of Science in “Mechanical engineering”, Leibniz Universität Hannover, Germany

Scientific career

since 2016: Research associate at the Institute of Structural Analysis, Leibniz Universität Hannover, Germany

Awards

2014: “Niedersachsen Stipendium” award for outstanding academic achievement

